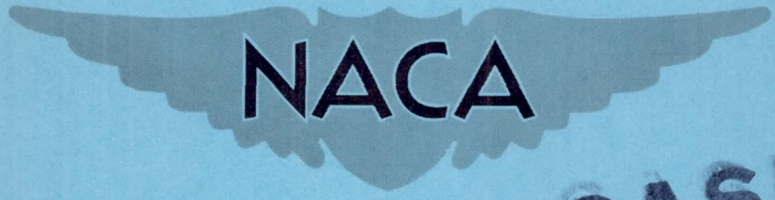


CONFIDENTIAL

Copy 264  
RM L53F05

NACA RM L53F05



CASE FILE  
COPY

# RESEARCH MEMORANDUM

AN INVESTIGATION OF THE AERODYNAMIC CHARACTERISTICS  
AT TRANSONIC MACH NUMBERS OF A SWEEPED-WING  
SUPERSONIC BOMBER CONFIGURATION

By Ralph P. Bielat and J. Lawrence Cooper

Langley Aeronautical Laboratory  
Langley Field, Va.

CLASSIFICATION CHANGED TO UNCLASSIFIED  
AUTHORITY: NACA RESEARCH ABSTRACT NO. 128  
DATE: JUNE 24, 1958

MHL

CLASSIFIED DOCUMENT

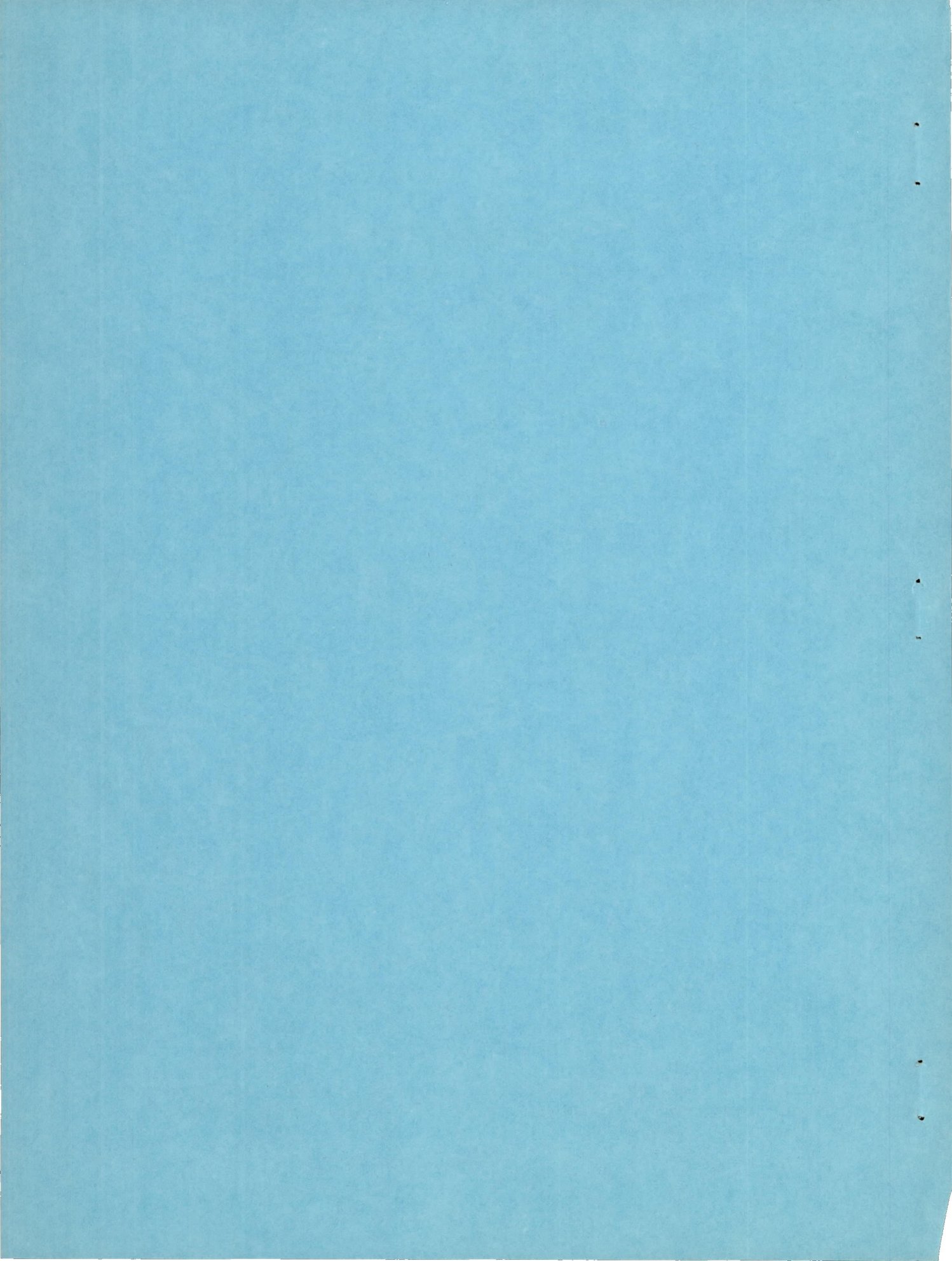
This material contains information affecting the National Defense of the United States within the meaning of the espionage laws, Title 18, U.S.C., Secs. 793 and 794, the transmission or revelation of which in any manner to an unauthorized person is prohibited by law.

## NATIONAL ADVISORY COMMITTEE FOR AERONAUTICS

WASHINGTON

February 1, 1956

CONFIDENTIAL



## NATIONAL ADVISORY COMMITTEE FOR AERONAUTICS

## RESEARCH MEMORANDUM

AN INVESTIGATION OF THE AERODYNAMIC CHARACTERISTICS  
AT TRANSONIC MACH NUMBERS OF A SWEEP-WING  
SUPERSONIC BOMBER CONFIGURATION

By Ralph P. Bielat and J. Lawrence Cooper

## SUMMARY

An investigation of the aerodynamic characteristics of a swept-wing supersonic bomber configuration was conducted in the Langley 8-foot transonic tunnel. The wing had an aspect ratio of 3.5, a taper ratio of 0.2,  $47^\circ$  sweepback of the 0.25-chord line, and airfoil sections which were 5.5 percent thick parallel to the plane of symmetry. The results reported herein consist of the longitudinal force characteristics of the complete model and of various combinations of its components. The effects of wing incidence, a modified wing, various auxiliary wing devices, and horizontal-tail height are also presented. The Mach number range extended from 0.70 to approximately 1.11, and the Reynolds number based on the wing mean aerodynamic chord varied from  $2.60 \times 10^6$  to  $2.95 \times 10^6$ .

The drag rise of the complete model occurred at a Mach number of 0.96, and the drag at transonic speeds increased over that at low speeds by a factor of 2.0. The value of trimmed maximum lift-drag ratio  $(L/D)_{\max}$  for the complete model decreased markedly through the transonic range; however, there was only a small increase in the lift coefficient for trimmed  $(L/D)_{\max}$  through the Mach number range.

Both the elevator and stabilizer effectiveness decreased through the transonic speed range; however, the loss in elevator effectiveness was about four times that noted for the stabilizer.

The model indicated pitch-up instability at lift coefficients near 0.6 through the Mach number range. A combination of leading-edge chord-extensions and a low position of the horizontal tail eliminated the pitch-up instability at a Mach number of 0.70 and reduced it at a Mach number of 0.90. Above a Mach number of 0.93, the leading-edge chord-extensions caused a slight delay in the pitch-up instability; and, generally, raising the horizontal tail above the extended wing-root-chord plane aggravated the pitch-up instability at lift coefficients above about 0.6.

The rate of change of effective downwash angle with angle of attack for the complete model with the horizontal tail located 0.06 semispan above the extended wing-root-chord plane was about the same for the angle-of-attack range from  $-5^\circ$  to  $6^\circ$  through the Mach number range and had a value less than 1.0. The downwash derivative for the model with buried nacelles and horizontal tail located 0.27 semispan above the extended wing-root-chord plane in the angle-of-attack range from  $6^\circ$  to  $12^\circ$  was approximately twice that at angles of attack from  $-6^\circ$  to  $1^\circ$  for subsonic Mach numbers and had a value greater than 1.0 for Mach numbers from 0.70 to 1.03; therefore, it had a destabilizing effect on the model at pitch-up.

## INTRODUCTION

An investigation of a swept-wing supersonic bomber configuration has been made at supersonic speeds in the Langley 4- by 4-foot supersonic pressure tunnel (ref. 1) and at transonic speeds in the Langley 8-foot transonic tunnel. The present paper presents the results of the investigation at transonic speeds.

The results reported herein consisted of the longitudinal characteristics of the complete model and of various combinations of its components. The effects of a modified wing, various auxiliary wing devices, and of horizontal-tail height are also presented. The Mach number range extended from 0.70 to approximately 1.11, and the Reynolds number range extended from  $2.60 \times 10^6$  to  $2.95 \times 10^6$  based on the wing mean aerodynamic chord.

## SYMBOLS

$A_1$	inlet area of ducts located in leading edge of wing root
$b$	wing span
$c$	wing-section chord
$\bar{c}$	wing mean aerodynamic chord
$C_D$	drag coefficient, $D/qS$
$C_{D_{\min}}$	minimum drag coefficient
$C_L$	lift coefficient, $L/qS$

$C_{L\alpha}$	lift-curve slope per degree, $dC_L/d\alpha$
$C_m$	pitching-moment coefficient, $M_{.35\bar{c}}/qS\bar{c}$
$C_{mC_L}$	static-longitudinal-stability parameter, $dC_m/dC_L$
$C_{m\delta}$	elevator effectiveness parameter, $\partial C_m/\partial\delta$
$C_{mi_t}$	stabilizer effectiveness parameter, $\partial C_m/\partial i_t$
D	drag
$h_t$	height of horizontal tail above extended wing-root-chord line
$i_t$	incidence angle of stabilizer chord line with respect to fuselage center line, positive when trailing edge is down
$i_w$	incidence angle of wing chord line with respect to fuselage center line
L	lift
L/D	lift-drag ratio
M	Mach number
$M_{.35\bar{c}}$	pitching moment of aerodynamic forces referred to 35-percent-chord station of wing mean aerodynamic chord
m	mass-flow rate
q	free-stream dynamic pressure, $\rho_0 V^2/2$
R	Reynolds number based on $\bar{c}$
S	wing area
$V_0$	free-stream velocity
$\alpha$	angle of attack of fuselage center line
$\epsilon$	effective downwash angle
$\delta$	deflection angle of elevator chord line with respect to stabilizer chord line, positive when trailing edge is down

$\rho_0$  free-stream density  
 $\Gamma$  dihedral angle

## APPARATUS AND MODELS

### Tunnel

The tests were conducted in the Langley 8-foot transonic tunnel, which is a dodecagonal, slotted-throat, single-return wind tunnel. This tunnel is designed to obtain aerodynamic data through the speed of sound without the usual effects of choking and blockage. The tunnel operates at atmospheric stagnation pressures. A more complete description of the tunnel can be found in reference 2.

### Models

A three-view drawing of the model is given in figure 1 and a photograph of it is shown in figure 2. The geometric characteristics of the model are presented in table I. The construction of the model was such that various components could be tested in combination. Symbols used to designate the various components of the model are given in table II.

Fuselage. - The fuselage B had a fineness ratio of 14.35. The fuselage could be shortened by the removal of a 4-inch section (fig. 1) between the midsection and afterbody, therefore making it possible to conduct some tests of the model with a shortened fuselage ( $B_4$ ) of fineness ratio 12.96. The rear end of the fuselage was of an arbitrary shape to accommodate a sting of adequate size for the loads involved.

Wing. - Two wings were tested: a basic wing W and a modified wing  $W_4$ . (See fig. 3.) The basic wing had an aspect ratio of 3.5, a taper ratio of 0.2,  $47^\circ$  sweepback of the quarter-chord line, and twist which varied linearly across the span to  $2\frac{1}{2}^\circ$  washout at the tip. The airfoil section was 5.5 percent thick measured parallel to the plane of symmetry. For the most part, the wing was tested at  $4^\circ$  incidence and  $0^\circ$  dihedral ( $W$ ), although some tests were conducted with  $2^\circ$  incidence and  $0^\circ$  dihedral ( $W_2$ ). The lower inboard section of the wing was removable for the installation of buried nacelles  $N_2$  which had an air inlet in the leading edge of the wing root ( $W_3$ ). (See fig. 2.) The leading-edge wing-root inlet was divided into two ducted passages as indicated in figure 4 and then exhausted through circular ducts at the rear of the buried nacelles. Air was permitted to flow through the ducts; however, no

provisions were made to control the flow quantity through the ducts. Airfoil coordinates for the basic wing W are given in table III.

The modified and basic wings were identical over the inboard 50 percent of the wing semispan. From the 80- to 100-percent-semispan stations, the forward 15 percent of the basic wing (fig. 3) was modified by adding the full camber of an NACA 230-series airfoil section to the mean line of the basic wing. (The mean line of the basic wing and the 230-series camber line were tangent at the 15-percent-chord station.) From the 50- to 80-percent-semispan stations, the amount of camber which was added to the basic wing mean line varied in an arbitrary manner. Airfoil coordinates for the modified wing W<sub>4</sub> are presented in table IV.

Since the results of reference 3 indicated pitch-up instability at lift coefficients near 0.6 and Mach numbers up to approximately 0.95, pitch-up instability was also expected for the present model with the basic wing even though the basic wing incorporated twist. Auxiliary wing devices in the form of leading-edge chord-extensions and wing fences were investigated in an attempt to eliminate or to reduce the severity of the pitch-up instability. Two of the leading-edge chord-extensions (figs. 4(a) and 4(b)) were geometrically similar in plan form but differed only in the droop of the chord-extension. The leading-edge chord-extensions covered the outboard span of the wing from the 68- to the 100-percent-semispan stations and the chords were 15 percent of the local wing chord. One leading-edge chord-extension (W<sub>5</sub>) had approximately 4° of nose droop which was obtained by moving forward the front 15 percent of the basic airfoil section along the camber line of the NACA 230-series airfoil section and fairing the remainder of the airfoil section in an arbitrary manner. (See fig. 4(a).) The airfoil coordinates for the basic wing with the drooped leading-edge chord-extension W<sub>5</sub> are given in table V and a photograph is shown in figure 5. The second leading-edge chord-extension W<sub>7</sub>, which had no droop, was obtained by moving forward the front 15 percent of the basic airfoil section along the chord line (fig. 4(b)). The airfoil coordinates for the undrooped leading-edge chord-extension W<sub>7</sub> are given in table VI.

A third leading-edge chord-extension W<sub>6</sub> had a "saw-toothed" plan form which was obtained by modifying the drooped leading-edge chord-extension. The chord-extension was 15 percent of the basic wing chord at the 68-percent-semispan station and varied linearly to zero chord at the 84-percent-semispan station. From the 84- to the 100-percent-semispan stations, the chord was 15 percent of the basic chord (figs. 4(c) and 6).

The wing fences investigated were located at the 50-percent-semispan station for wing W<sub>7</sub> and at the 84.3-percent-semispan station for wing W<sub>5</sub>. The fences were located on the upper surfaces of the wings

and were 0.033c high for wing  $W_7$  and 0.062c high for wing  $W_5$ . The leading edges of the fences were located at approximately the point of maximum wing thickness. Details of the wing fences are shown in figure 7

Horizontal stabilizer.- The horizontal stabilizer was geometrically similar to the basic wing in plan form and was identical in thickness ratio. Provisions were made for testing the horizontal stabilizer in three positions  $H$ ,  $H_1$ , and  $H_2$  above the extended wing-root-chord plane as shown in figure 8. It was necessary to use a modified vertical tail in order to test the horizontal stabilizer at the  $0.56b/2$  position above the extended wing-root-chord plane (fig. 8). The elevator, which was included as a part of the horizontal stabilizer, had an area which was approximately 15 percent of the complete exposed stabilizer area and a chord which was 21 percent of the stabilizer chord. Elevator deflections were obtained by installing elevator sections which had been machined to the desired deflections. Coordinates for the horizontal stabilizer are given in table VII.

Vertical tail.- The vertical tail  $V$  had the same taper ratio and thickness ratio as the horizontal stabilizer, but had an aspect ratio of 1.50. The modified vertical tail  $V_1$  (fig. 9) also had the same thickness ratio as the horizontal stabilizer, but had a taper ratio of 0.74 and an aspect ratio of 1.04. Airfoil coordinates for the vertical tails are presented in table VII.

#### Model Support System

The model was attached to the sting support through a six-component, internal, electrical strain-gage balance. Angle-of-attack changes of the model were accomplished by pivoting the sting about a point which was located approximately 80 inches downstream of the  $0.35\bar{c}$  station. A  $15^\circ$  coupling located ahead of the pivot point made it possible to keep the model position reasonably close to the tunnel axis for the  $6^\circ$  to  $12^\circ$  angle-of-attack range. The angle mechanism was controlled from outside the test section and, therefore, permitted angle changes while the tunnel was in operation.

A temperature-compensated, pendulum-type inclinometer, calibrated against angle of attack and located within the sting downstream of the model, was used to indicate the angles of the model relative to the air stream. For actual testing conditions, however, it was necessary to apply a correction to the angle of attack of the model caused by the elasticity of the sting-support system.

The use of the calibrated inclinometer in conjunction with the remotely controlled angle-of-attack changing mechanism allowed the model angle to be set within  $\pm 0.1^\circ$  at all test Mach numbers.



## TESTS

The variation with Mach number of the range of test Reynolds number calculated from several runs and based on the mean aerodynamic chord of the wing is presented in figure 10. For the present tests, the Reynolds number varied from  $2.60 \times 10^6$  to  $2.95 \times 10^6$ .

## Measurements

Lift, drag, and pitching moment were determined by means of an electrical strain-gage balance located inside the fuselage. Static-pressure measurements were taken in the ducts of the buried nacelles to determine the mass flow and internal-drag coefficient. The methods used to determine the mass flow and internal-drag coefficient are discussed in reference 1. Results of the mass-flow measurements are presented in figure 11. In general, dependent on model configuration, measurements were taken for two angle-of-attack ranges:  $-6^\circ$  to  $16^\circ$  and  $-6^\circ$  to  $8^\circ$  at Mach numbers varying from 0.70 to approximately 1.11. Load limits on the balance, however, prevented the attainment of measurements over the entire angle-of-attack range at all test Mach numbers.

## Corrections and Accuracy

No corrections to the free-stream Mach number and dynamic pressure for the effects of model and wake blockage are necessary for tests in the slotted test section of the 8-foot transonic tunnel (ref. 4). There is a range of Mach number above a Mach number of 1.00, however, where the data are affected by the reflected compressions and expansions from the test-section boundary. On the basis of the results of reference 5, it is believed that, for Mach numbers up to approximately 1.03, the effects of these disturbances on the measurements made in the present investigation may be considered to be negligible. For test Mach numbers above 1.03, however, the data were influenced by the boundary-reflected disturbances but the extent to which the data were affected by these disturbances is not known for these tests. A study of the effects of boundary interference on the force and moment characteristics of a wing-body configuration at transonic Mach numbers has been made in reference 6. From these studies it is concluded that the effects of shock reflection would be small on the lift characteristics presented herein. As shown in references 5 and 6, the effects of boundary interference on the drag characteristics at Mach numbers above 1.03 cause the drag to be first overestimated and then underestimated; however, it is believed that these effects on the drag results of the present investigation are small. No data are available which show the effects of shock reflection on pitching moment for a wing-body configuration having horizontal-tail surfaces; however, on the basis of the studies of

reference 6, it is believed that these effects on the pitching-moment data presented herein are also small.

It was assumed that bending of the swept wings had a negligible effect on the aerodynamic data presented herein.

No corrections for interference forces caused by the sting support have been applied to the data. As indicated in reference 7 the significant corrections would be limited to small increments in pitching moment and drag and to the effective downwash angle.

The drag data have been corrected for base pressure such that the drag corresponds to conditions where the body base pressure is equal to the free-stream static pressure. The drag data for the configurations with the buried nacelles include the internal drag of the ducts. The measured internal drag coefficient based on wing area for four ducts was of the order of 0.0024 and was essentially constant throughout the Mach number range.

The estimated consistency of the balance based on the design of the balance and the repeatability of the data is as follows:

$C_L$ . . . . .	$\pm 0.003$
$C_D$ . . . . .	$\pm 0.0015$
$C_m$ . . . . .	$\pm 0.003$

The reference axes of the data presented in the figures are the wind axes.

## PRESENTATION OF RESULTS AND DISCUSSION

Throughout the discussion, the model configuration having the basic wing, fuselage, vertical tail, and horizontal tail with incidence angle of  $-0.1^\circ$  and located  $0.06b/2$  above the extended wing-root-chord line (WBHV) is identified as the complete model. Unless otherwise stated, wing incidence is  $4^\circ$  and wing dihedral is  $0^\circ$ . An index of the figures presenting the results is given in table VIII.

### Lift and Drag Characteristics

The variations with angle of attack of the lift and drag characteristics of the various combinations of the model components are presented in figure 12. The effects of wing incidence on the lift and drag characteristics for the wing-fuselage configuration are shown in figure 13

and the effects of vertical location of the horizontal tail on the lift and drag characteristics of the model with buried nacelles are shown in figure 14. A comparison of the lift and drag characteristics of the complete model with the basic wing and the modified wing is made in figure 15. Figures 16 and 17 present the effects of stabilizer incidence on the lift and drag characteristics of the complete model and of the model with buried nacelles, respectively. The effects of elevator deflection on the lift and drag characteristics of the model with the horizontal tail located  $0.27b/2$  above the extended wing-root-chord line are given in figure 18.

It can be seen that the lift characteristics of the various complete model configurations (see, for example, fig. 16) were linear up to a lift coefficient of approximately 0.5. Above a lift coefficient of 0.6 and Mach numbers up to 0.96, the lift-curve slope decreased such that it was less than one-half the value in the low-lift range (-0.2 to 0.5). The decrease in the lift-curve slope at high lift coefficients ( $C_L > 0.6$ ), compared with the low-lift-coefficient range at Mach numbers 1.00 and above, was less than that observed at subsonic speeds.

The effects of compressibility on the values of lift-curve slope measured for a lift-coefficient range of 0 to 0.3 are shown in figure 19. The lift-curve slopes increased with increase in Mach number up to 0.96 and then decreased rapidly through the transonic speed range. In general, a change in the vertical location of the horizontal tail (fig. 19(a)), a change in the wing incidence (fig. 19(b)), or a wing modification (fig. 19(c)) had only a small effect on the lift-curve slopes. There is also shown in figure 19 the values of the lift-curve slopes at supersonic speeds taken from reference 1. Curves have been faired from the transonic data through the supersonic data in order to illustrate the trends in the lift-curve-slope characteristics in these speed ranges.

The variations with Mach number of the minimum drag coefficients for several of the model configurations are presented in figure 20. The minimum drag values at supersonic speeds taken from reference 1 are also included. The minimum drag coefficient of the complete model (fig. 20(a)) was approximately 0.012, the drag rise occurred at a Mach number of 0.96, and the drag at transonic speeds increased over the low-speed value by a factor of 2.0.

It can be seen that horizontal-tail location (fig. 20(a)) and wing incidence (fig. 20(c)) had a small effect on the minimum drag coefficient throughout the Mach number range. Figure 20(b) indicates that the buried nacelles ( $h_t = 0.27b/2$ ) increased the drag of the basic model approximately 20 percent throughout the Mach number range.

A comparison of the results obtained from tests of the complete model and the complete model with the modified wing  $W_4$  is made in figure 20(d). The modified wing  $W_4$  increased the minimum drag coefficient of the complete model approximately 15 percent throughout the speed range. A comparison of the results in figure 15, however, indicates that the modified wing  $W_4$  reduced the drag due to lift of the complete model for Mach numbers up to 0.98.

The variation through the Mach number range of the trimmed lift-drag ratio with lift coefficient for the model with two positions of the horizontal tail ( $H$  and  $H_1$ ) and for the model configuration with buried nacelles ( $h_t = 0.27b/2$ ) is presented in figure 21. The data for this figure were calculated from that presented in figures 16, 17, and 18. It can readily be seen that the trimmed  $(L/D)_{\max}$  for all three configurations dropped off very rapidly for an increase in Mach number from 0.93 to 1.05. For higher Mach numbers, however, there was very little change in the values of trimmed  $(L/D)_{\max}$ . It can also be seen that there was only a slight increase in the lift coefficient for trimmed  $(L/D)_{\max}$  through the Mach number range. Curves of trimmed  $(L/D)_{\max}$  against Mach number are shown in figure 22. The trimmed  $L/D$  curves for sea level and an altitude of 35,000 feet calculated for the lift coefficients shown in figure 23 are also shown in figure 22. Supersonic data of reference 1 are presented with the transonic data. A comparison of the data of figure 22(c) with figure 22(b) indicates that the buried nacelles decreased the trimmed  $(L/D)_{\max}$  of the basic model from a value of 14.6 to a value of 12.1 at a Mach number of 0.70. The values of trimmed  $(L/D)_{\max}$  for the basic model and the model with buried nacelles were approximately 6.3 and 6.6, respectively, at a Mach number of 1.10.

The effects of leading-edge chord-extensions and fences on the aerodynamic characteristics of the model with buried nacelles are presented in figures 24 and 25. In general, the addition of the various leading-edge chord-extensions or the fences to the basic wing had negligible effect on the lift characteristics and had little or no effect on the drag characteristics at low lift coefficients.

### Longitudinal Stability and Control Characteristics of Model

#### Without Auxiliary Wing Devices

Stability characteristics. - A comparison of the variation of pitching-moment coefficient with angle of attack for the various components of the

model presented in figure 12 indicated that fuselage B alone was an unstable configuration. Addition of either wing W or the horizontal tails H and  $H_1$  to the fuselage produced a stable configuration; however, above a lift coefficient of 0.50, the wing-fuselage configuration WBV (see fig. 16, for instance) had a pitch-up instability which was due primarily to the flow changes occurring over the wing. The model configurations with the tail, WBHV and  $WBH_1V$ , also indicated pitch-up instability at lift coefficients above 0.50.

A comparison of the pitching-moment characteristics for the configurations having  $2^\circ$  and  $4^\circ$  wing incidence,  $W_2B$  and WB, indicated that the effects on stability of changing the wing incidence were small throughout the Mach number range (fig. 13).

The effects of vertical location of the horizontal tail (H,  $H_1$ , and  $H_2$ ) on the pitching-moment characteristics of the model configuration with the basic wing  $W_3$  and buried nacelles (fig. 14) indicated that an increase in tail height from 0.06 to 0.56 semispan above the extended wing-root-chord plane resulted in an increase in the longitudinal stability of the model for an approximate lift-coefficient range from -0.20 to 0.50 throughout the Mach number range. An increase in tail height, however, aggravated the pitch-up instability at lift coefficients above about 0.60 which indicates an increase in the value of the downwash derivative  $\partial\epsilon/\partial\alpha$  with increase in tail height.

The variations with Mach number of the static-longitudinal-stability parameter  $C_{mC_L}$  for the configurations having  $2^\circ$  and  $4^\circ$  wing incidence and the configurations having the buried nacelles and various vertical locations of the horizontal tail are given in figure 26. The static-longitudinal-stability parameter was averaged over the lift-coefficient range from 0 to 0.3. A large increase in the negative value of  $C_{mC_L}$  for both the tail-on and tail-off configurations occurred through the transonic speed range which, if expressed in terms of the aerodynamic-center location, would represent a shift in the aerodynamic-center location of 13 to 19 percent of the mean aerodynamic chord. An increase in tail height from 0.06 to 0.56 semispan above the extended wing-root-chord plane (fig. 26(b)) increased the negative value of the static-stability parameter approximately 50 percent throughout the Mach number range.

The variations with Mach number of the neutral-point locations for several of the model configurations presented in figure 27 were determined from the data given in figures 16, 17, and 18. It can be seen that there was a large rearward movement of the neutral-point location through the transonic speed range which amounted to about 15 percent of the mean aerodynamic chord and which was comparable to the shift in the

static-stability parameter  $C_{mCL}$ . This shift in the neutral-point location would be expected since the curves of pitching-moment coefficient against stabilizer incidence (figs. 16 and 17) and pitching-moment coefficient against elevator deflection (fig. 18) are linear for the angle-of-attack range corresponding to data given in figures 26 and 27. Changes in model configuration caused only small differences in the neutral-point location.

Stabilizer and elevator effectiveness.- The longitudinal stability characteristics of the model presented in figures 16, 17, and 18 were used to calculate the stabilizer effectiveness and elevator effectiveness parameters given in figure 28. The data were averaged over a lift-coefficient range from 0 to 0.3. The supersonic tunnel data of reference 1 are included to illustrate the trends of the effectiveness parameters through the speed range. The effectiveness of the stabilizer increased gradually up to a Mach number of 0.98 and then decreased approximately 10 percent through the transonic speed range. Vertical location of the stabilizer had a small effect on the effectiveness parameter  $C_{mit}$ .

At subsonic Mach numbers, the elevator was about one-third as effective as the stabilizer in producing control. The elevator lost approximately 41 percent of its effectiveness when the Mach number was increased from 0.93 to 1.10 and, therefore, as a control producing device, was only one-fifth as effective as the stabilizer in the same range of Mach numbers.

Effective downwash characteristics.- The variation of effective downwash angle with angle of attack for the complete model with horizontal tail located 0.06 semispan above the extended wing-root-chord line (H) and the model with buried nacelles and horizontal tail located 0.27 semispan above the extended wing-root-chord line ( $H_1$ ) is presented in figure 29. The effective downwash angle at a given angle of attack was determined by finding the stabilizer incidence setting at which the pitching-moment coefficient of the complete model was equal to the pitching-moment coefficient of the model without the horizontal tail. The sum of the stabilizer incidence thus found and the angle of attack gave the effective downwash in the region of the horizontal tail. The effect of the horizontal-tail drag on the pitching moment was neglected. Since only three stabilizer incidence settings were used, some of the data at the low and at the high angles of attack given in figure 29 were extrapolated. In general, the variation of the effective downwash angle with angle of attack showed no large changes for the complete model with horizontal tail H (fig. 29(a)); whereas, on the other hand, the effective downwash angle increased markedly above  $3^\circ$  angle of attack (fig. 29(b)) for the model with buried nacelles and horizontal tail  $H_1$ .

The effect of Mach number on the rate of change of effective downwash angle with angle of attack for the complete model with horizontal tail  $H$  and for the model with buried nacelles and horizontal tail  $H_1$  is shown in figure 30. The effective downwash derivative  $\partial\epsilon/\partial\alpha$  for the complete model ( $h_t = 0.06b/2$ ) was about the same for the angle-of-attack range of  $-5^\circ$  to  $6^\circ$  and had a value less than 1.0. The effective downwash derivative  $d\epsilon/d\alpha$  indicated a rather large increase followed by a rapid decrease in the range of Mach number from 0.90 to 1.00. For angles of attack from  $1^\circ$  to  $6^\circ$  (fig. 30(a)), the value of the downwash derivative decreased approximately 0.20 through the transonic speed range.

A comparison of figure 30(b) with figure 30(a) indicates that, at angles of attack from approximately  $-6^\circ$  to  $1^\circ$ , the downwash derivative  $\partial\epsilon/\partial\alpha$  for the model with buried nacelles ( $h_t = 0.27b/2$ ) was essentially the same as for the complete model ( $h_t = 0.06b/2$ ). At angles of attack from  $6^\circ$  to  $12^\circ$ , however, the value of the downwash derivative was approximately twice that obtained at angles of attack from  $-6^\circ$  to  $1^\circ$  for subsonic Mach numbers and had a value greater than 1.0 for Mach numbers of 0.70 to 1.03. The increase in the derivative  $\partial\epsilon/\partial\alpha$  was the cause of the marked increase in the pitch-up characteristics at high angles of attack for the model with the horizontal tail located 0.27 semispan above the extended wing-root-chord plane as was previously discussed.

#### Effects of Wing Modification, Chord-Extensions, and Fences on Longitudinal Stability Characteristics

Because the model exhibited undesirable pitch-up characteristics at lift coefficients near 0.6, a program was initiated in an attempt to eliminate or to reduce the severity of the pitch-up instability. A wing modification, various leading-edge chord-extensions, wing fences, and various locations of the horizontal tail in combination with leading-edge chord-extensions were investigated to determine their effects on the stability characteristics of the model.

Wing modification.- The pitching-moment characteristics of the complete models with the modified wing  $W_4$  and the basic wing  $W$  are compared in figure 15. It can be seen that the modified wing had only a small effect in delaying the point at which pitch-up occurred.

Leading-edge chord-extensions.- The effects of drooped leading-edge chord-extensions  $W_5$  and undrooped leading-edge chord-extensions  $W_7$  on the longitudinal stability characteristics of the complete model with buried nacelles ( $h_t = 0.06b/2$ ) are shown in figure 24. At a Mach number of 0.70, both leading-edge chord-extensions eliminated the pitch-up instability noted for the model configuration  $W_3$  and reduced the pitch-up

instability at a Mach number of 0.90. In the range of Mach numbers from 0.93 to 1.10, the addition of the leading-edge chord-extensions caused a small delay in the lift coefficient for pitch-up.

Figure 25 shows the effects of drooped  $W_5$  and saw-toothed  $W_6$  leading-edge chord-extensions on the aerodynamic characteristics of the complete model with buried nacelles and horizontal tail located 0.56 semispan above the extended wing-root-chord plane ( $H_2$ ). Through the Mach number range 0.70 to 1.00, the leading-edge chord-extensions delayed the break in the pitching-moment curve to slightly higher lift coefficients; however, the pitch-up instability was about as severe as that noted for the model without leading-edge chord-extensions. At Mach numbers of 1.04 and 1.11, the data indicated that the saw-toothed leading-edge chord-extensions  $W_6$  eliminated the pitch-up for the range of lift coefficients investigated.

Horizontal-tail location.- The effects of vertical location of the horizontal tail ( $H$ ,  $H_1$ , and  $H_2$ ) on the aerodynamic characteristics of the model with the basic wing with leading-edge chord-extensions  $W_5$  and buried nacelles are presented in figure 31. In general, for the locations of the horizontal tail investigated herein, an increase in the height of the horizontal tail from 0.06 to 0.56 semispan above the extended wing-root-chord plane resulted in an increase in the longitudinal stability of the model for an approximate lift-coefficient range from -0.2 to 0.5 throughout the Mach number range. Raising the horizontal tail from  $H$  to  $H_1$  increased the pitch-up instability at a lift coefficient above 0.6; however, with a further increase in tail height to  $H_2$ , the pitch-up instability was intermediate between that of the  $H$  and  $H_1$  locations.

Fences.- The effects of fences (fig. 7) on the aerodynamic characteristics of the model are presented in figures 24 and 32. Since no drag data, due to balance operational difficulties, were obtained during the investigation of the model configurations given in figure 32, the conversion from body axes to wind axes was computed by neglecting the contribution to the lift component of the axial force; however, this omission does not affect the analysis of the data. The addition of the fences (figs. 24 and 32) had little effect on the longitudinal stability characteristics of the models for the Mach number range investigated.

#### SUMMARY OF RESULTS

An investigation of the aerodynamic characteristics of a swept-wing supersonic bomber configuration was conducted in the Langley 8-foot transonic tunnel at Mach numbers varying from 0.70 to 1.11 and Reynolds



numbers varying from  $2.60 \times 10^6$  to  $2.95 \times 10^6$ . The wing had an aspect ratio of 3.5, a taper ratio of 0.2,  $47^\circ$  sweepback of the 0.25-chord line, and airfoil sections which were 5.5 percent thick parallel to the plane of symmetry. The following results are indicated:

1. The minimum drag coefficient of the complete model was approximately 0.012, the drag rise occurred at a Mach number of 0.96, and the drag at transonic speeds increased over the low-speed value by a factor of 2.0. Addition of buried nacelles to the basic model (horizontal tail located 0.27 semispan above the extended wing-root-chord plane) increased the drag approximately 20 percent throughout the Mach number range. The modified wing increased the drag of the complete model approximately 15 percent throughout the Mach number range; however, the modified wing reduced the drag due to lift of the complete model for subsonic Mach numbers.

2. The values of trimmed maximum lift-drag ratio  $(L/D)_{\max}$  for the various model configurations decreased markedly through the transonic speed range; however, there was only a small increase in the lift coefficient for trimmed  $(L/D)_{\max}$  through the Mach number range. Buried nacelles decreased the values of trimmed  $(L/D)_{\max}$  of the basic model from 14.6 to 12.1 at a Mach number of 0.70, and these values decreased to 6.3 and 6.6 for the basic model and the model with buried nacelles, respectively, at a Mach number of 1.10.

3. The aerodynamic-center location for both the tail-on and tail-off configurations and the neutral-point location moved rearward approximately 15 percent of the mean aerodynamic chord through the transonic speed range.

4. The stabilizer effectiveness decreased about 10 percent through the transonic speed range. Vertical location of the stabilizer had a small effect on the stabilizer effectiveness. The elevator lost approximately 41 percent of its effectiveness when the Mach number was increased from 0.93 to 1.10 and was about one-third to one-fifth as effective as the stabilizer in producing control for the same range of Mach number.

5. The model indicated pitch-up instability at lift coefficients near 0.6 through the Mach number range. The modified wing had only a small effect in delaying the point at which pitch-up occurred.

6. A combination of leading-edge chord-extensions and a low position of the horizontal tail eliminated the pitch-up instability at a Mach number of 0.70 and reduced the pitch-up instability at a Mach number of 0.90. The leading-edge chord-extensions caused a slight delay in the pitch-up instability at Mach numbers above 0.93.

7. Generally, raising the horizontal tail above the extended wing-root-chord plane aggravated the pitch-up instability at lift coefficients above about 0.6.

8. The range of change of effective downwash angle with angle of attack for the complete model with the horizontal tail located 0.06 semi-span above the extended wing-root-chord plane was about the same for the angle-of-attack range from  $-5^{\circ}$  to  $6^{\circ}$  through the Mach number range and had a value less than 1.0. The downwash derivative for the model with buried nacelles and horizontal tail located 0.27 semispan above the extended wing-root-chord plane in the angle-of-attack range from  $6^{\circ}$  to  $12^{\circ}$  was approximately twice that at angles of attack from  $-6^{\circ}$  to  $1^{\circ}$  for subsonic Mach numbers and had a value greater than 1.0 for Mach numbers from 0.70 to 1.03 and, therefore, had a destabilizing effect on the model at pitch-up.

Langley Aeronautical Laboratory,  
National Advisory Committee for Aeronautics,  
Langley Field, Va., May 14, 1953.

## REFERENCES

1. Smith, Norman F., and Hasel, Lowell E.: An Investigation at Mach Numbers of 1.41 and 2.01 of the Aerodynamic Characteristics of a Swept-Wing Supersonic Bomber Configuration. NACA RM L52J17, 1956.
2. Wright, Ray H., and Ritchie, Virgil S.: Characteristics of a Transonic Test Section With Various Slot Shapes in the Langley 8-Foot High-Speed Tunnel. NACA RM L51H10, 1951.
3. Bielat, Ralph P., Harrison, Daniel E., and Coppolino, Domenic A.: An Investigation at Transonic Speeds of the Effects of Thickness Ratio and of Thickened Root Sections on the Aerodynamic Characteristics of Wings With  $47^\circ$  Sweepback, Aspect Ratio 3.5, and Taper Ratio 0.2 in the Slotted Test Section of the Langley 8-Foot High-Speed Tunnel. NACA RM L51I04a, 1951.
4. Wright, Ray H., and Ward, Vernon G.: NACA Transonic Wind-Tunnel Test Sections. NACA RM L8J06, 1948.
5. Ritchie, Virgil S., and Pearson, Albin O.: Calibration of the Slotted Test Section of the Langley 8-Foot Transonic Tunnel and Preliminary Experimental Investigation of Boundary-Reflected Disturbances. NACA RM L51K14, 1952.
6. Whitcomb, Charles F., and Osborne, Robert S.: An Experimental Investigation of Boundary Interference on Force and Moment Characteristics of Lifting Models in the Langley 16- and 8-Foot Transonic Tunnels. NACA RM L52L29, 1953.
7. Osborne, Robert S.: High-Speed Wind-Tunnel Investigation of the Longitudinal Stability and Control Characteristics of a 1/16-Scale Model of the D-558-2 Research Airplane at High Subsonic Mach Numbers and at a Mach Number of 1.2. NACA RM L9C04, 1949.

TABLE I.- GEOMETRIC CHARACTERISTICS OF MODEL

Wing:	
Area, sq ft (includes area blanketed by fuselage)	1.367
Span, ft	2.188
Aspect ratio	3.5
Sweepback of quarter-chord line, deg	47
Taper ratio	0.2
Mean aerodynamic chord, ft	0.718
Airfoil section thickness in streamwise direction, percent (see tables III and IV for ordinates)	5.5
Twist, deg (linear variation from root to tip)	0 to 2.5 washout at tip
Horizontal tail H (see table II):	
Area (includes area blanketed by fuselage), sq ft	0.191
Span, ft	0.837
Aspect ratio	3.65
Sweepback of quarter-chord line, deg	47
Taper ratio	0.2
Airfoil section thickness in streamwise direction, percent (see table VII for ordinates)	5.5
Total elevator area, sq ft	0.0226
Horizontal tails H <sub>1</sub> and H <sub>2</sub> :	
Area (includes area blanketed by vertical tail), sq ft	0.154
Span, ft	0.733
Aspect ratio	3.5
Sweepback of quarter-chord line, deg	47
Taper ratio	0.2
Airfoil section thickness in streamwise direction, percent (see table VII for ordinates)	5.5
Total elevator area, sq ft	0.0226
Vertical tail:	
Area (exposed), sq ft	0.121
Span (exposed), ft	0.425
Aspect ratio (based on exposed span and area)	1.5
Sweepback of quarter-chord line, deg	47
Taper ratio	0.2
Airfoil section thickness in streamwise direction, percent (see table VII for ordinates)	5.5
Rudder area, sq ft	0.0166
Modified vertical tail:	
Area (exposed), sq ft	0.175
Span (exposed), ft	0.425
Aspect ratio (based on exposed span and area)	1.04
Sweepback of quarter-chord line, deg	25.5
Taper ratio	0.74
Airfoil section thickness in streamwise direction, percent (see table VII for ordinates)	5.5
Fuselage:	
Fineness ratio (original fuselage)	14.35
Fineness ratio (shortened fuselage)	12.96
Frontal area, sq ft	0.0452
Miscellaneous:	
Tail length from 0.35 wing M.A.C. to 0.35 tail M.A.C. (original fuselage), ft	1.636
Tail length from 0.35 wing M.A.C. to 0.35 tail M.A.C. (shortened fuselage), ft	1.302

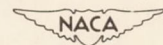


TABLE II.- SYMBOLS FOR MODEL COMPONENTS

B	Long fuselage
B <sub>4</sub>	Short fuselage
V	Vertical tail
V <sub>1</sub>	Modified vertical tail
H	Horizontal tail; $h_t = 0.06b/2$
H <sub>1</sub>	Horizontal tail; $h_t = 0.27b/2$
H <sub>2</sub>	Horizontal tail; $h_t = 0.56b/2$
W	Basic wing; $i_w = 4^\circ$ ; $\Gamma = 0^\circ$
W <sub>2</sub>	Basic wing; $i_w = 2^\circ$ ; $\Gamma = 0^\circ$
W <sub>3</sub>	Basic wing with leading-edge inlet; $i_w = 4^\circ$ ; $\Gamma = 0^\circ$
W <sub>4</sub>	Modified wing; $i_w = 4^\circ$ ; $\Gamma = 0^\circ$
W <sub>5</sub>	Basic wing, leading-edge inlet, and drooped leading-edge chord-extensions; $i_w = 4^\circ$ ; $\Gamma = 0^\circ$
W <sub>6</sub>	Basic wing, leading-edge inlet, and drooped saw-toothed leading-edge chord-extensions; $i_w = 4^\circ$ ; $\Gamma = 0^\circ$
W <sub>7</sub>	Basic wing, leading-edge inlet, and undrooped leading-edge chord-extensions; $i_w = 4^\circ$ ; $\Gamma = 0^\circ$
N <sub>2</sub>	Buried nacelles

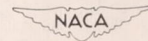


TABLE III.- ORDINATES FOR BASIC WING W

[Values expressed in percent of total chord length]

Chord	Upper ordinate	Lower ordinate
0	0.051	0
.50	.532	.337
.75	.662	.399
1.25	.861	.474
2.50	1.214	.540
5.00	1.801	.650
7.50	2.193	.744
10	2.506	.861
15	2.976	1.057
20	3.250	1.292
25	3.445	1.488
30	3.641	1.605
35	3.680	1.723
40	3.720	1.762
45	3.680	1.801
50	3.563	1.723
55	3.406	1.644
60	3.132	1.488
65	2.819	1.292
70	2.467	1.096
80	1.684	.744
90	.861	.391
100	.098	.098

L.E. radius: 0.196

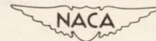


TABLE IV.- ORDINATES FOR MODIFIED WING  $W_4$ 

[Values expressed in percent of total chord length]

Chord	Upper ordinate	Lower ordinate
0	-2.075	2.193
.50	-1.410	2.349
.75	-1.175	2.349
1.25	-.861	2.271
2.50	-.157	2.036
5.00	.901	1.605
7.50	1.684	1.292
10	2.232	1.135
15	2.937	1.096
20	3.250	1.292
30	3.602	1.605
40	3.720	1.762
50	3.563	1.723
60	3.132	1.488
70	2.467	1.096
80	1.684	.744
90	.861	.391
100	.098	.098

L.E. radius: 0.196

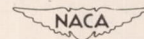


TABLE V.- ORDINATES FOR WINGS  $W_5$  AND  $W_6$ 

[Values expressed in percent of total chord length]

Chord	Upper ordinate	Lower ordinate
-15.00	-1.292	1.370
-14.50	-.783	1.566
-14.25	-.666	1.644
-13.75	-.470	1.723
-12.50	-.039	1.801
-10.00	.626	1.801
-7.50	1.175	1.801
-5.00	1.566	1.801
0	2.232	1.801
5	2.584	1.801
10	2.897	1.801
15	3.132	1.801
20	3.289	1.801
25	3.445	1.801
30	3.641	1.801
35	3.680	1.801
40	3.720	1.801
45	3.680	1.801
50	3.563	1.723
55	3.406	1.644
60	3.132	1.488
65	2.819	1.292
70	2.467	1.096
80	1.684	.744
90	.861	.391
100	.098	.098

L.E. radius: 0.196

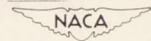
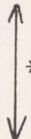
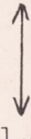




TABLE VI.- ORDINATES FOR WING W<sub>7</sub>

[Values expressed in percent of total chord length]

Chord	Upper ordinate	Lower ordinate
-15.00	0.051	0
-14.50	.532	.337
-14.25	.662	.399
-13.75	.861	.474
-12.50	1.214	.540
-10.00	1.801	.650
-7.50	2.193	.744
-5.00	2.506	.861
0	2.976	1.057
5	 *	 *
10		
15		
20		
25		
30	3.641	1.488
35	3.680	1.605
40	3.720	1.723
45	3.680	1.762
50	3.563	1.801
55	3.406	1.723
60	3.132	1.644
65	2.819	1.488
70	2.467	1.292
80	1.684	1.096
90	.861	.744
100	.098	.391
L.E. radius: 0.196		

\*Faired in an arbitrary manner.

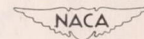


TABLE VII.- ORDINATES FOR HORIZONTAL AND VERTICAL TAILS

[Values expressed in percent of total chord length]

Chord	Symmetrical ordinate
0	0
.50	.436
.75	.526
1.25	.657
2.50	.876
5.00	1.201
7.50	1.456
10.00	1.672
15.00	2.014
20.00	2.275
25.00	2.472
30.00	2.614
40.00	2.748
50.00	2.658
60.00	2.308
70.00	1.774
100.00	0
L.E. radius: 0.202	

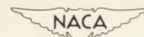
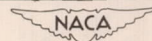


TABLE VIII.- INDEX OF FIGURES

Figure	Type of plot	Configuration	Remarks
11	$m/\rho_0 V_0 A_1$ against M	$W_2BH_1VN_2$	
12	$C_L$ , $C_D$ , and $C_m$ against $\alpha$	B; WBV BHV; WBHV $BH_1V$ ; $WBH_1V$	Effects of model components
13	$\alpha$ , $C_D$ , and $C_m$ against $C_L$	WB $W_2B$	Effects of wing incidence
14	$\alpha$ , $C_D$ , and $C_m$ against $C_L$	$W_2BVN_2$ $W_3BHVN_2$ $W_2BH_1VN_2$ $W_3BH_2V_1N_2$	Effects of horizontal-tail location
15	$\alpha$ , $C_D$ , and $C_m$ against $C_L$	WBHV $W_1BHV$	Effects of wing modification
16	$\alpha$ , $C_D$ , and $C_m$ against $C_L$	WBV WBHV; $i_t = -3.0^\circ$ ; $-0.1^\circ$ ; $2.0^\circ$	Effects of stabilizer incidence
17	$\alpha$ , $C_D$ , and $C_m$ against $C_L$	$W_2BVN_2$ $W_3BH_1VN_2$ ; $i_t = -3.0^\circ$ ; $-0.1^\circ$ ; $2.0^\circ$	Effects of stabilizer incidence
18	$\alpha$ , $C_D$ , and $C_m$ against $C_L$	$WBH_1V$ ; $\delta_e = 0^\circ$ ; $-5^\circ$ ; $-10^\circ$	Effects of elevator deflection
19	$C_{L\alpha}$ against M	WB; WBHV; $W_1BHV$ $W_2B$ ; $WBH_1V$	
20	$C_{Dmin}$ against M	WB; WBHV; $W_1BHV$ $W_2B$ ; $WBH_1V$ ; $W_3BH_1VN_2$	
21	Trimmed L/D against $C_L$	WBHV $WBH_1V$ $W_3BH_1VN_2$	
22	Trimmed $(L/D)_{max}$ against M	WBHV $WBH_1V$ $W_3BH_1VN_2$	
23	Level flight $C_L$ against M for sea level and 35,000-foot altitude; wing loading of 100 pounds per square foot		
24	$\alpha$ , $C_D$ , and $C_m$ against $C_L$	$W_3BHVN_2$ $W_7BHVN_2$ $W_5BHVN_2$ $W_5BHVN_2$ with fences	Effects of leading-edge chord-extensions and fences; $h_t = 0.06b/2$
25	$\alpha$ , $C_D$ , and $C_m$ against $C_L$	$W_2BH_2V_1N_2$ $W_6BH_2V_1N_2$ $W_6BH_2V_1N_2$	Effects of leading-edge chord-extensions; $h_t = 0.56b/2$
26	$C_{mC_L}$ against M	WB; $W_2BH_1VN_2$ $W_2B$ ; $W_3BH_2V_1N_2$ $W_3BHVN_2$	
27	Neutral-point location against M	WBHV $WBH_1V$ $W_3BH_1VN_2$	
28	$C_{m\alpha}$ and $C_{m1t}$ against M	WBHV $WBH_1V$ $W_3BH_1VN_2$	
29	$\epsilon$ against $\alpha$	WBHV $W_3BH_1VN_2$	
30	$\partial\epsilon/\partial\alpha$ against M	WBHV $W_3BH_1VN_2$	
31	$\alpha$ , $C_D$ , and $C_m$ against $C_L$	$W_5BVN_2$ $W_5BHVN_2$ $W_5BH_1VN_2$ $W_5BH_2V_1N_2$	Effect of horizontal-tail location on model with leading-edge chord-extensions
32	$\alpha$ and $C_m$ against $C_L$	$W_7B_4N_2V_1$ $W_7B_4N_2V_1$ with fences	Effect of fences on model with shortened fuselage



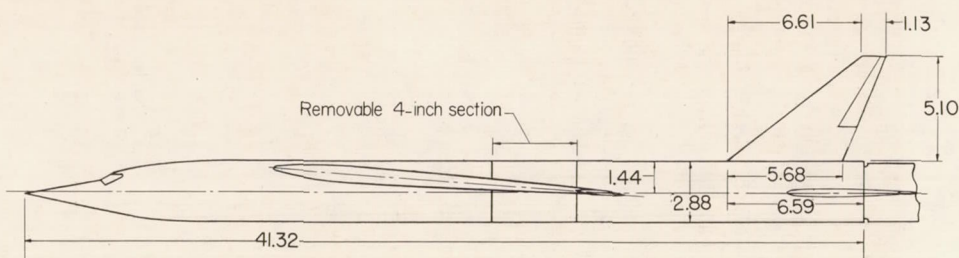
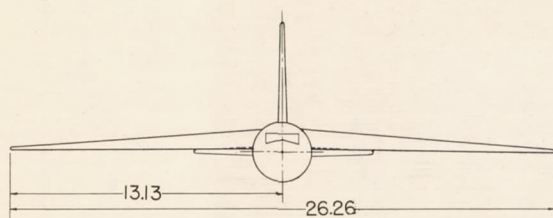
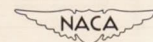
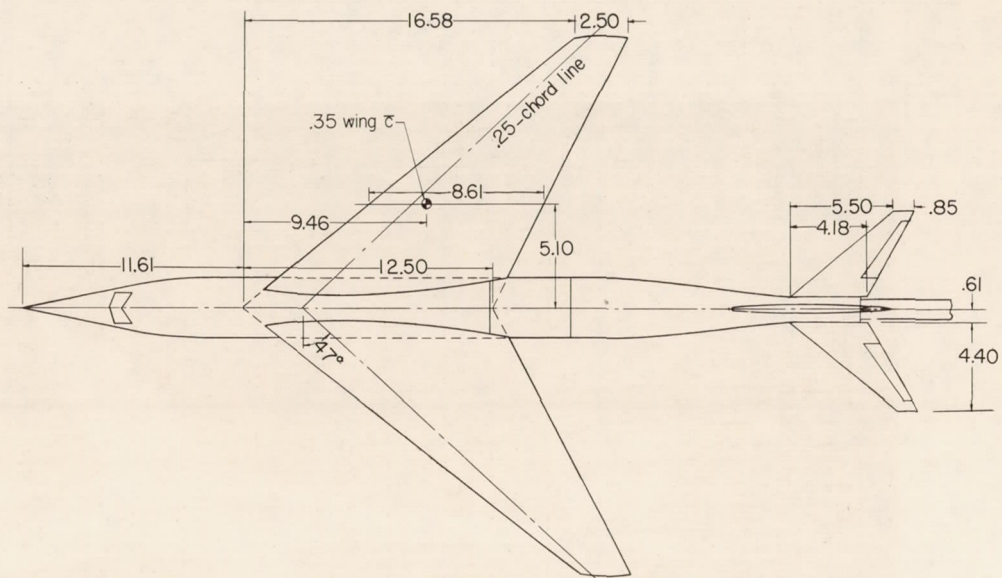
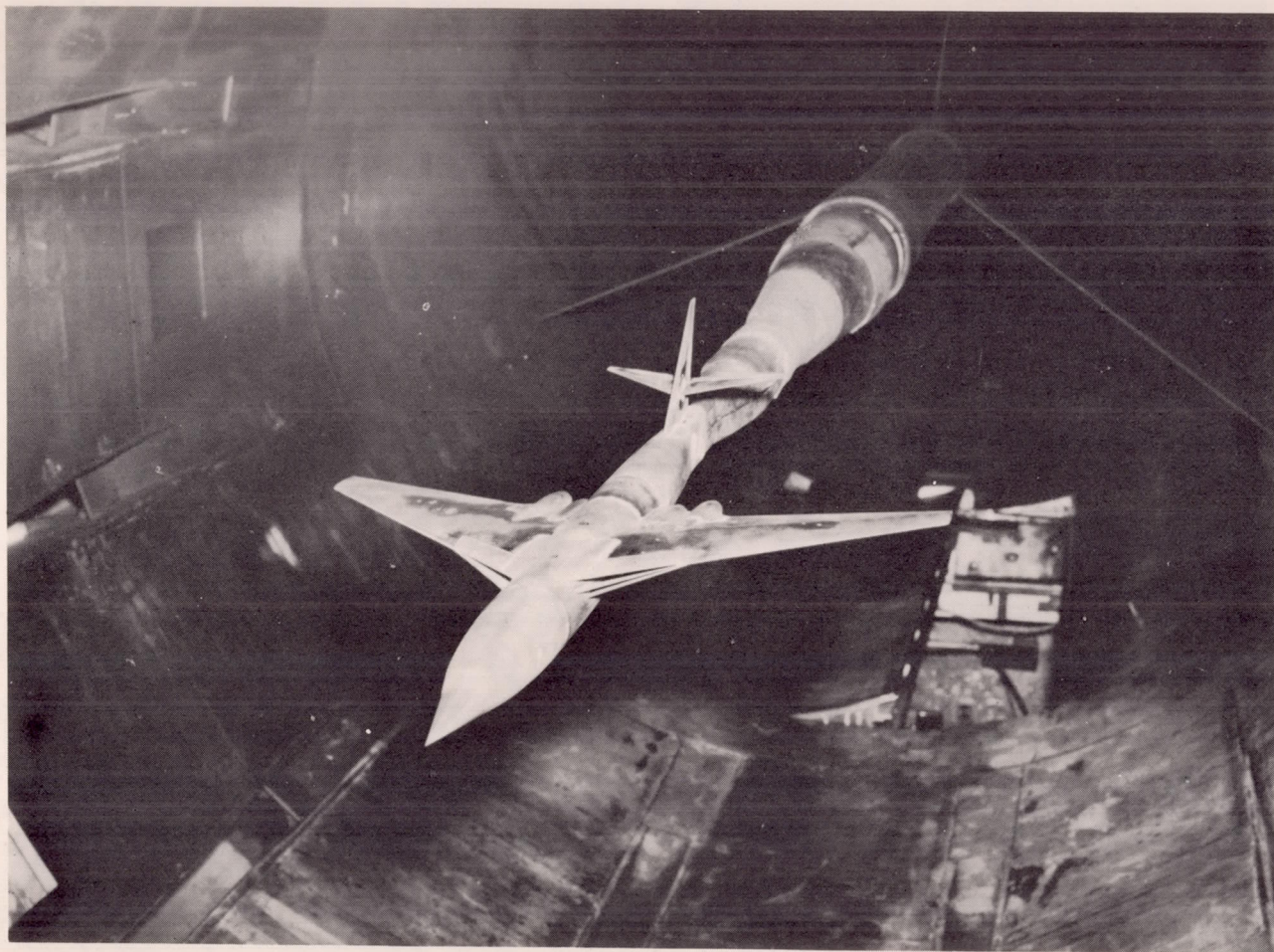


Figure 1.- Details of test model. All dimensions in inches.

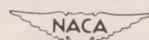
CONFIDENTIAL

CONFIDENTIAL

NACA RM L53F05



CONFIDENTIAL



L-73935

Figure 2.- Test model installed in the Langley 8-foot transonic tunnel.

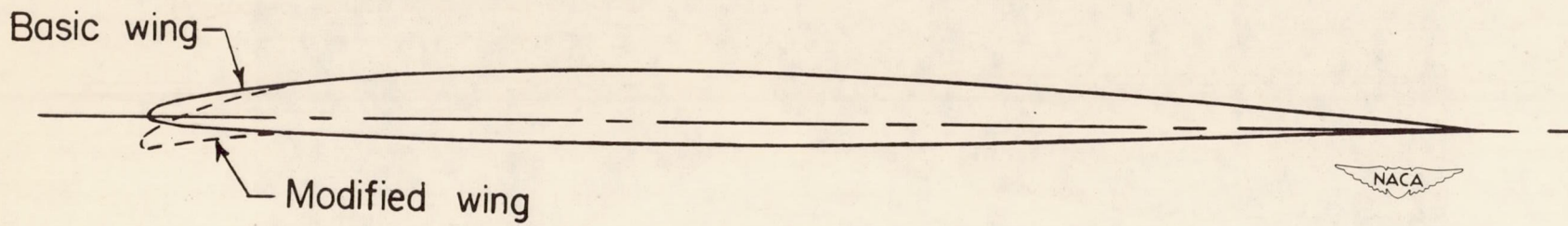
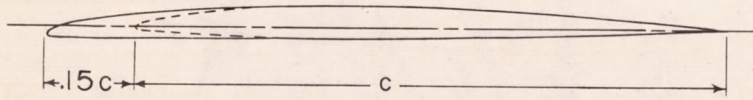
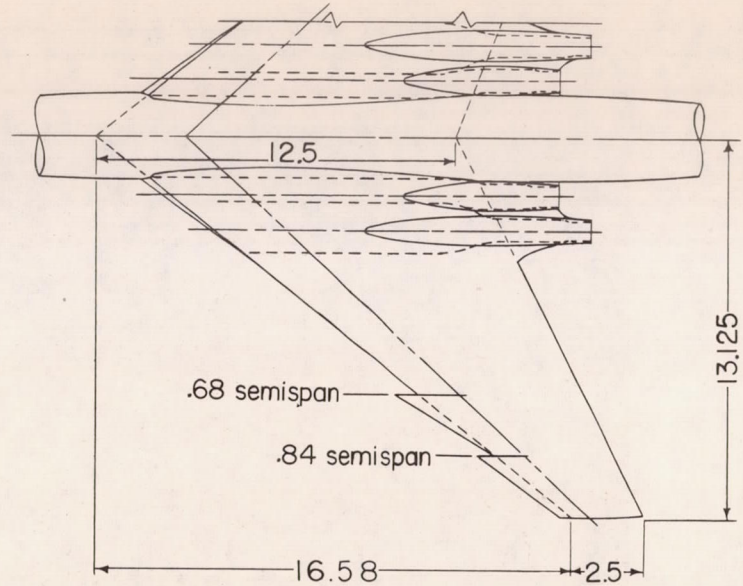
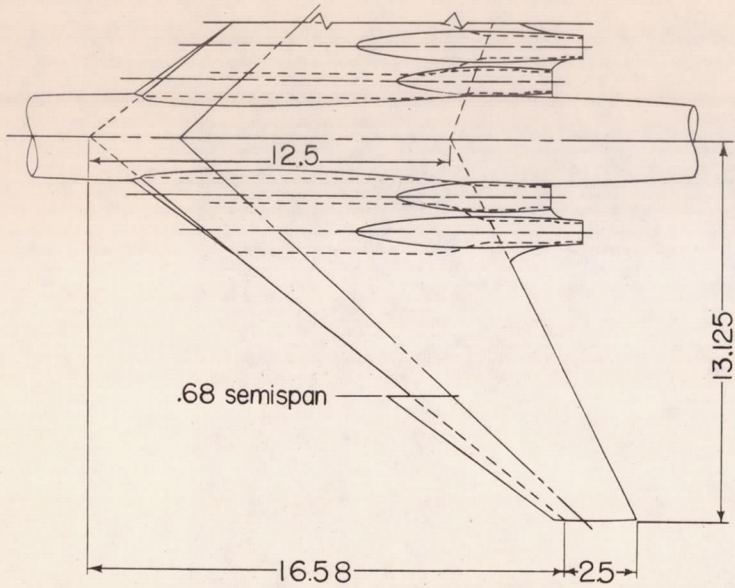
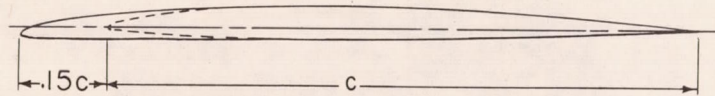


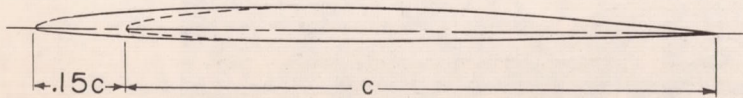
Figure 3.- Comparison of the basic and modified wing sections outboard of the 80-percent-semispan station.



(a) Drooped leading-edge chord-extension.

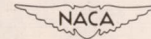


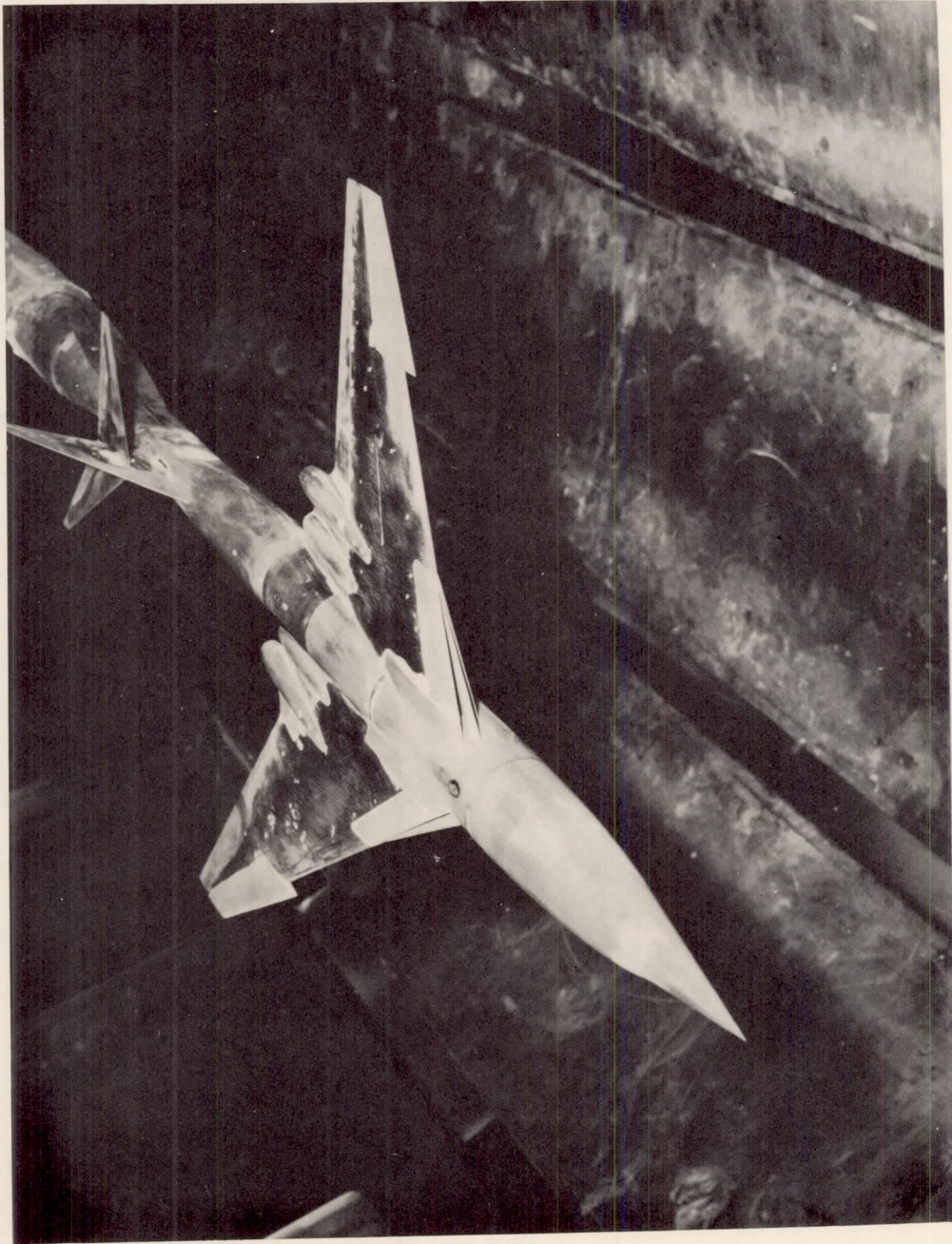
(c) Saw-toothed leading-edge chord-extension.

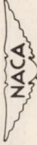


(b) Undrooped leading-edge chord-extension.

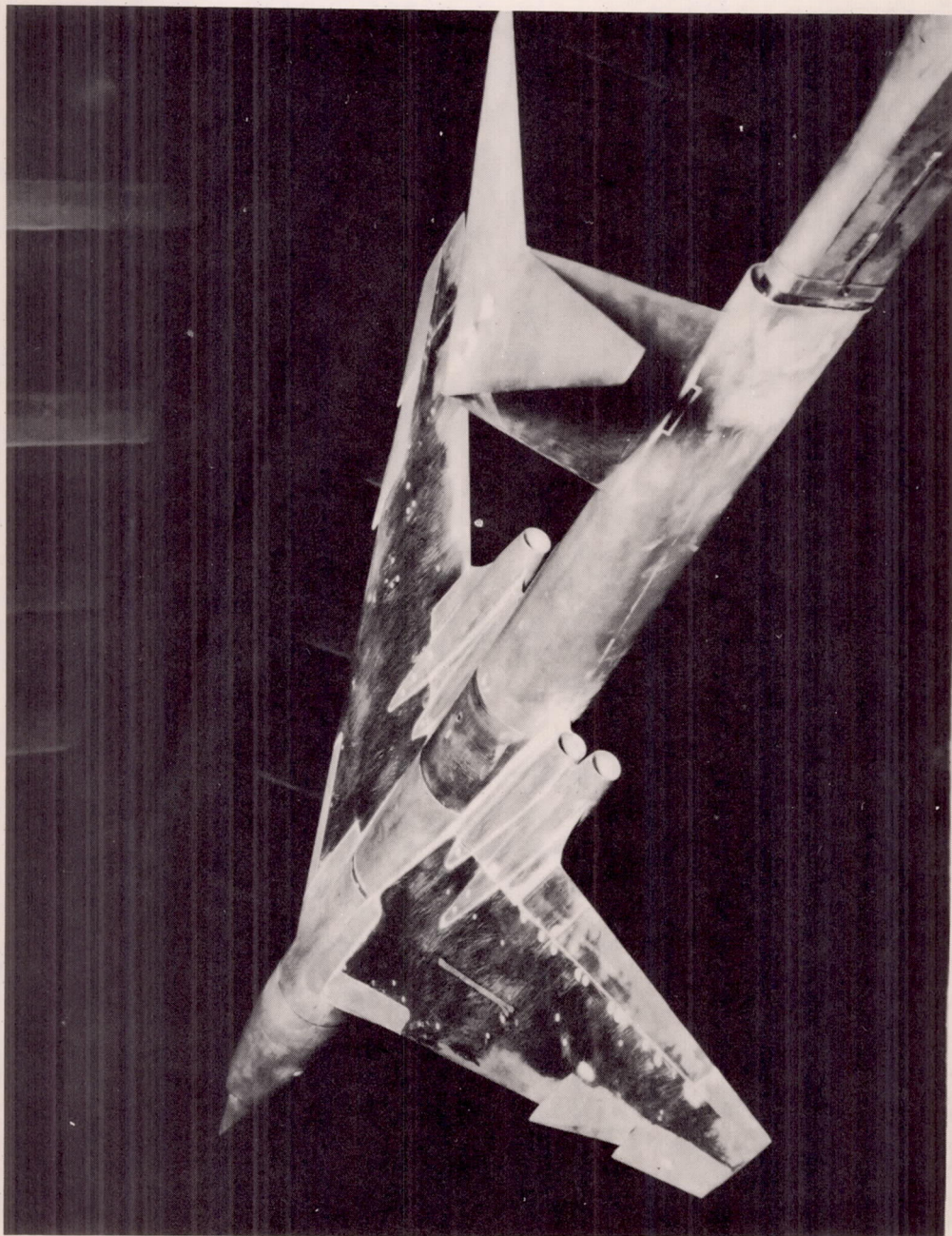
Figure 4.- Comparisons of the various leading-edge chord-extensions investigated. All dimensions in inches except as noted.





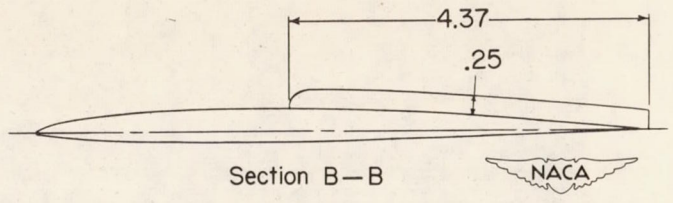
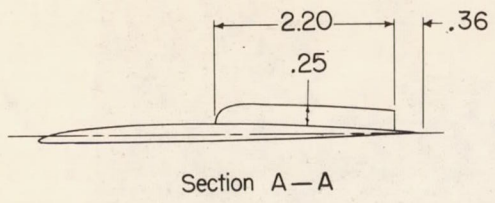
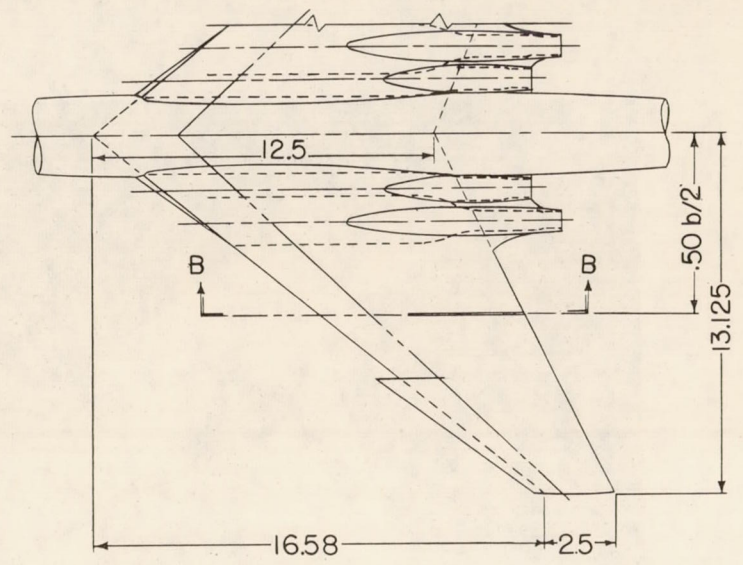
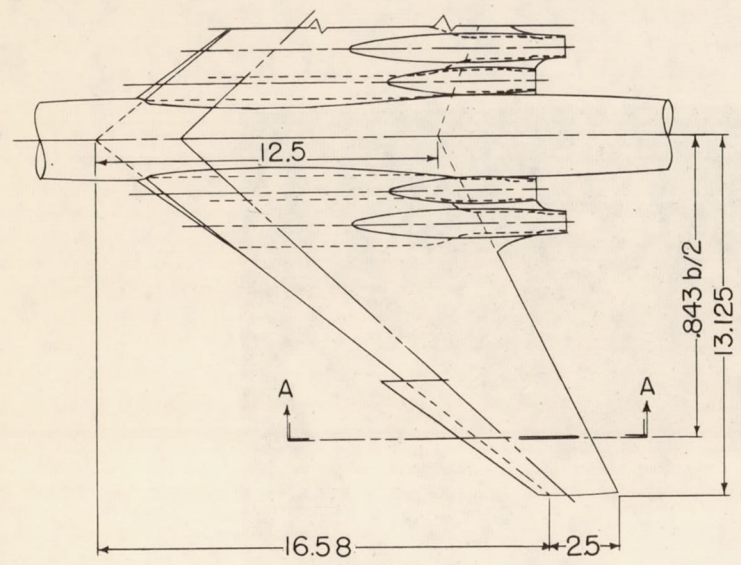
 Figure 5.- Model with drooped leading-edge chord-extension. L-74307





NACA  
I-74436

Figure 6.- Model with "saw-toothed" leading-edge chord-extension.



(a) Fences with drooped leading-edge chord-extensions.

(b) Fences with undrooped leading-edge chord-extensions.

Figure 7.- Details of wing fences investigated. All dimensions in inches except as noted.

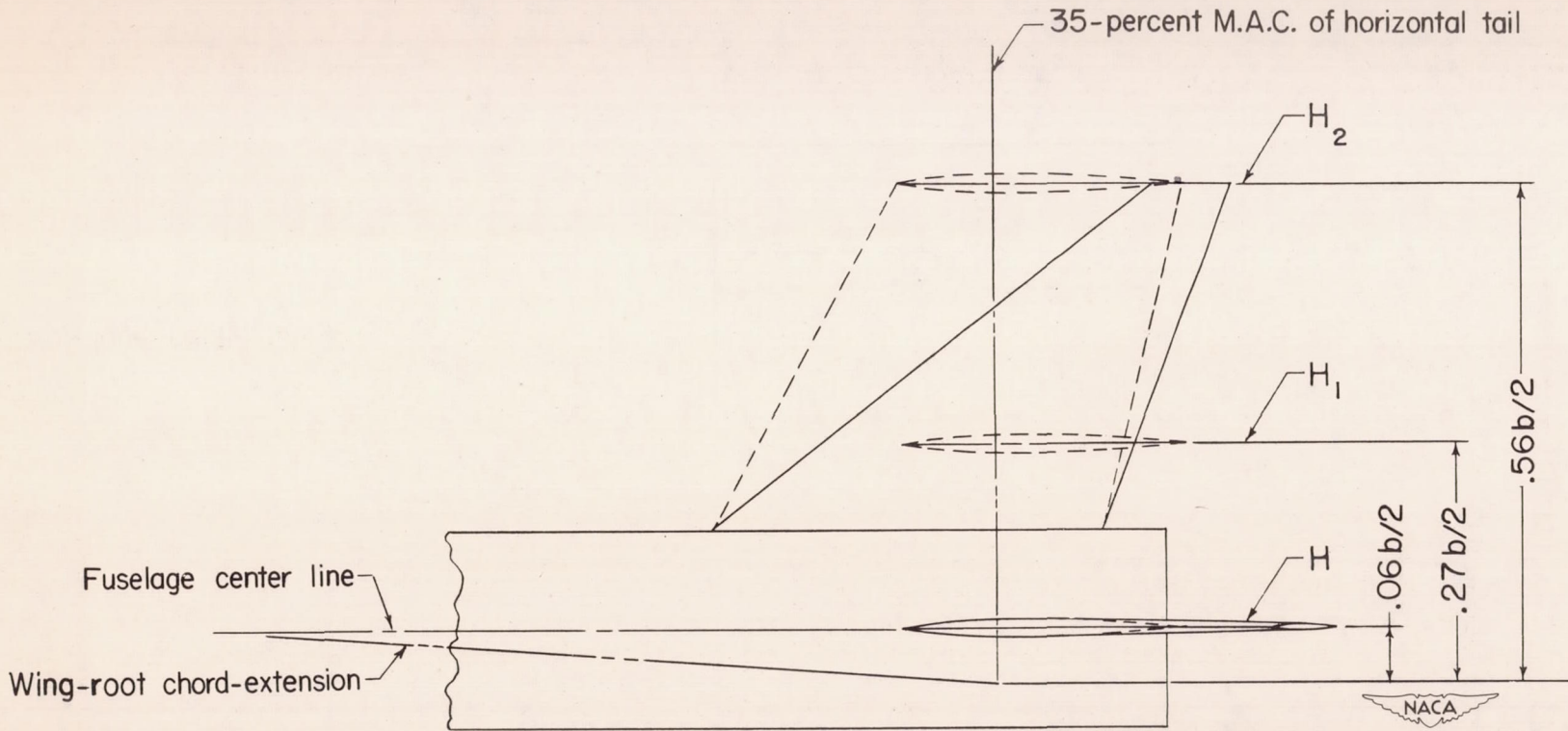


Figure 8.- Vertical locations of horizontal stabilizer relative to wing-root chord plane extended.

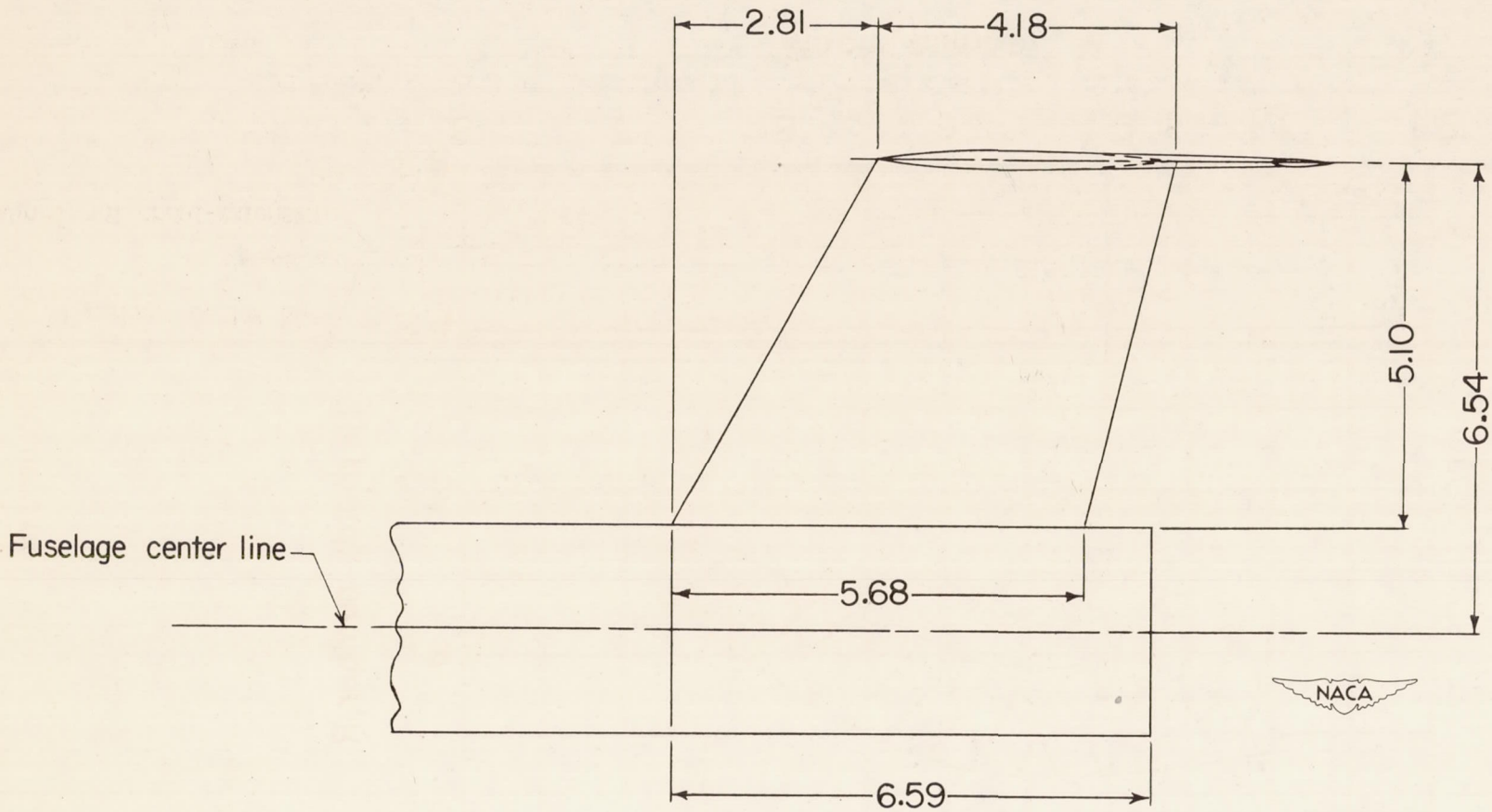


Figure 9.- Details of modified vertical tail V<sub>1</sub>. All dimensions in inches.

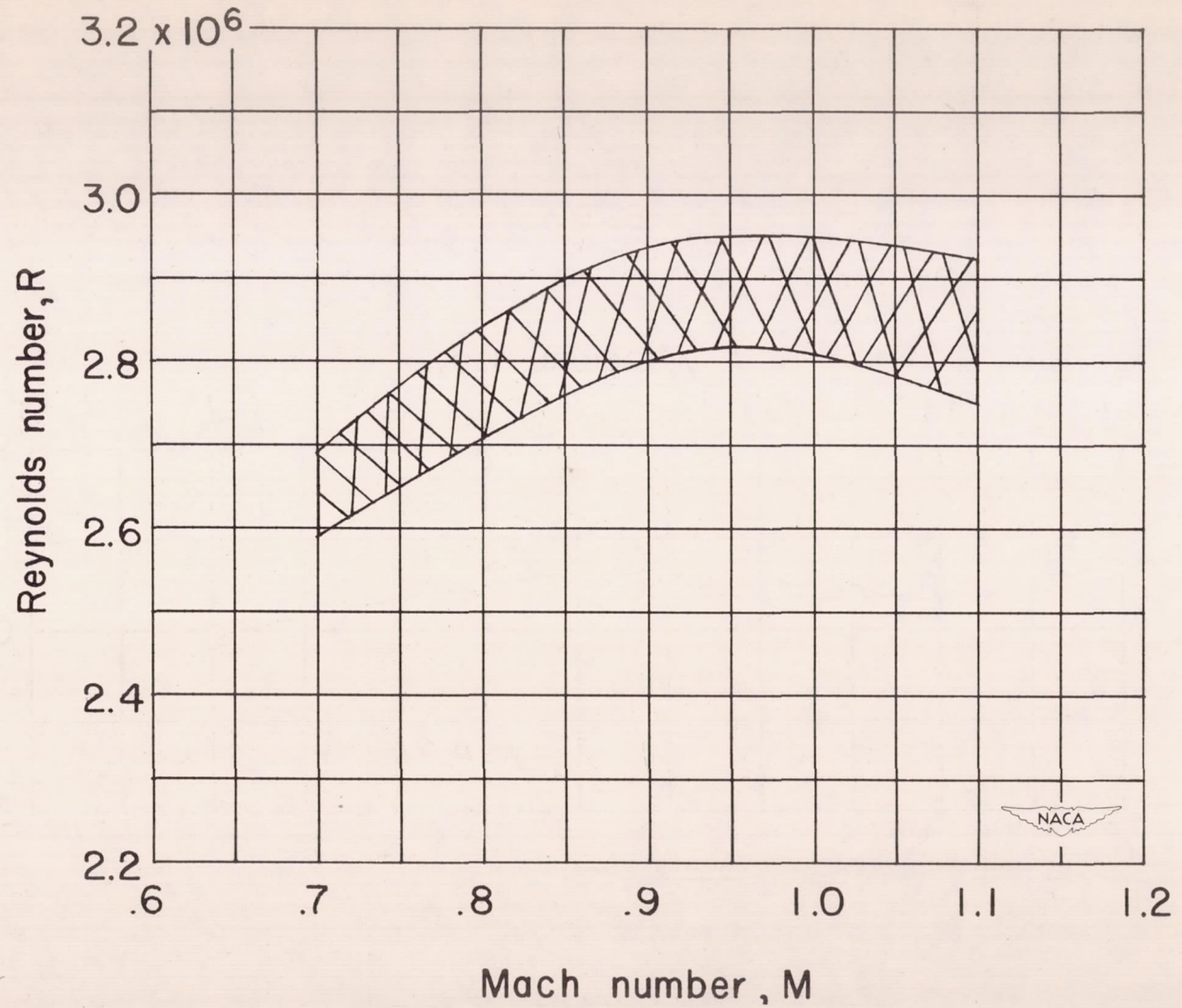
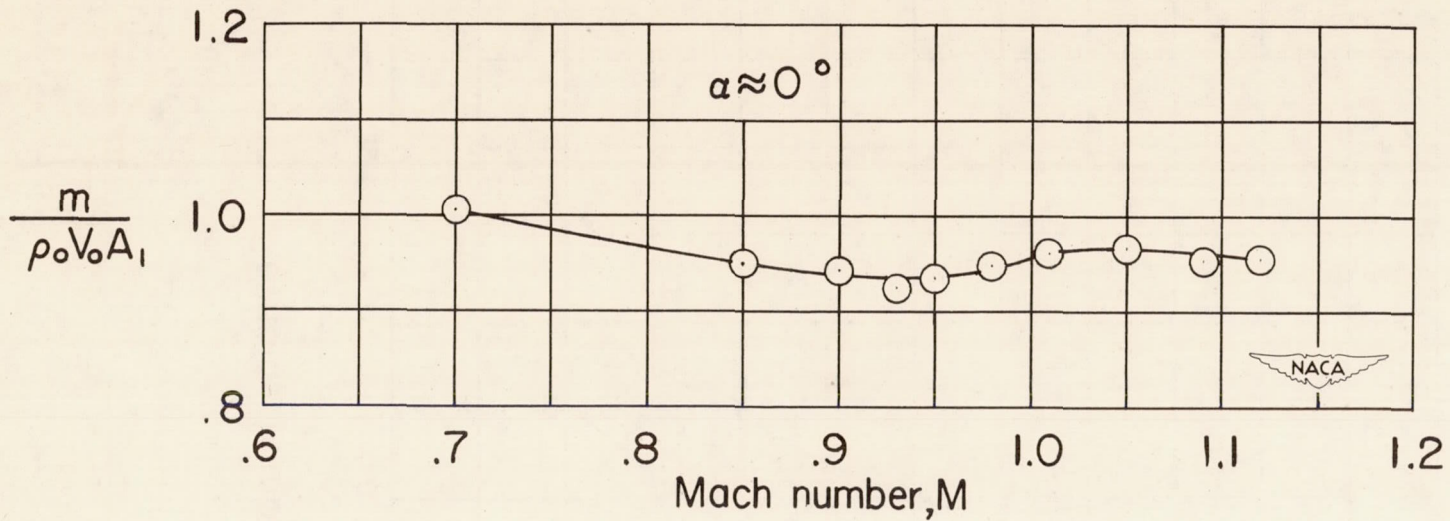


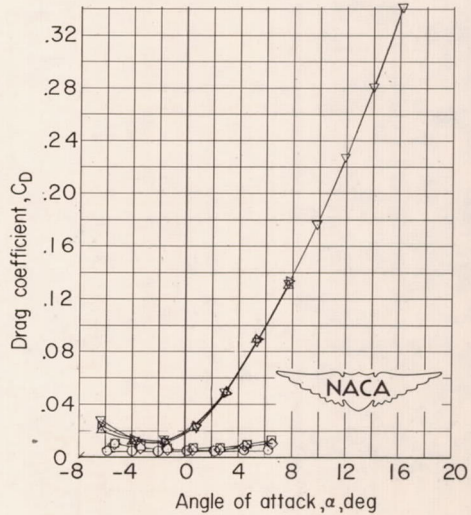
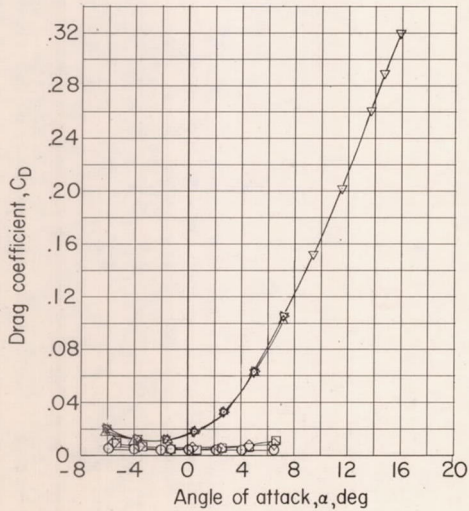
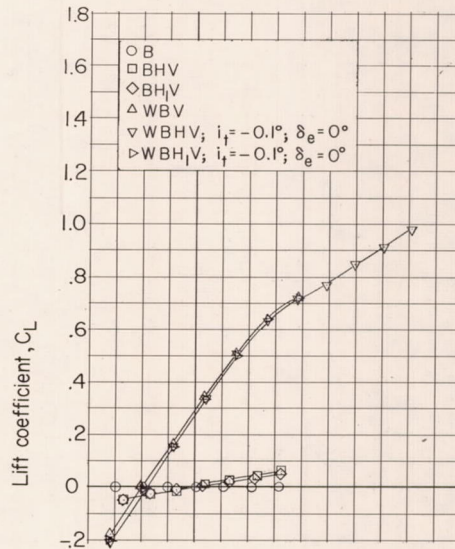
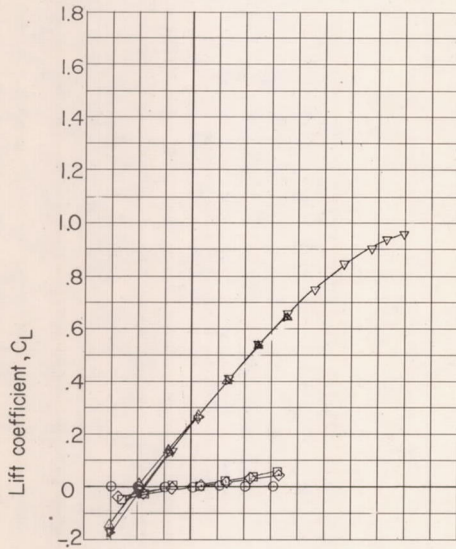
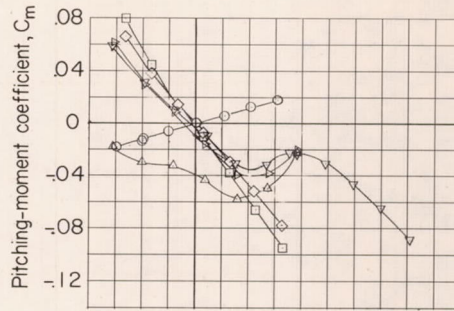
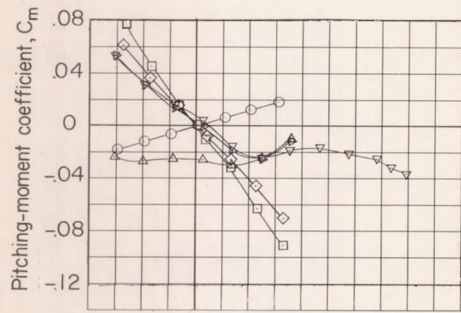
Figure 10.- Variation with Mach number of the test Reynolds number range based on the wing mean aerodynamic chord.

CONFIDENTIAL



CONFIDENTIAL

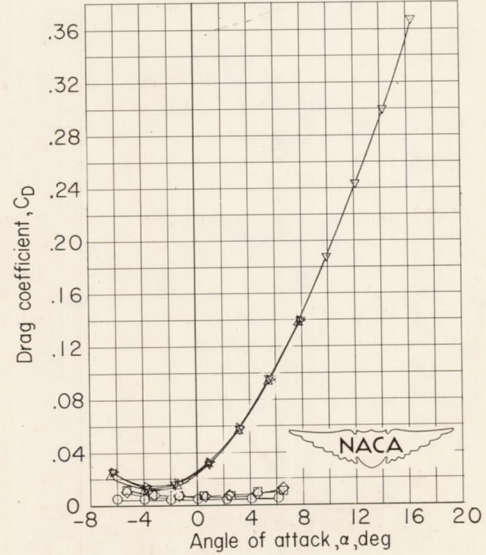
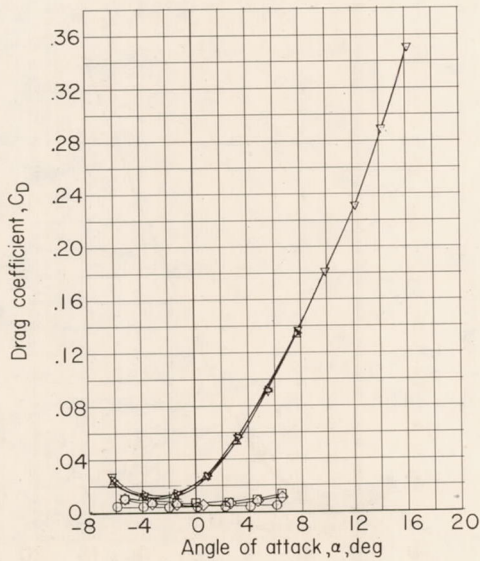
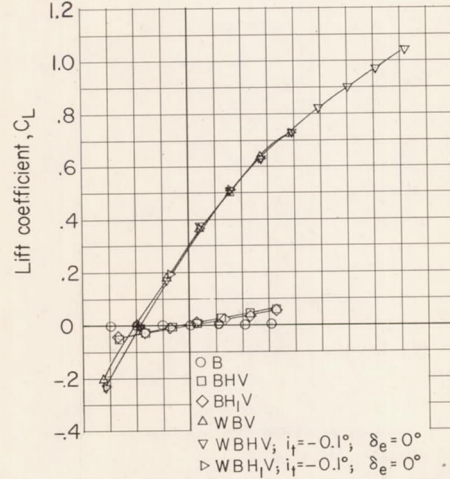
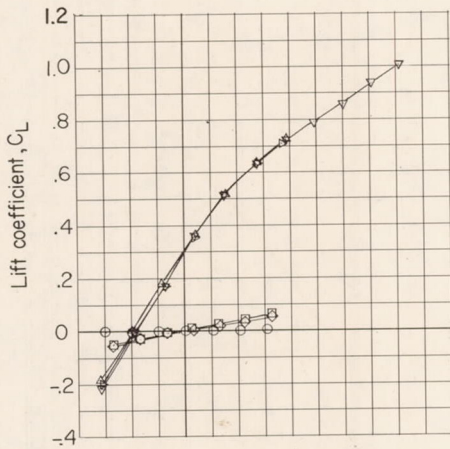
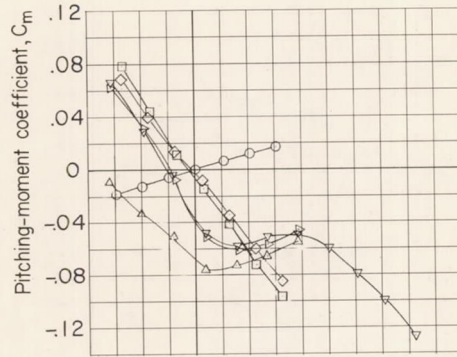
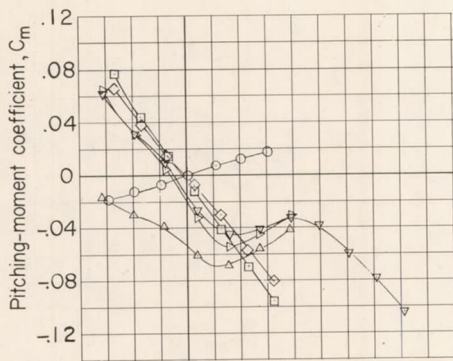
Figure 11.- Variation of mass-flow ratio with Mach number.  
Configuration  $W_3BH_1VN_2$ .



(a)  $M = 0.70$ .

(b)  $M = 0.91$ .

Figure 12.- Aerodynamic characteristics of various combinations of fuselage, wing, and tail.

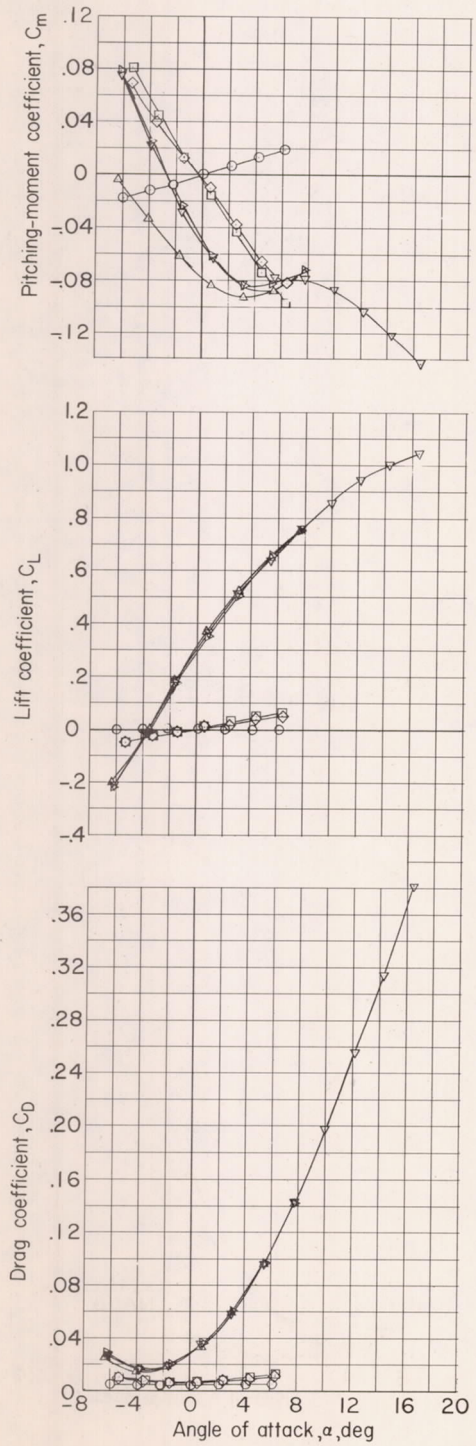


(c)  $M = 0.93$ .

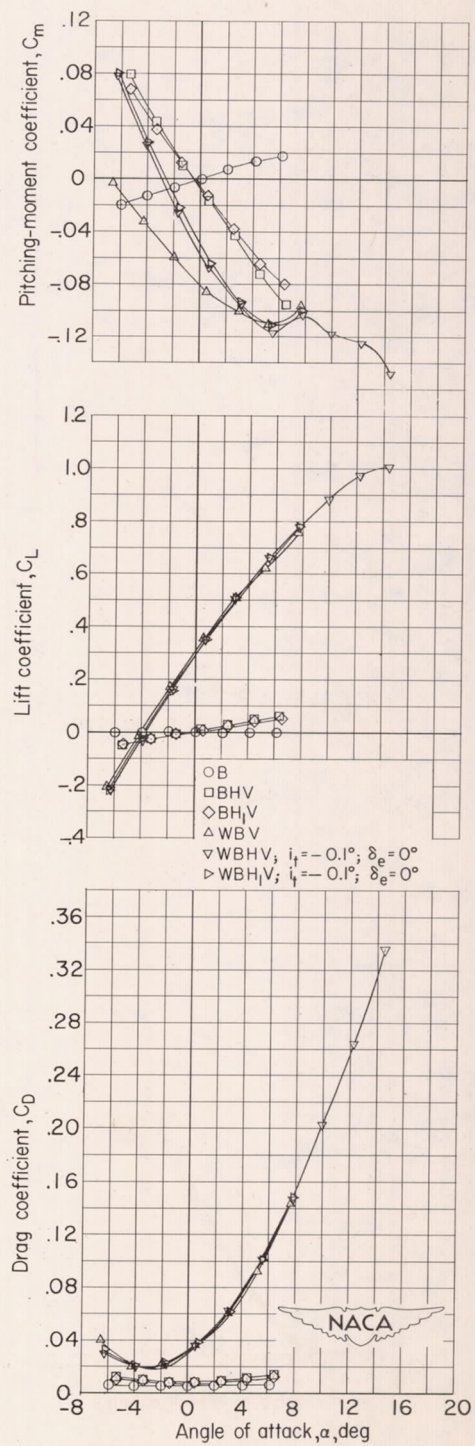
(d)  $M = 0.96$ .

Figure 12.- Continued.



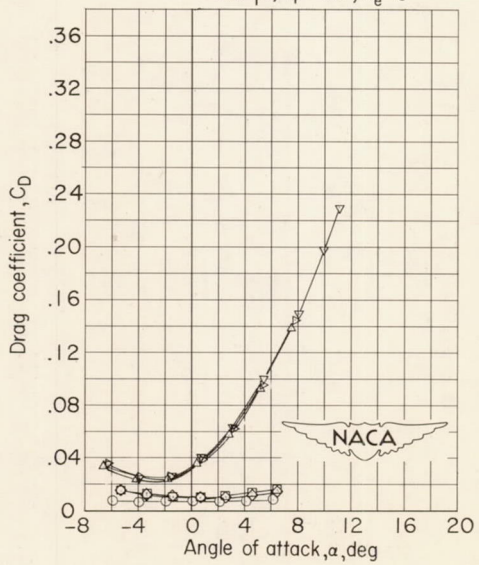
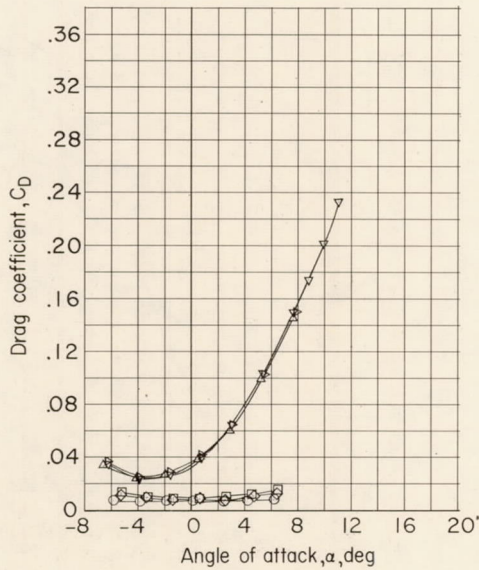
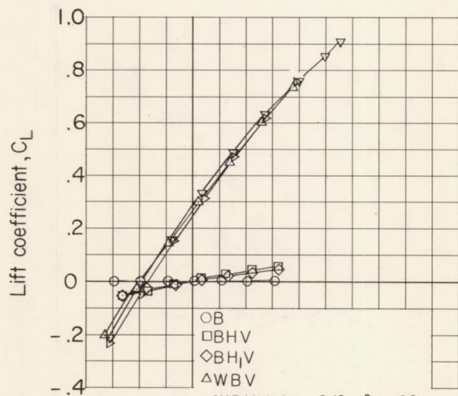
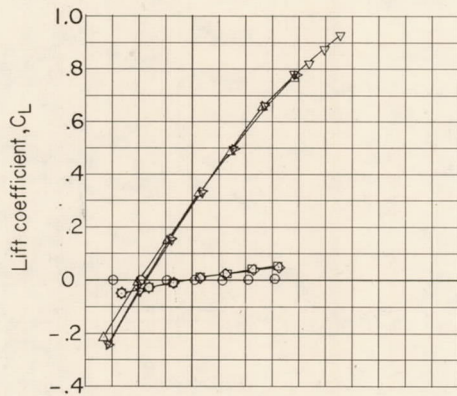
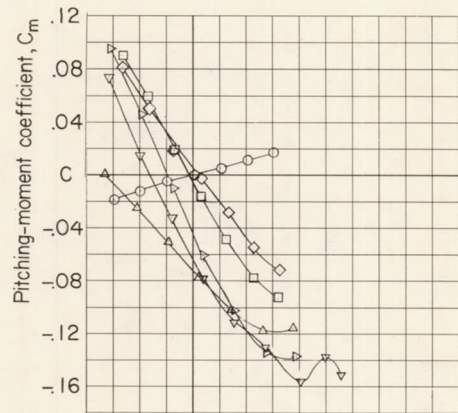
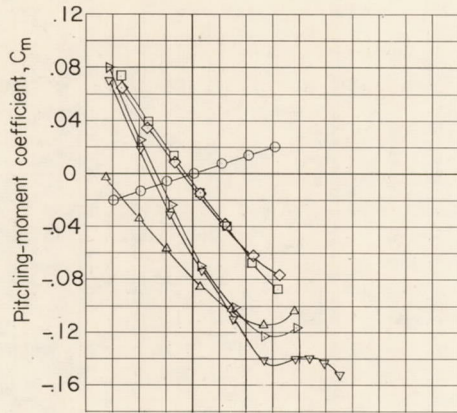


(e)  $M = 0.98$ .



(f)  $M = 1.00$ .

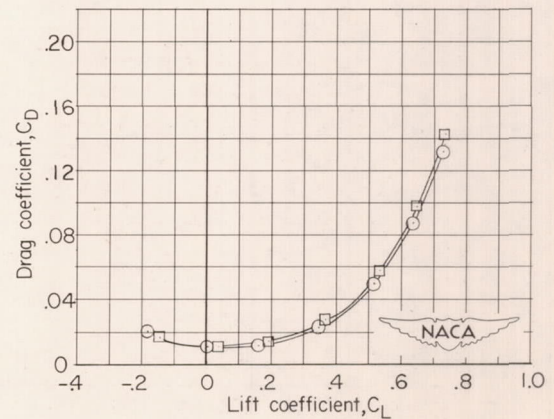
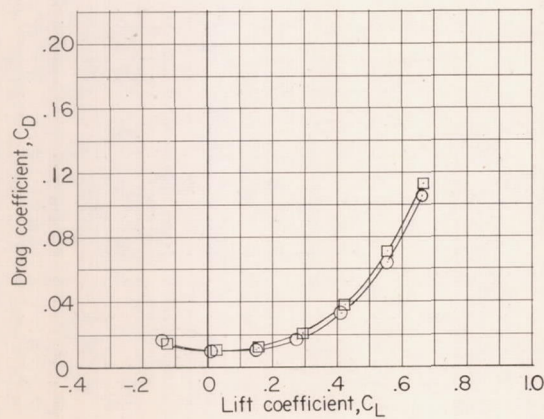
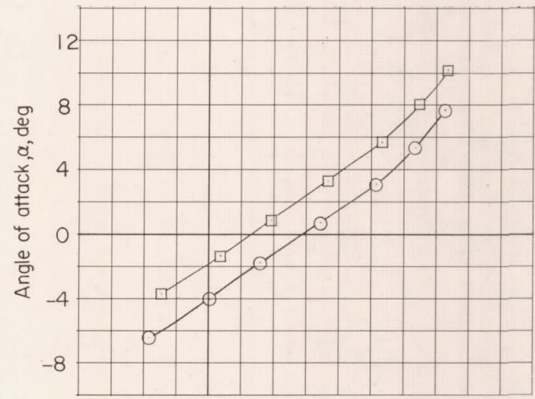
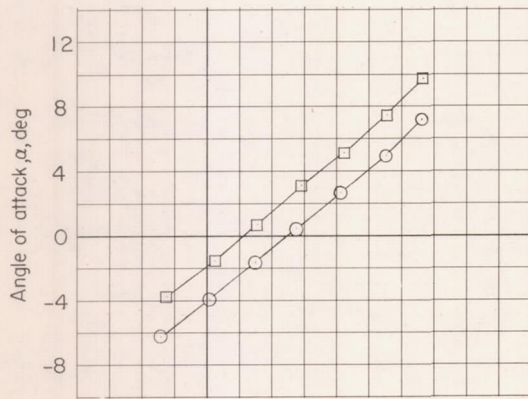
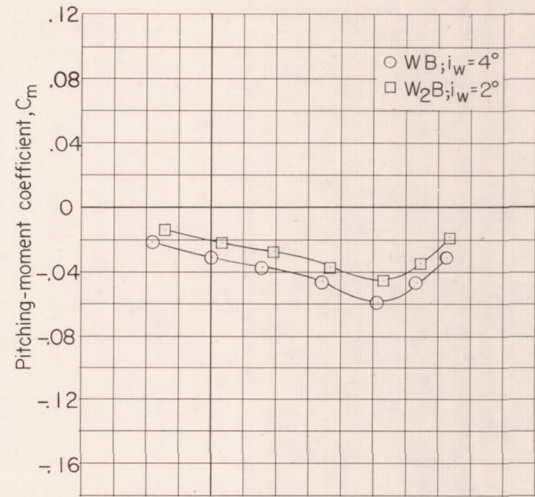
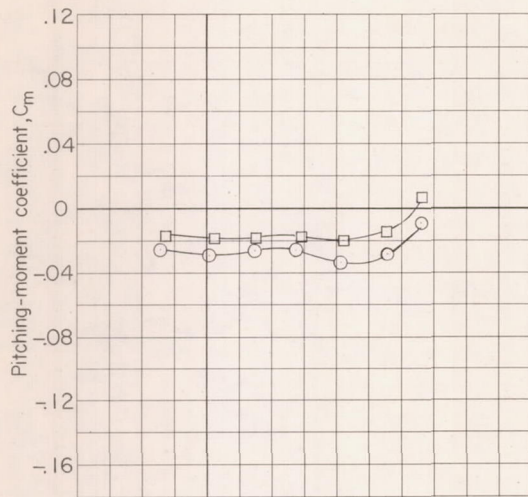
Figure 12.- Continued.



(g)  $M = 1.04$ .

(h)  $M = 1.11$ .

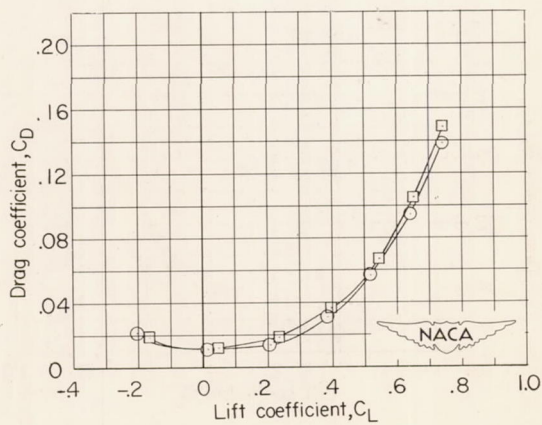
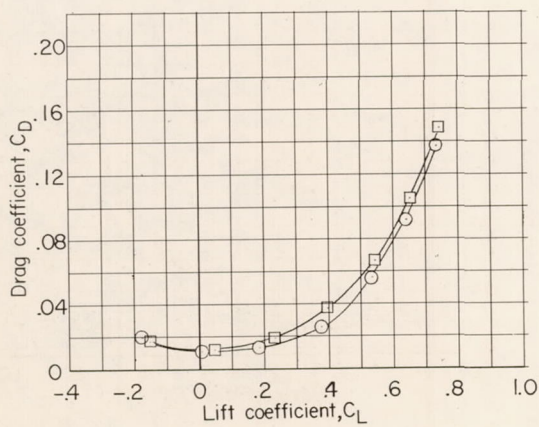
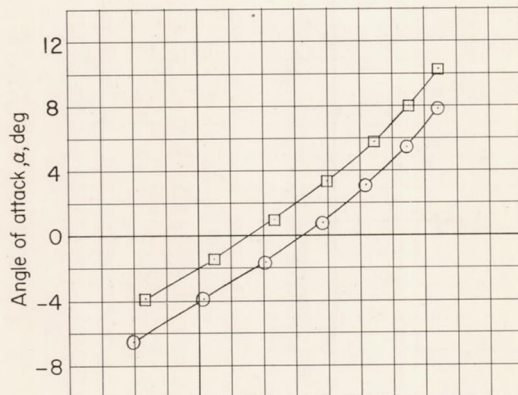
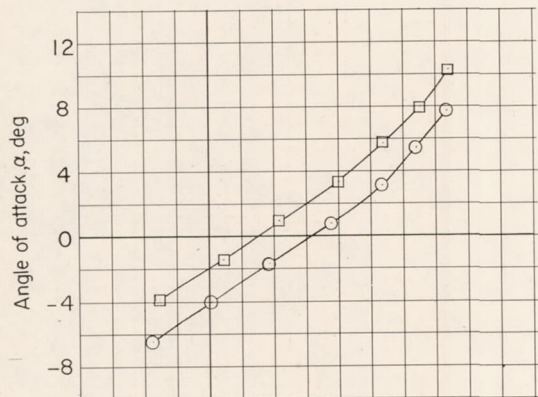
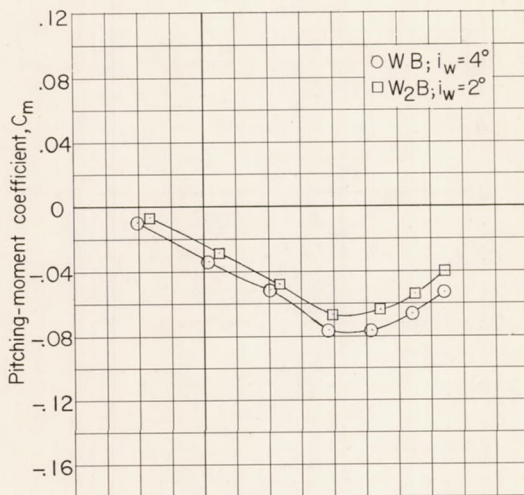
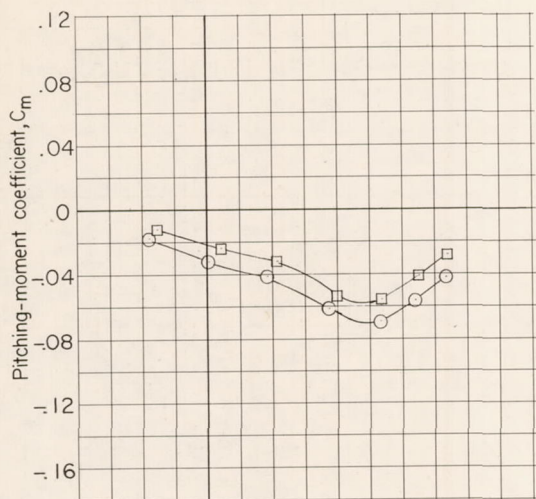
Figure 12.- Concluded.



(a)  $M = 0.70$ .

(b)  $M = 0.90$ .

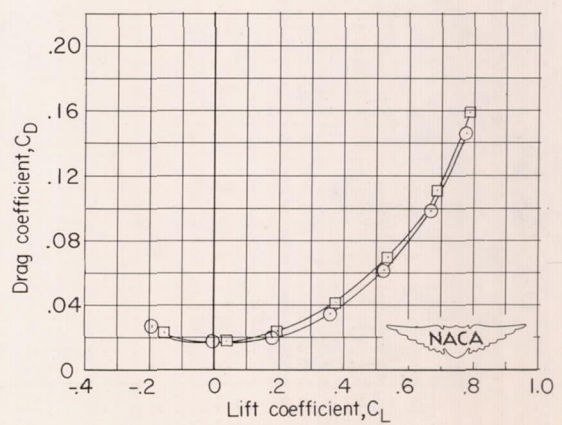
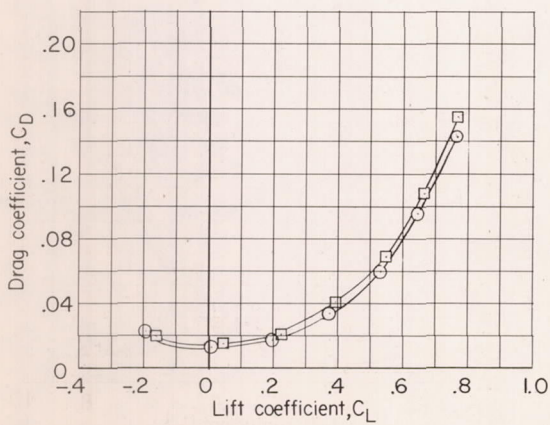
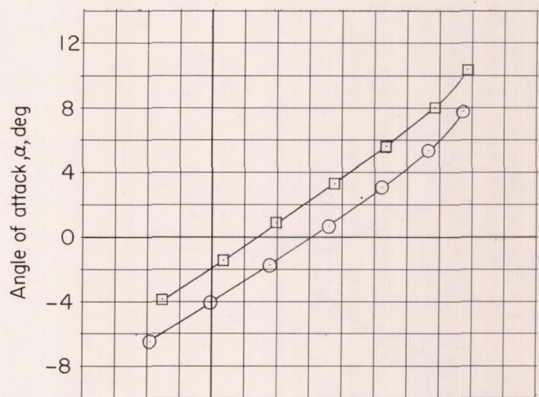
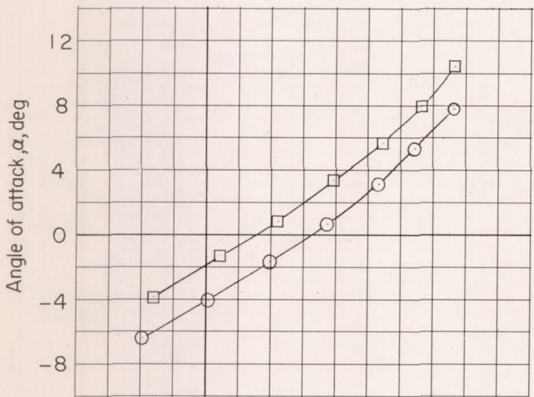
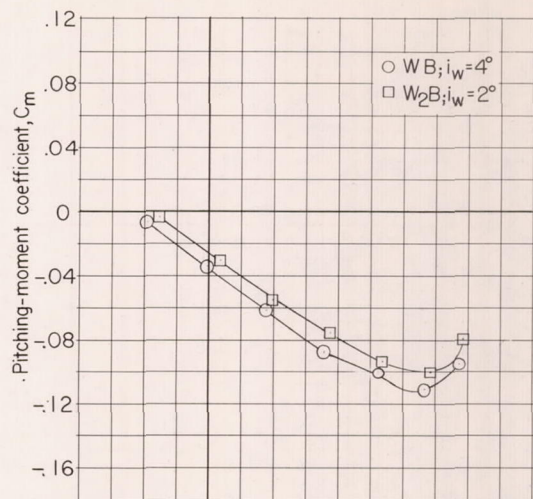
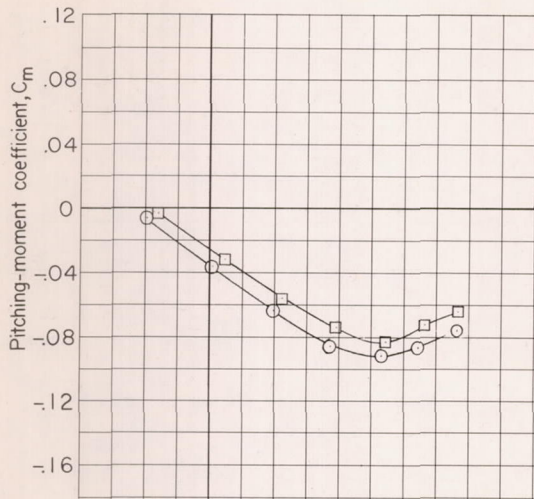
Figure 13.- Effects of wing incidence on the aerodynamic characteristics of the wing-fuselage combination.



(c)  $M = 0.93$ .

(d)  $M = 0.95$ .

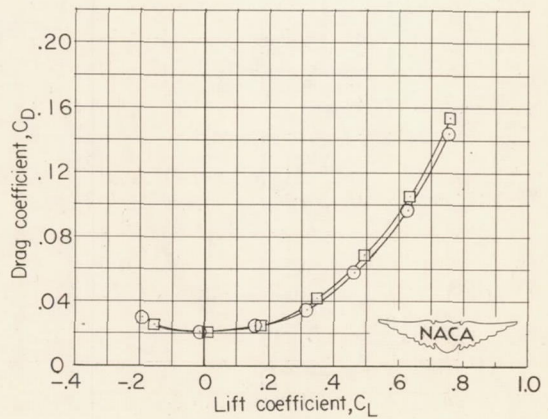
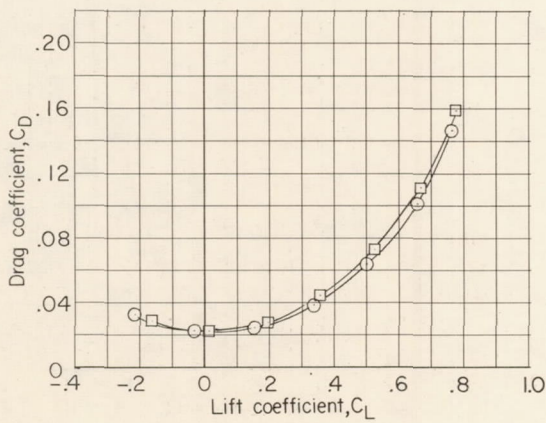
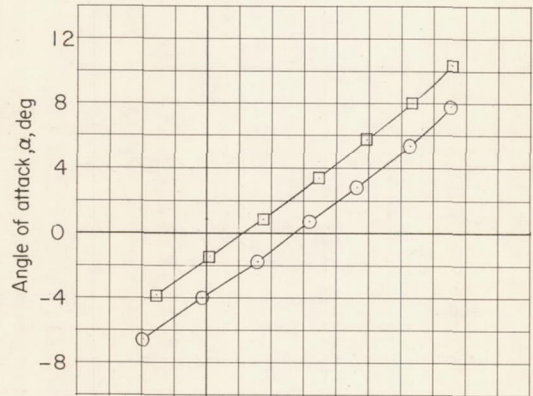
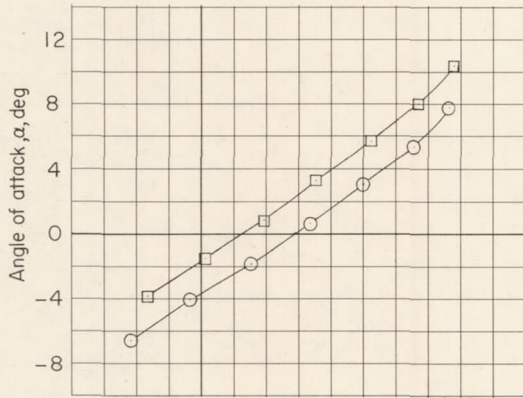
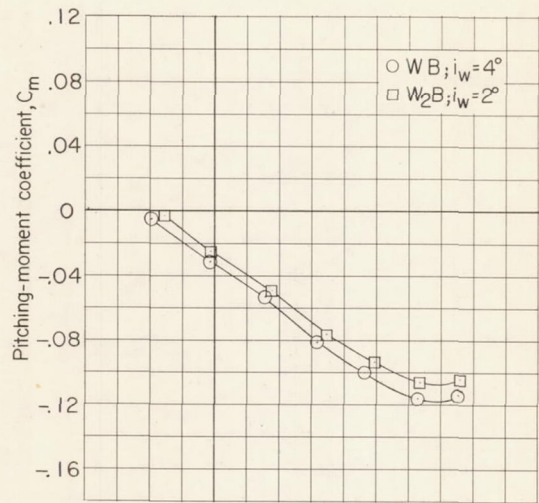
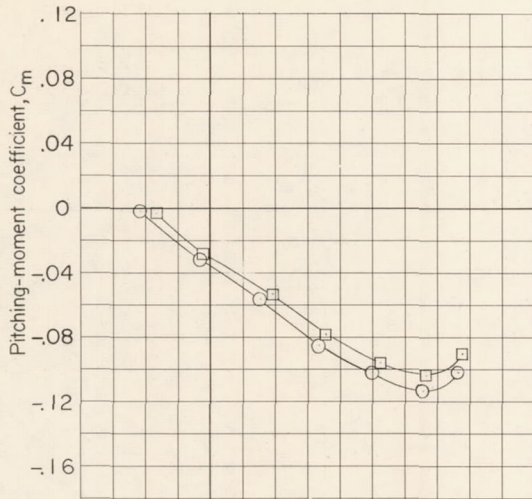
Figure 13.- Continued.



(e)  $M = 0.98$ .

(f)  $M = 1.00$ .

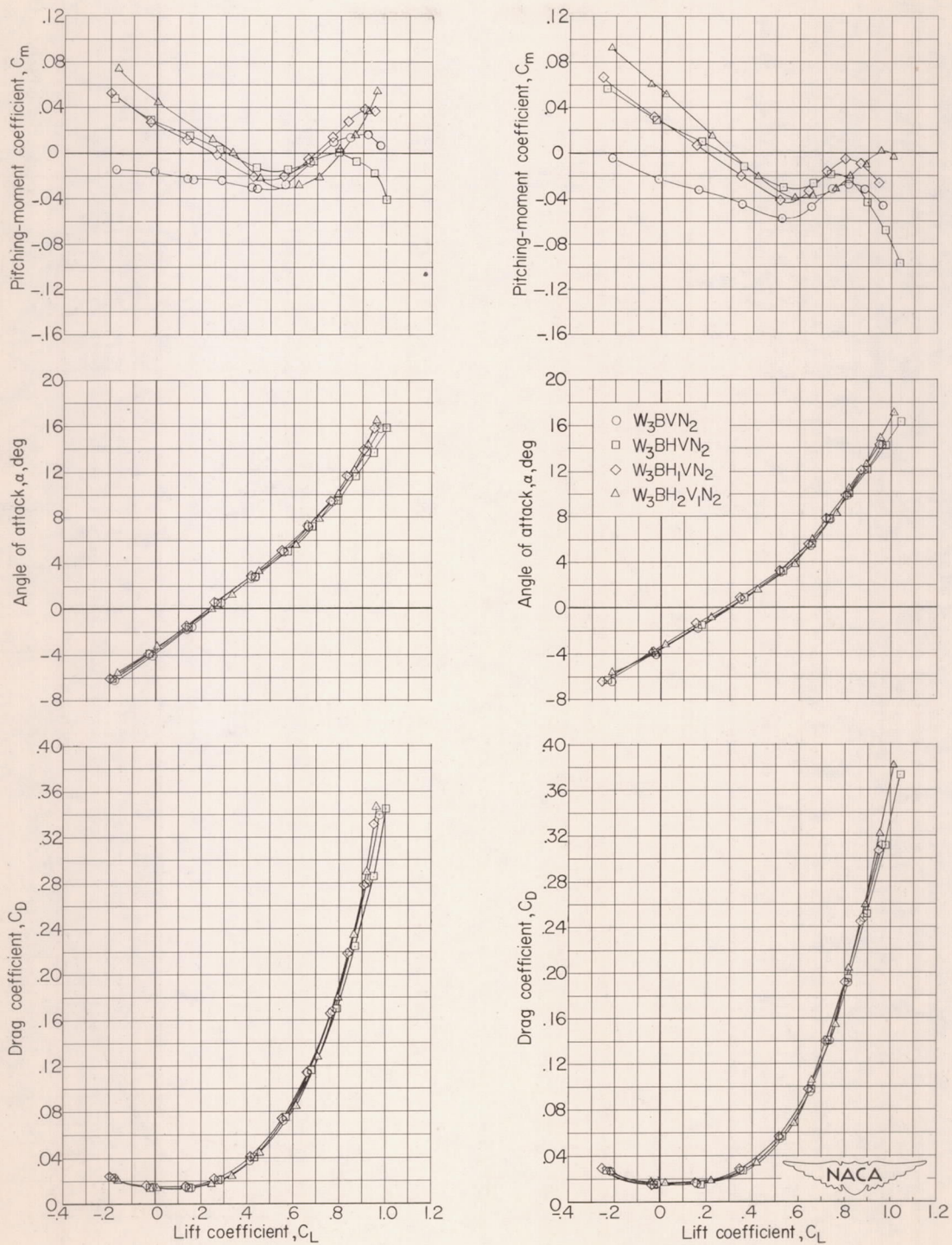
Figure 13.- Continued.



(g)  $M = 1.05$ .

(h)  $M = 1.11$ .

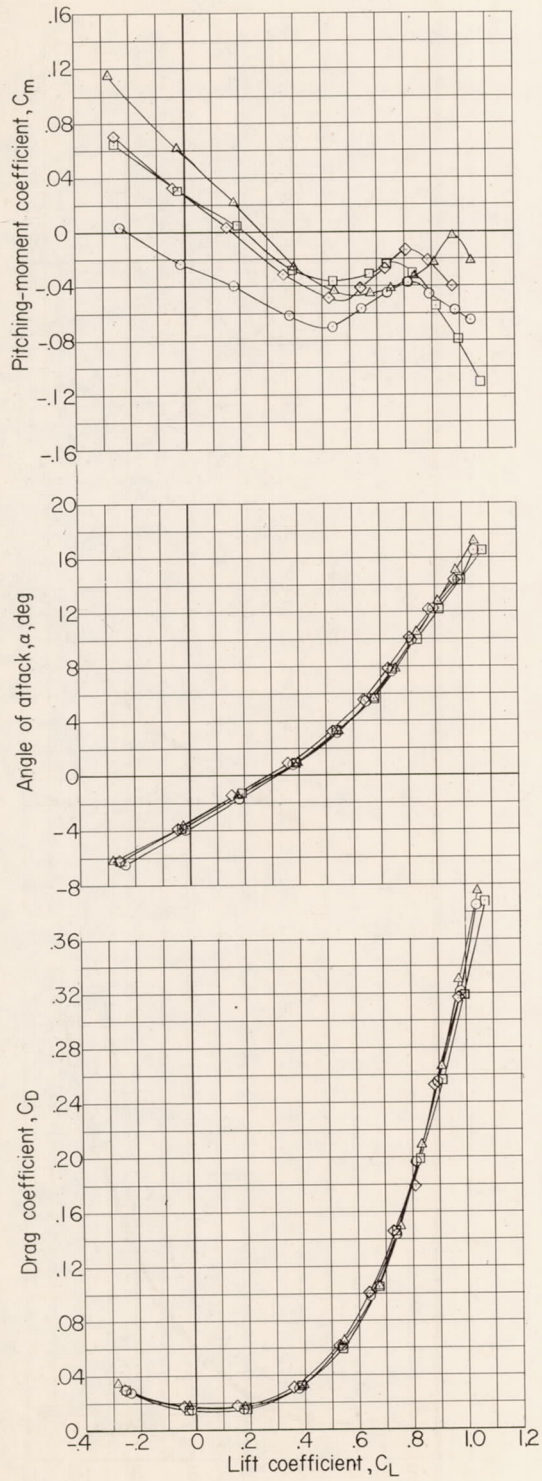
Figure 13.- Concluded.



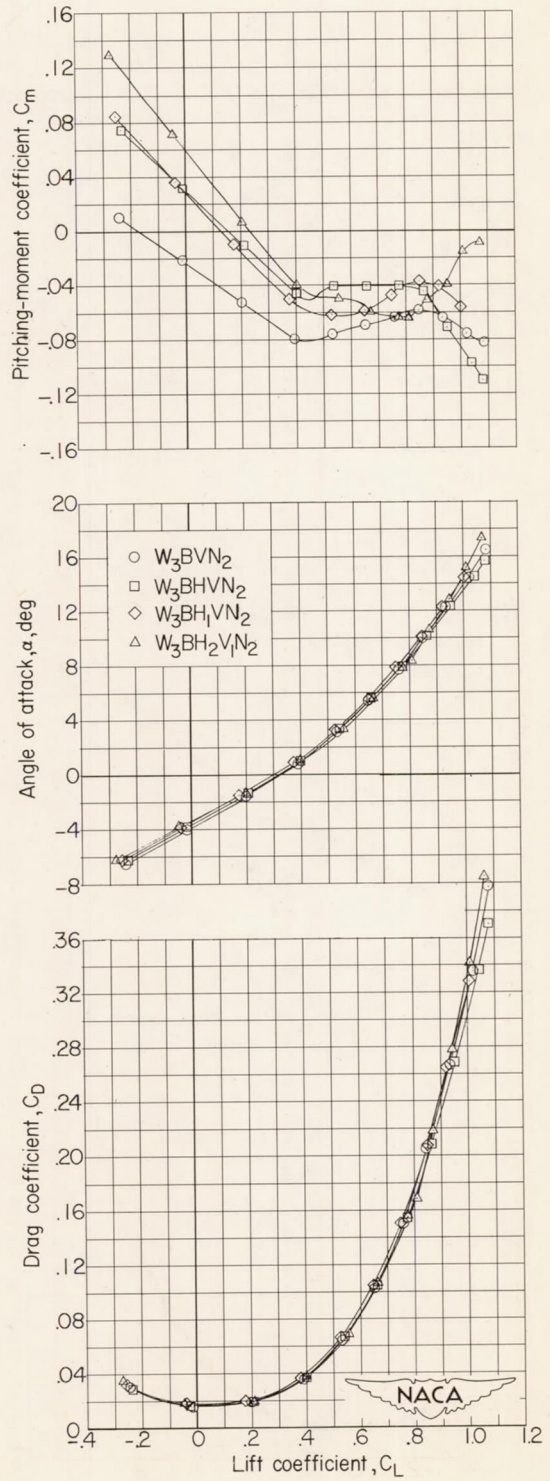
(a)  $M = 0.70$ .

(b)  $M = 0.90$ .

Figure 14.- Effects of vertical location of horizontal tail on the aerodynamic characteristics of the model with buried nacelles.



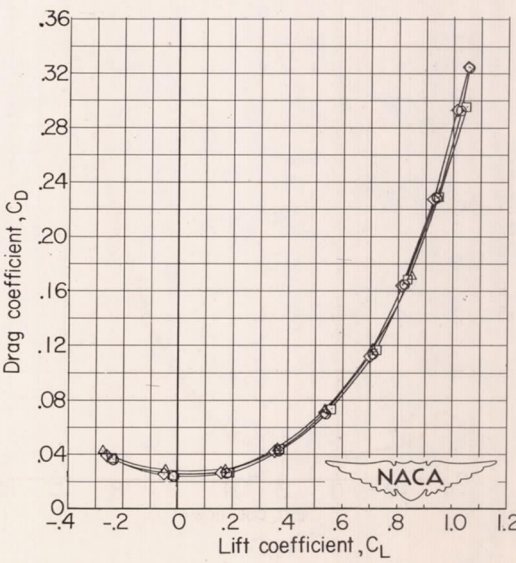
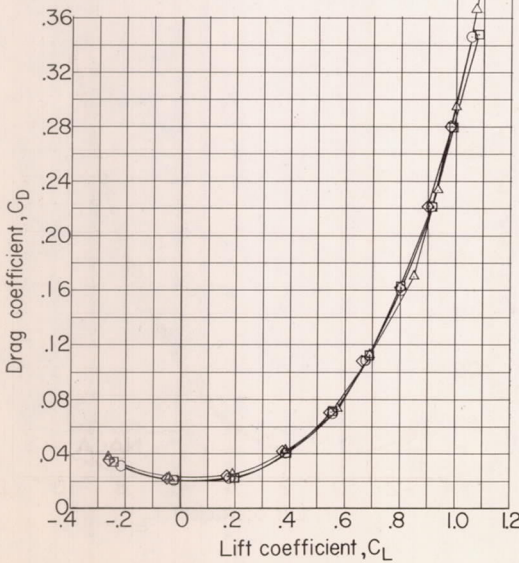
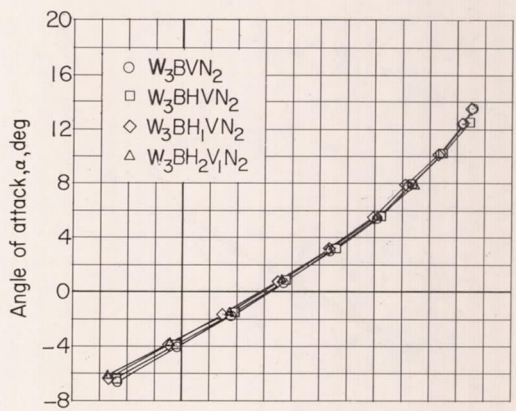
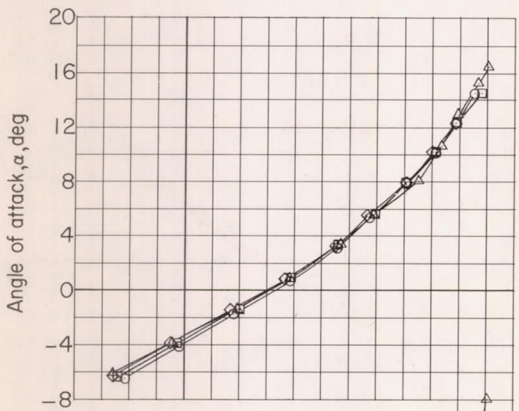
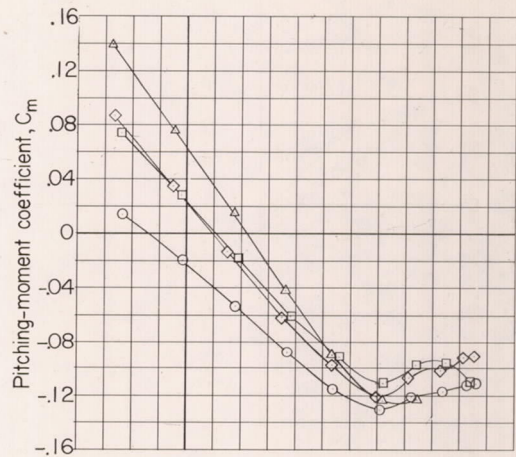
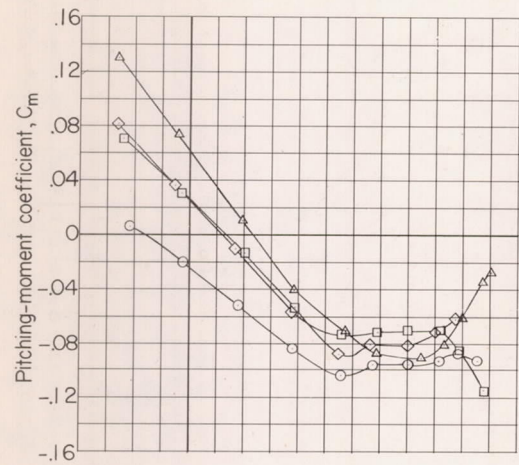
(c)  $M = 0.93$ .



(d)  $M = 0.95$ .

Figure 14.- Continued.

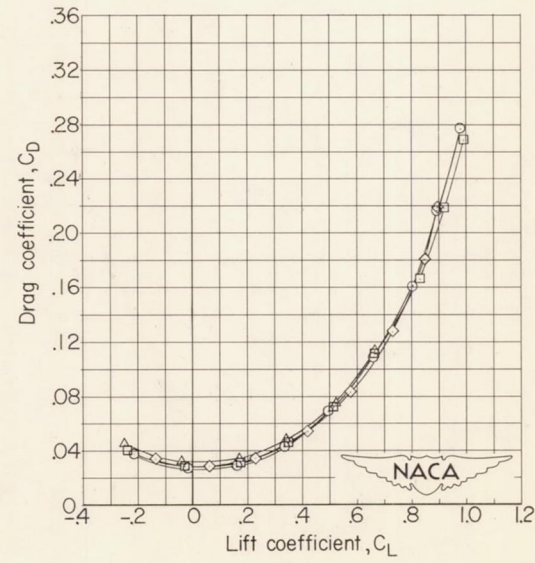
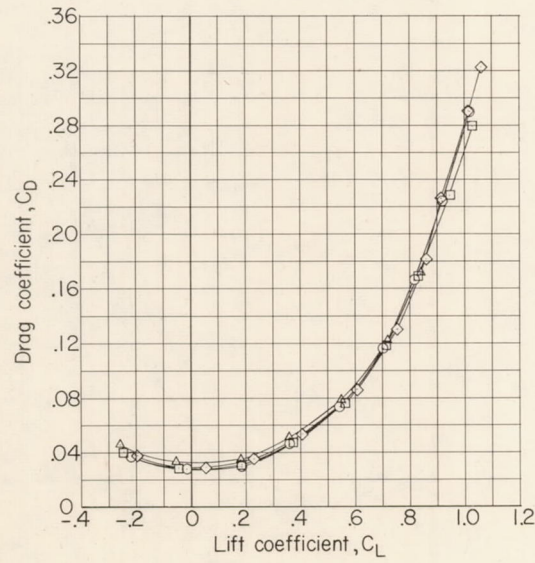
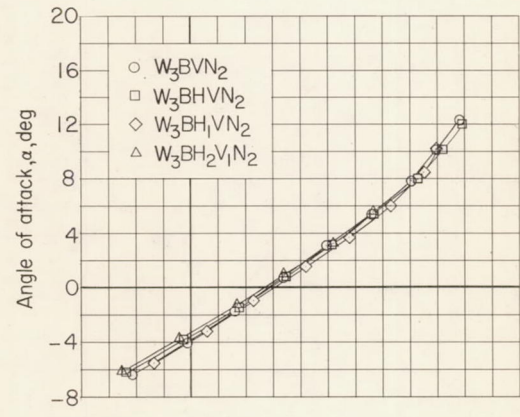
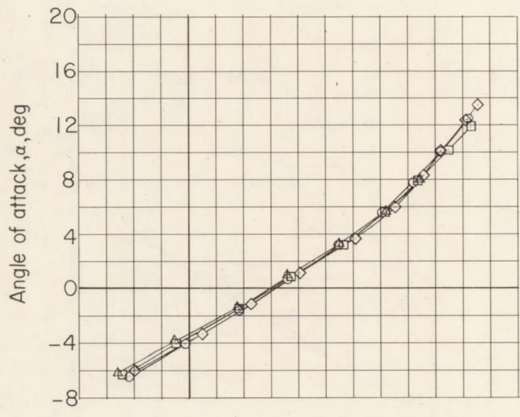
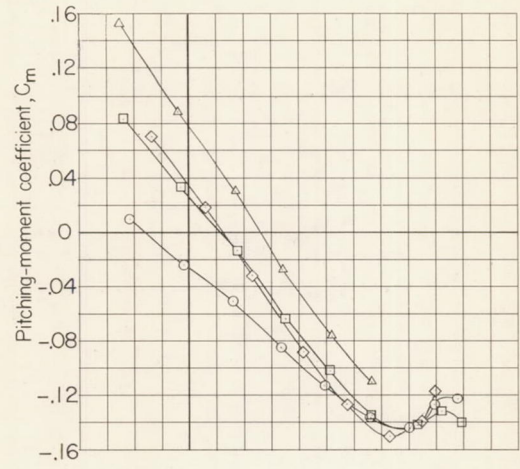
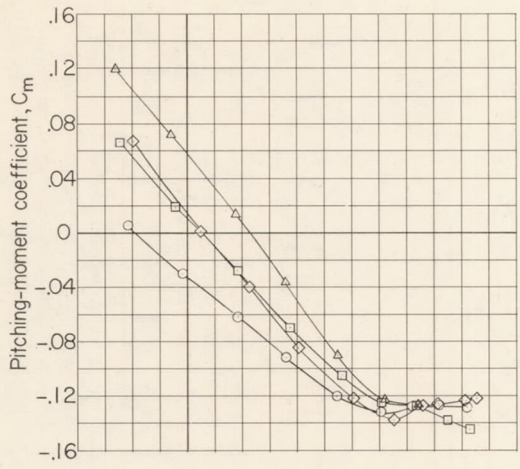




(e)  $M = 0.98$ .

(f)  $M = 1.00$ .

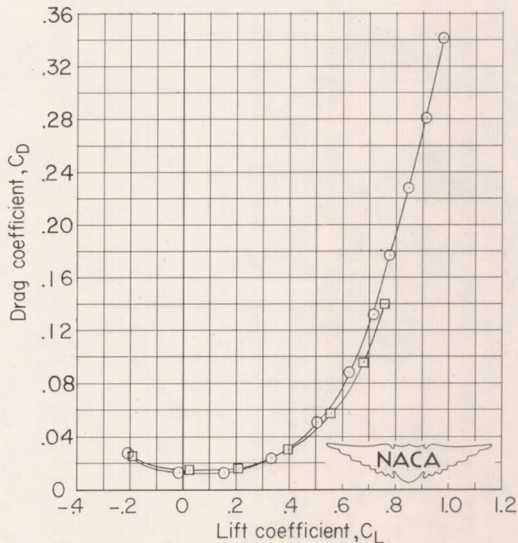
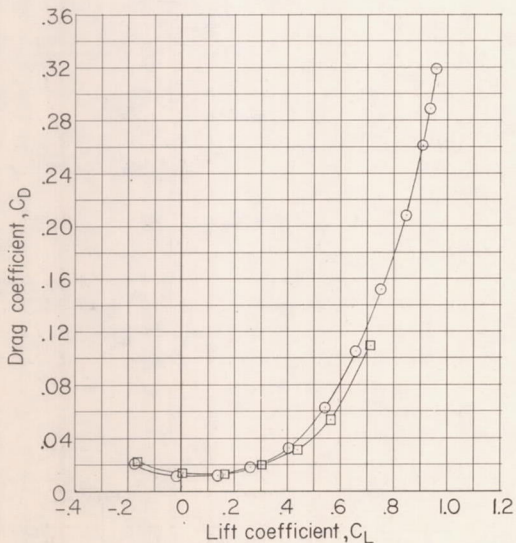
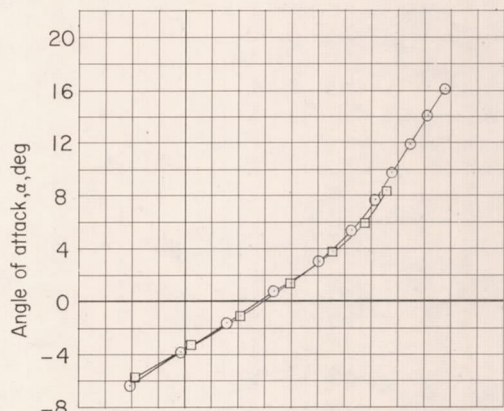
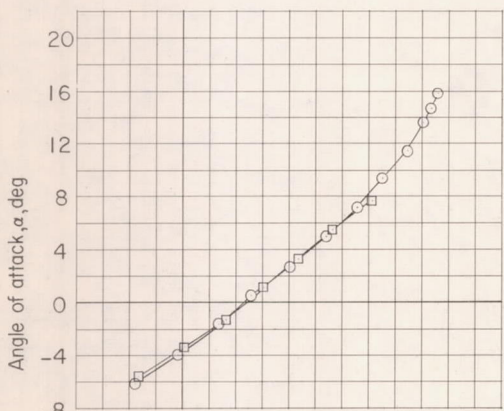
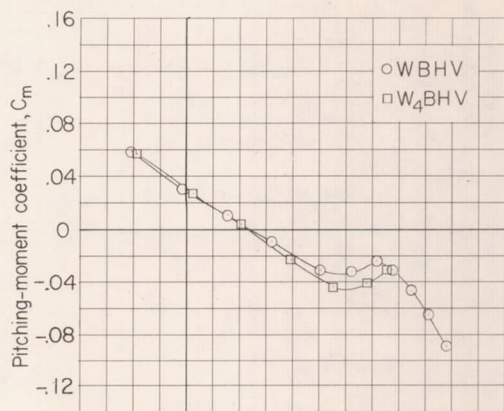
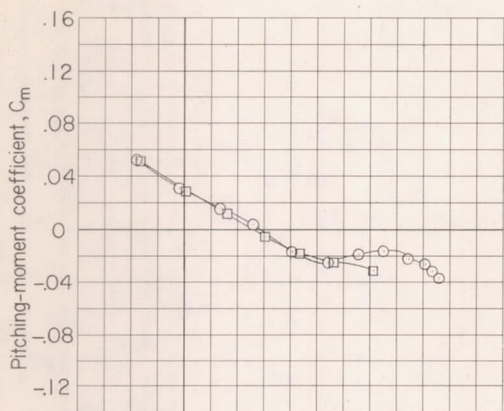
Figure 14.- Continued.



(g) M = 1.04.

(h) M = 1.11.

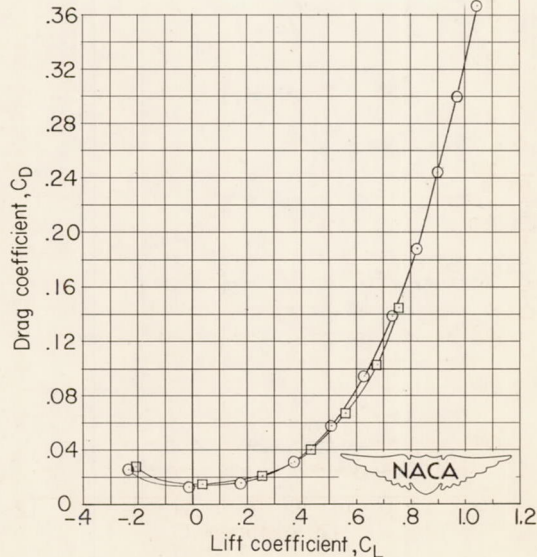
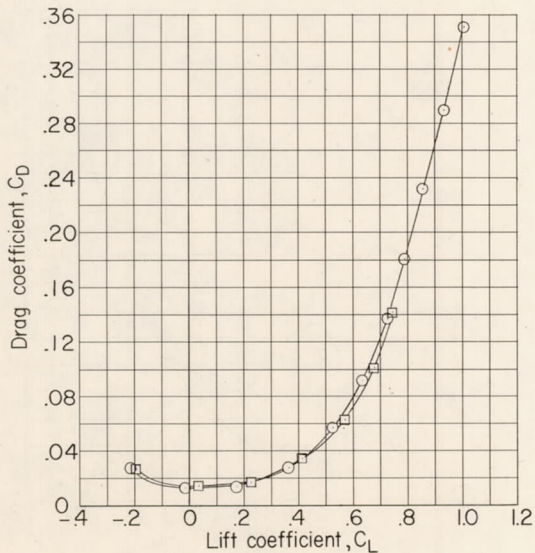
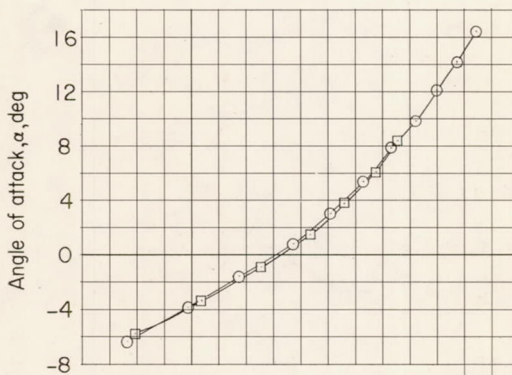
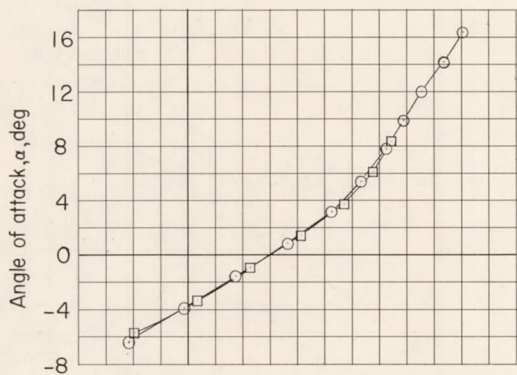
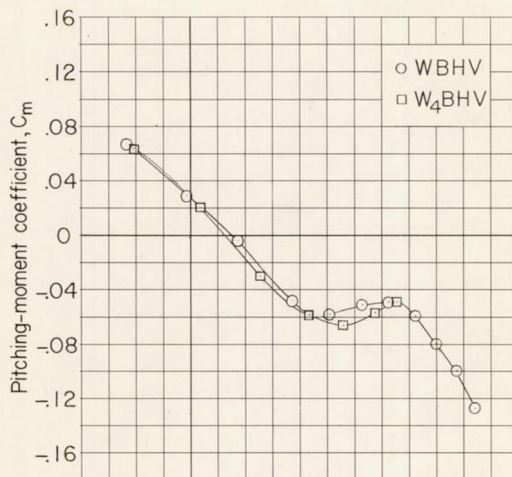
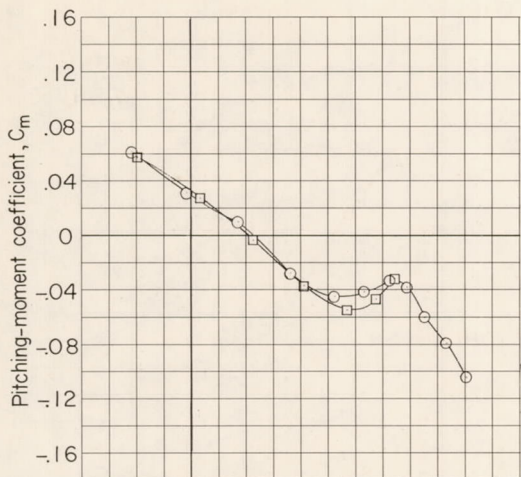
Figure 14.- Concluded.



(a)  $M = 0.70$ .

(b)  $M = 0.90$ .

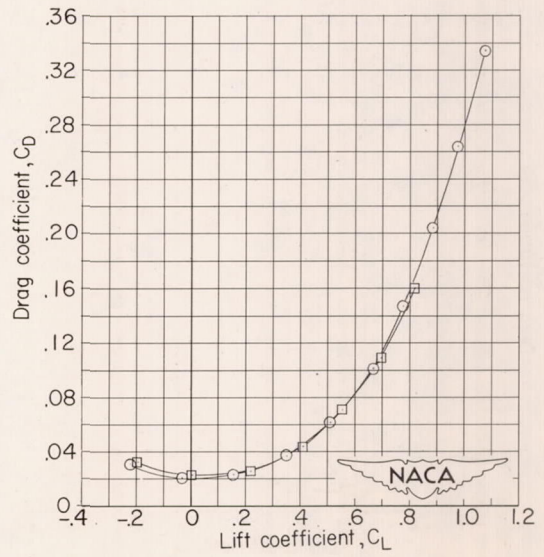
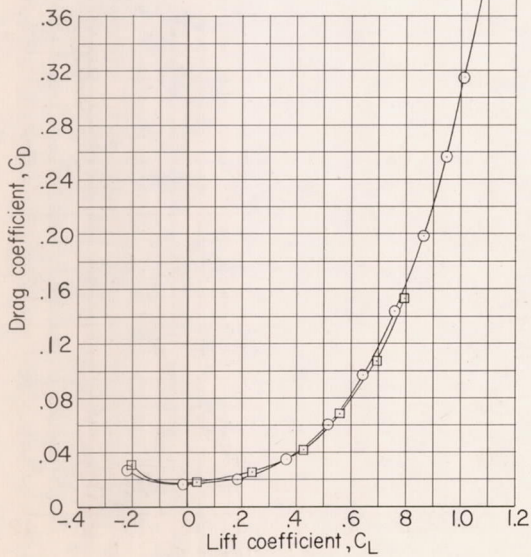
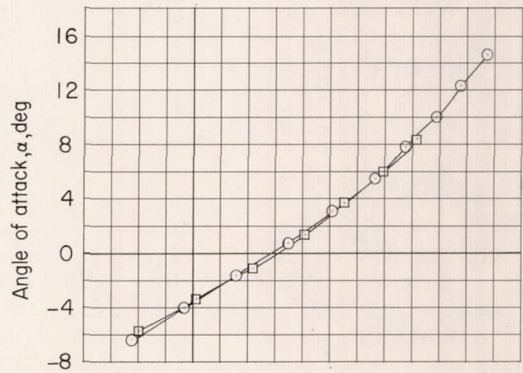
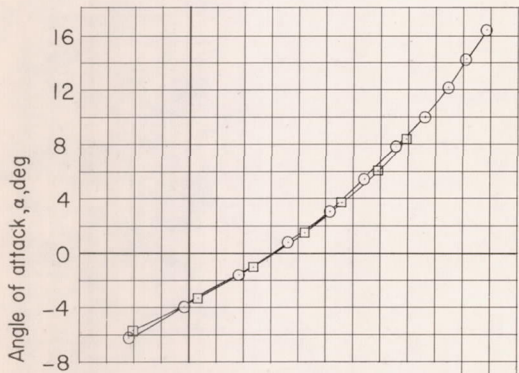
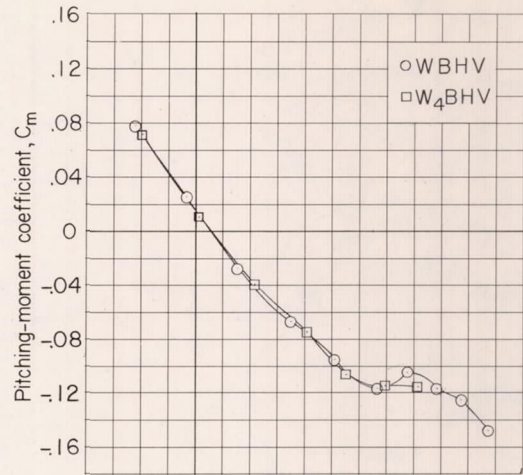
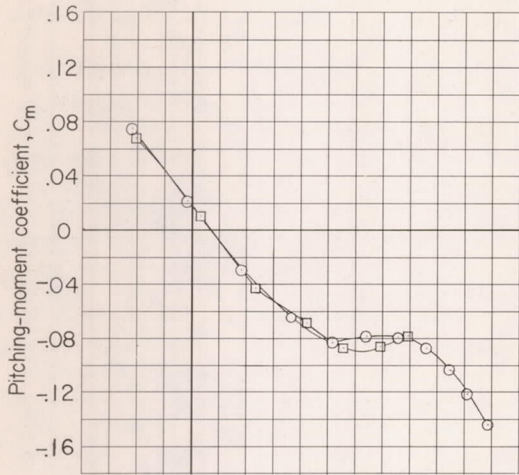
Figure 15.- Effects of wing modification on the aerodynamic characteristics of the model.



(c)  $M = 0.93$ .

(d)  $M = 0.96$ .

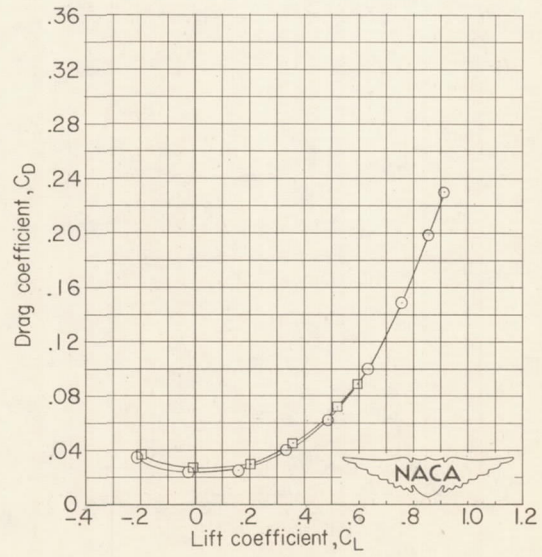
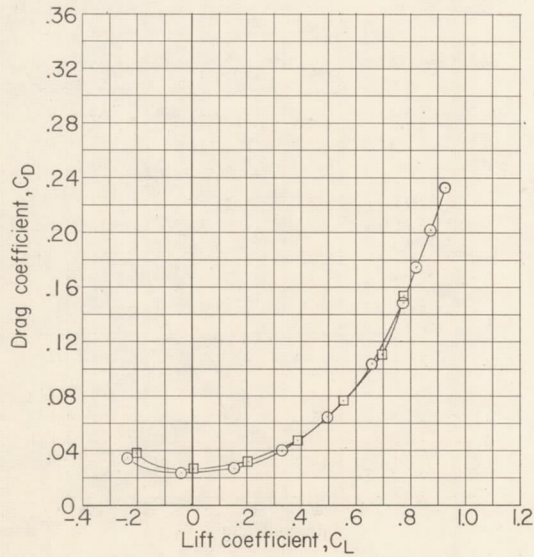
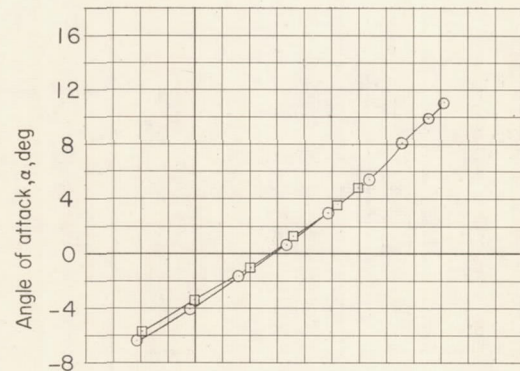
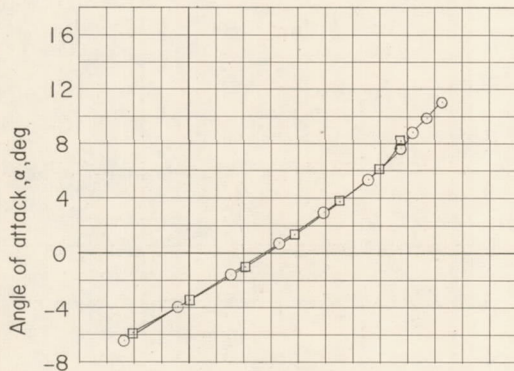
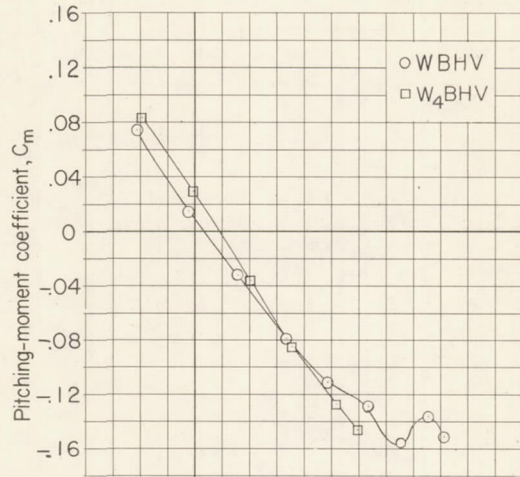
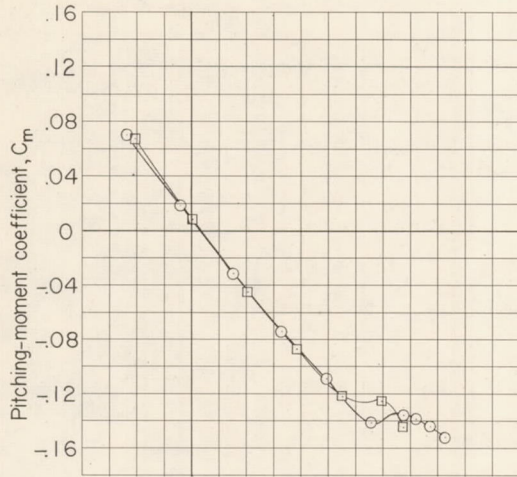
Figure 15.- Continued.



(e)  $M = 0.98$ .

(f)  $M = 1.01$ .

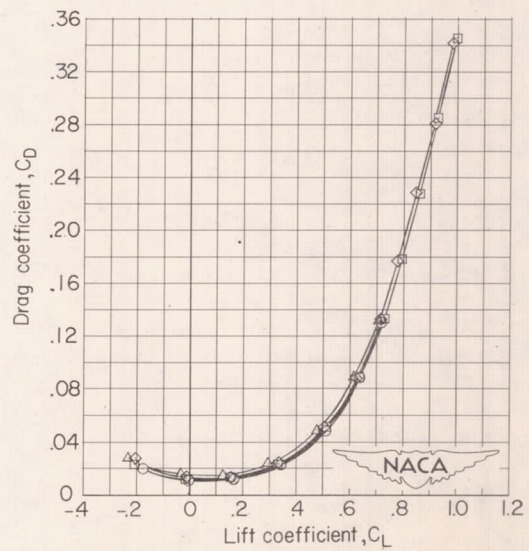
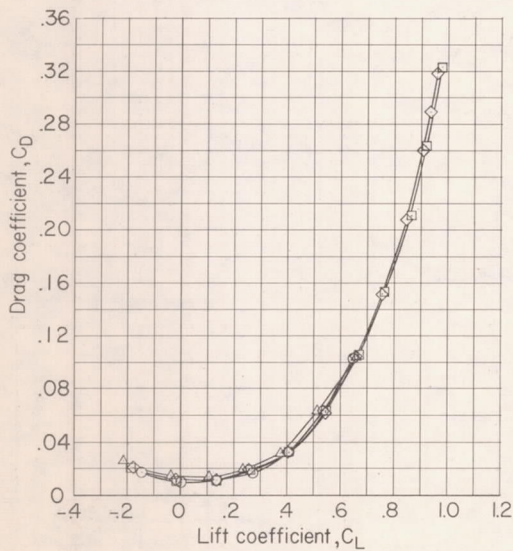
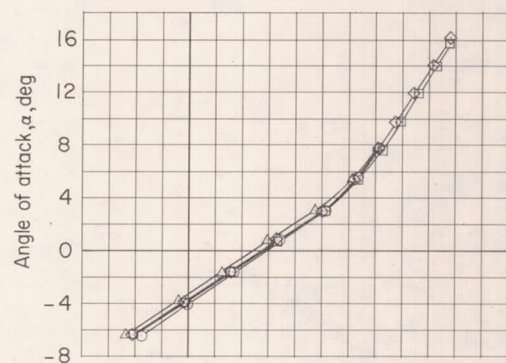
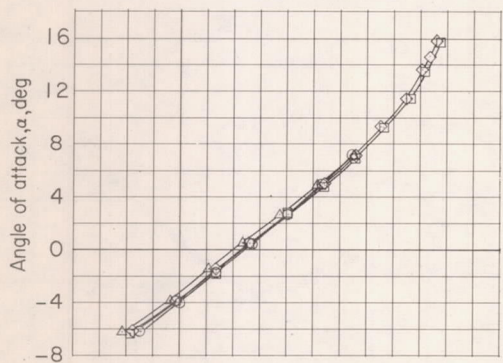
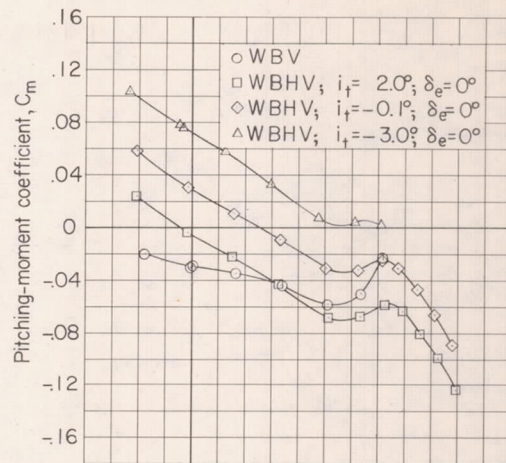
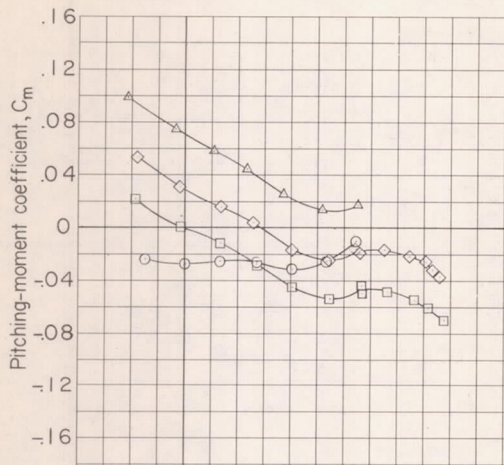
Figure 15.- Continued.



(g)  $M = 1.05$ .

(h)  $M = 1.10$ .

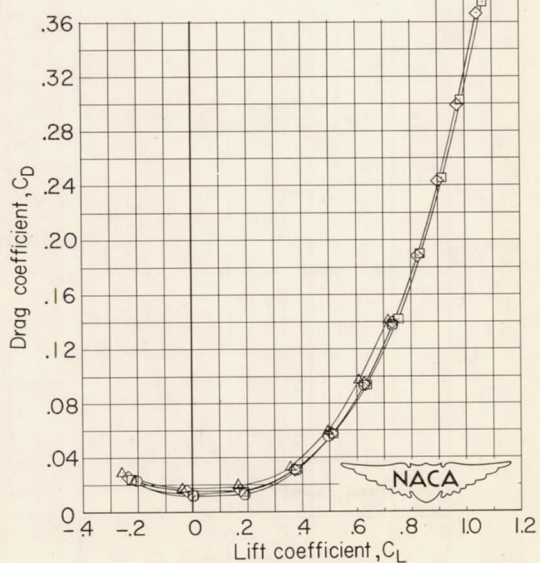
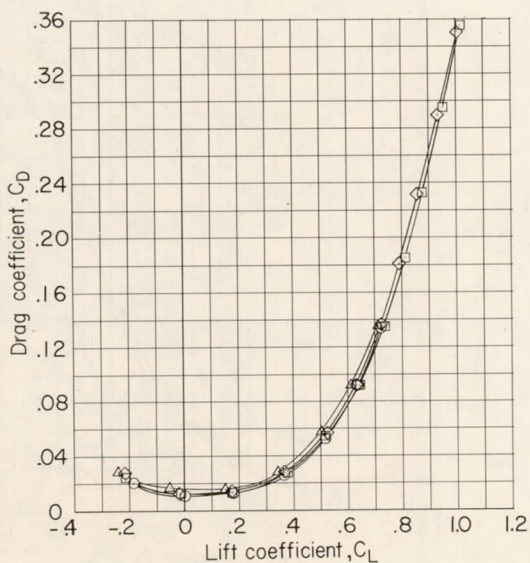
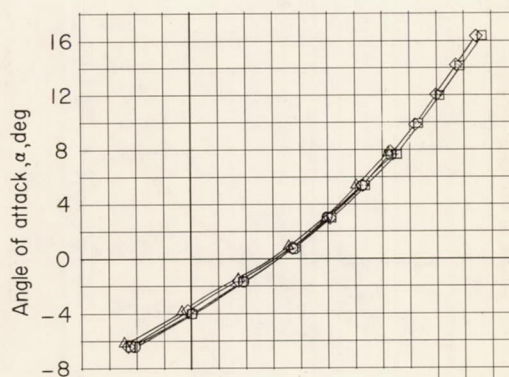
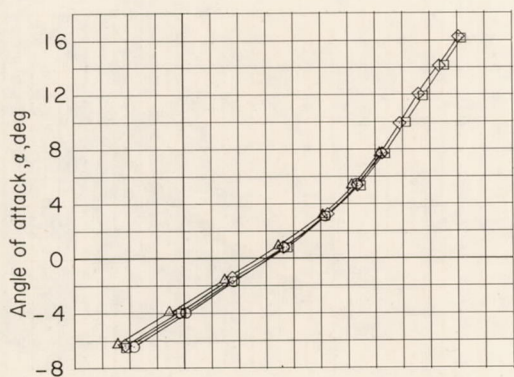
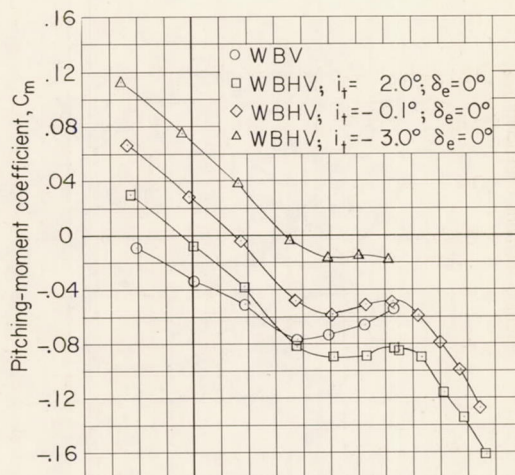
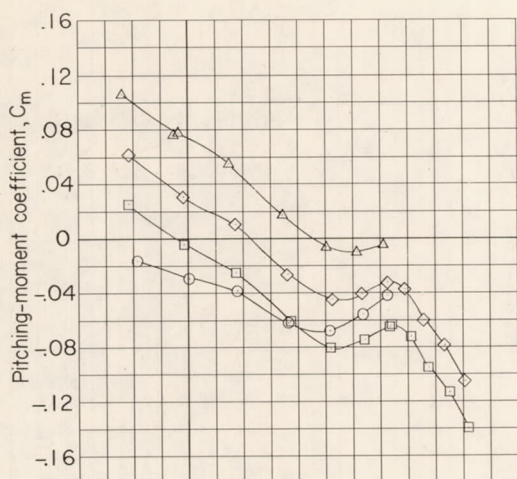
Figure 15.- Concluded.



(a)  $M = 0.70$ .

(b)  $M = 0.91$ .

Figure 16.- Effects of stabilizer incidence on the aerodynamic characteristics of the model.

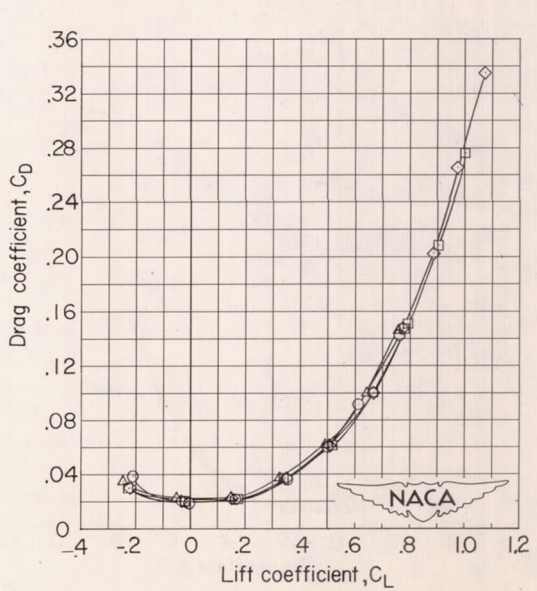
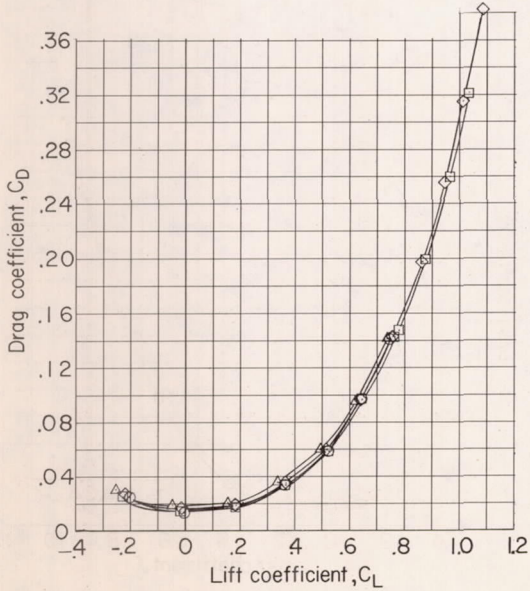
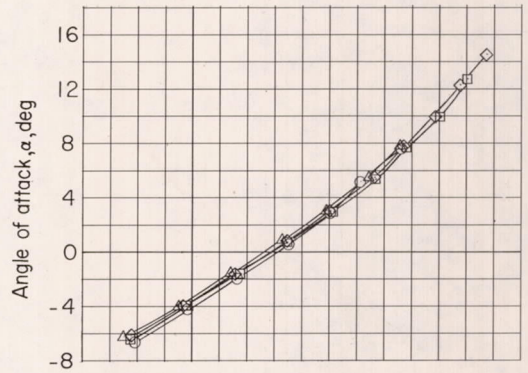
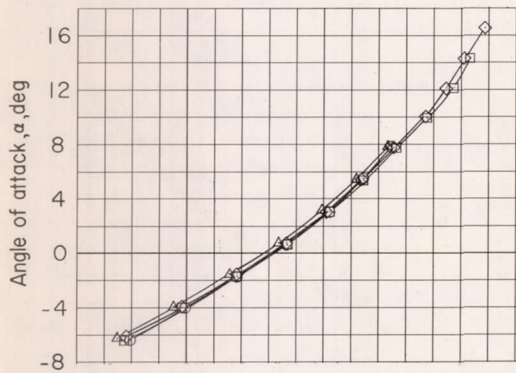
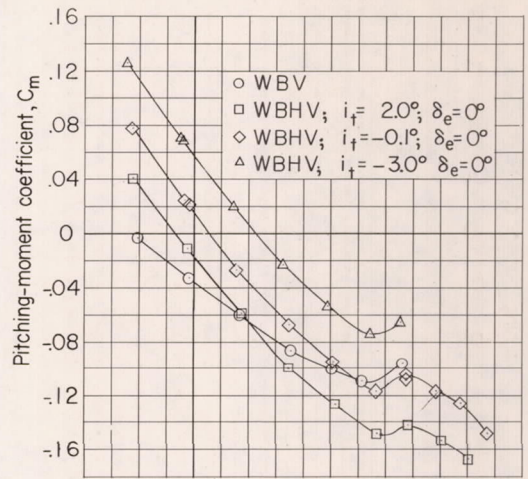
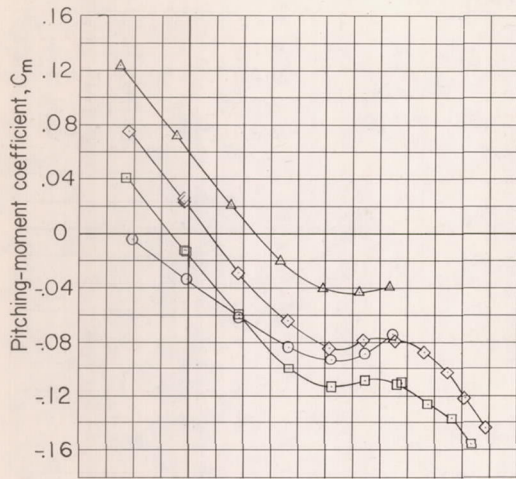


(c)  $M = 0.93$ .

(d)  $M = 0.96$ .

Figure 16.- Continued.

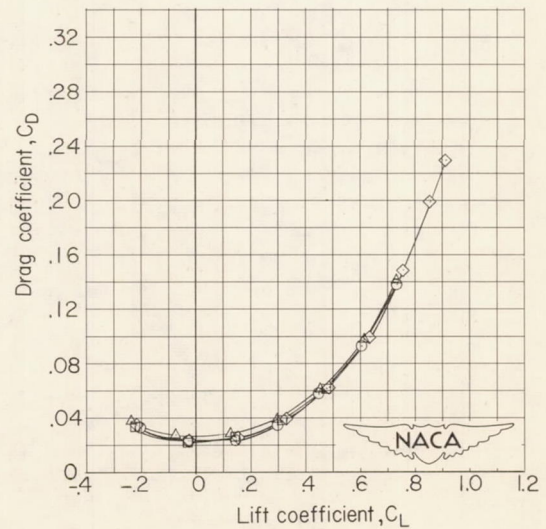
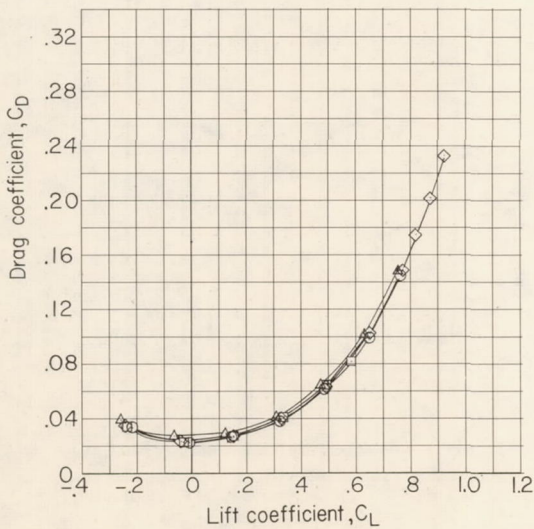
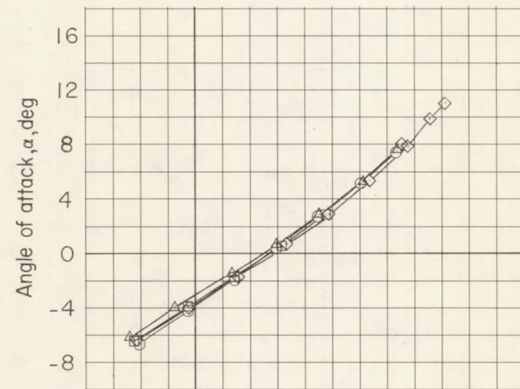
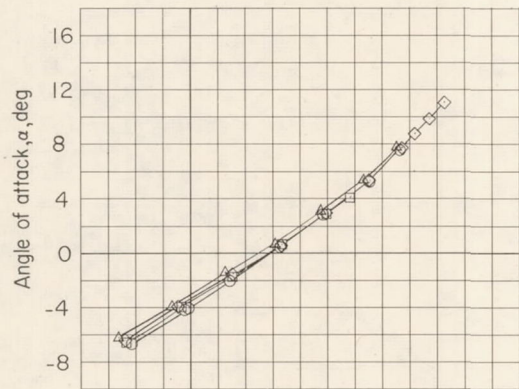
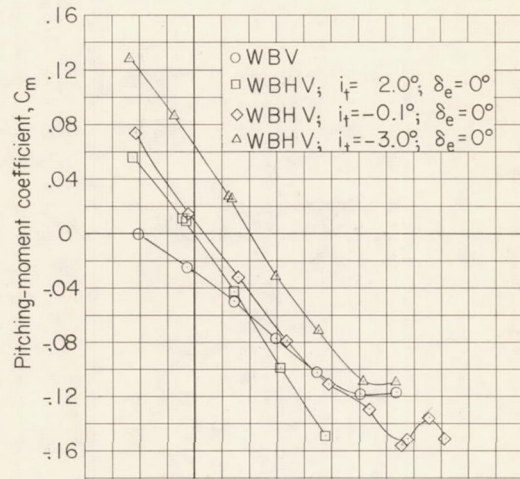
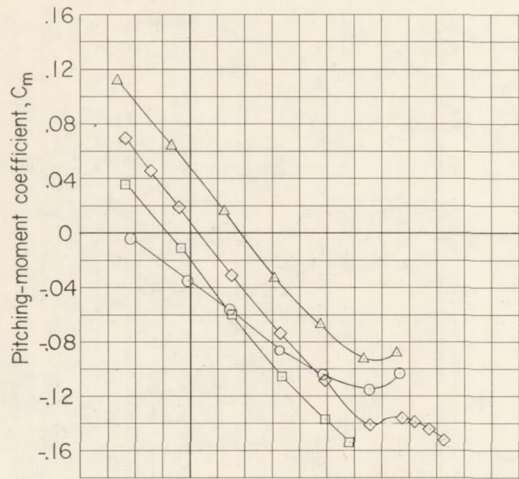




(e)  $M = 0.98$ .

(f)  $M = 1.01$ .

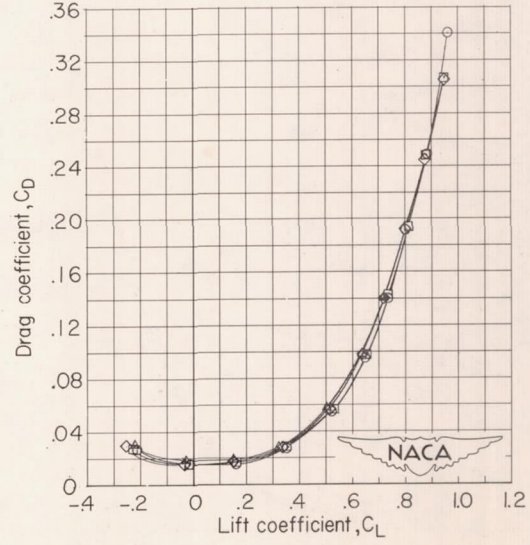
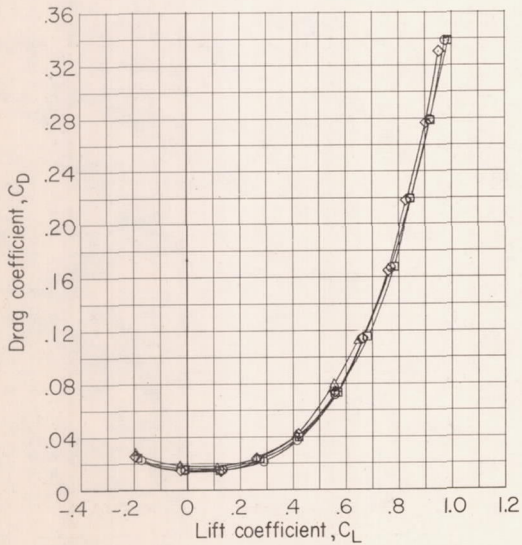
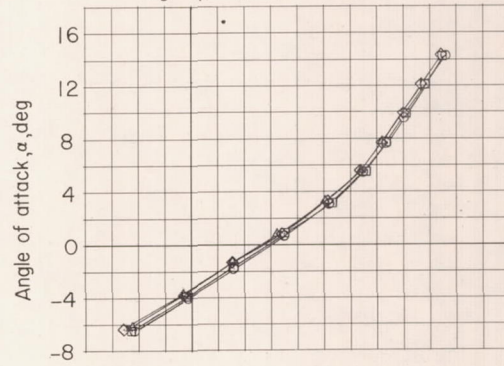
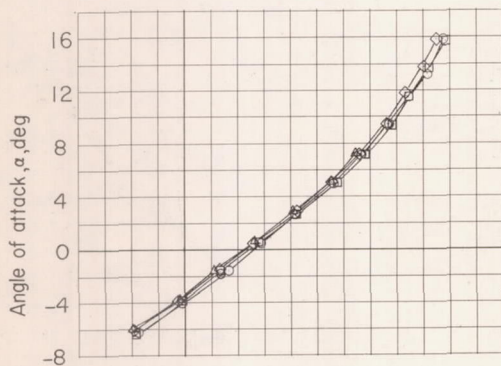
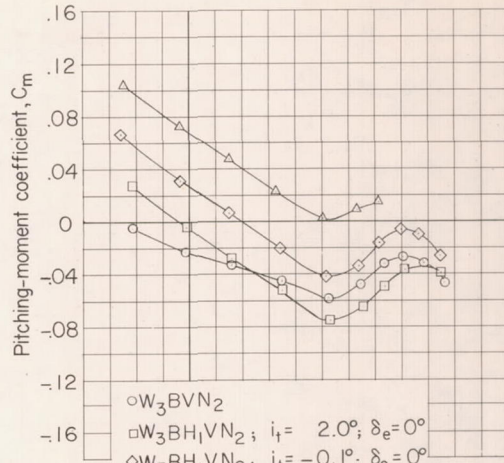
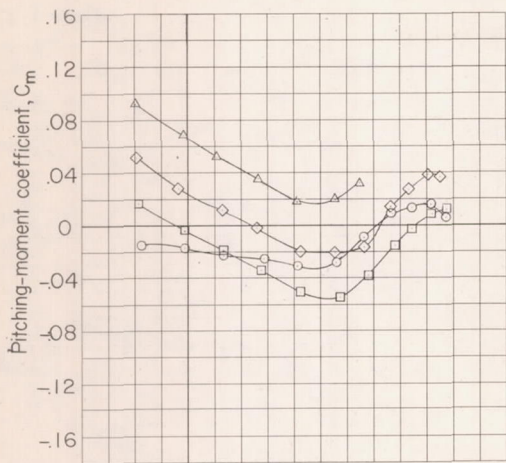
Figure 16.- Continued.



(g)  $M = 1.05$ .

(h)  $M = 1.11$ .

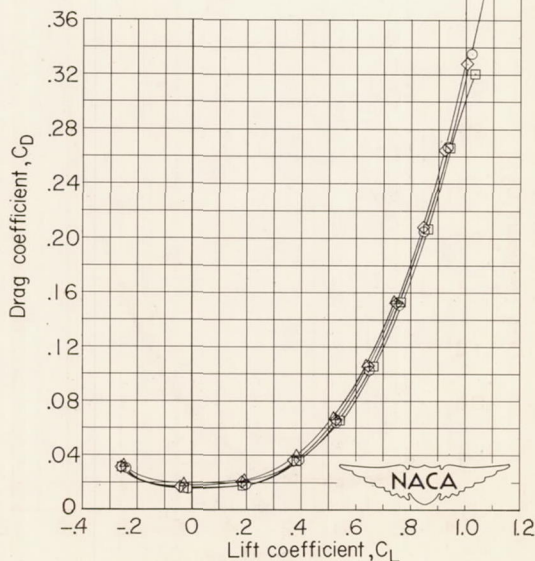
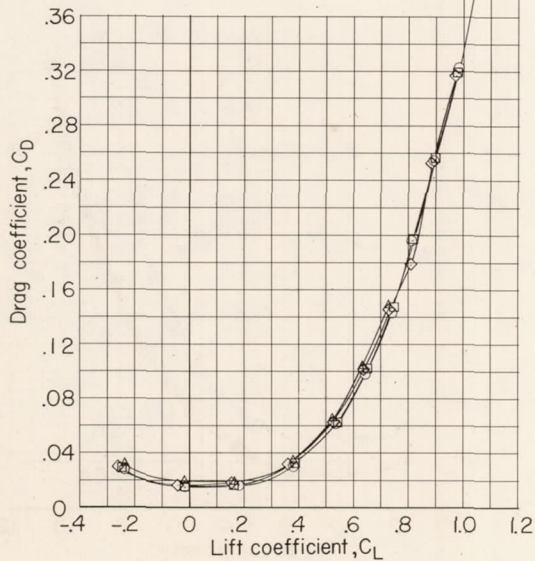
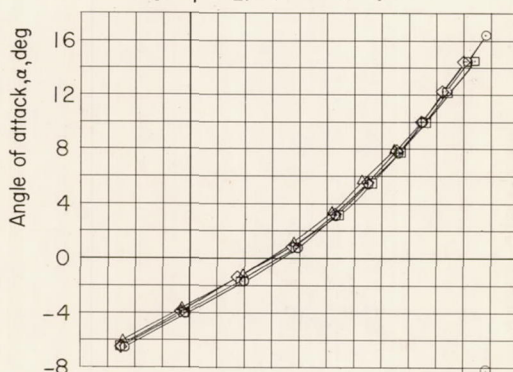
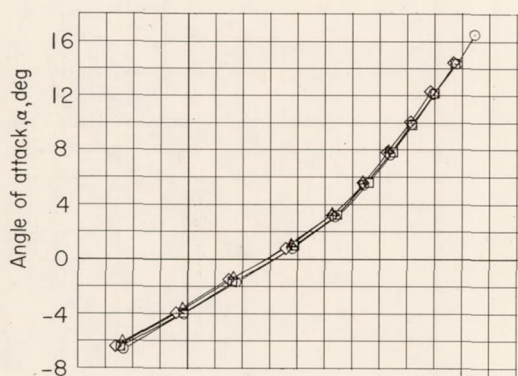
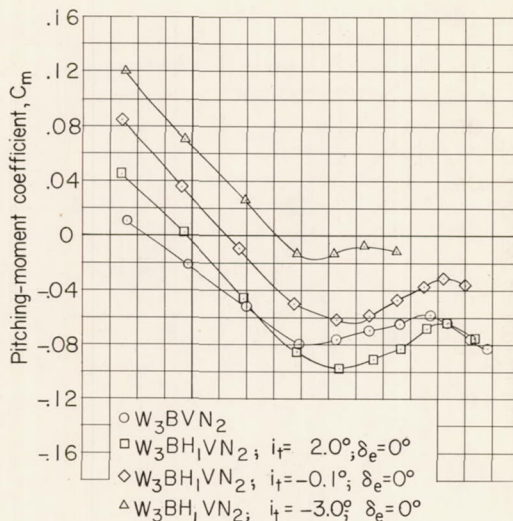
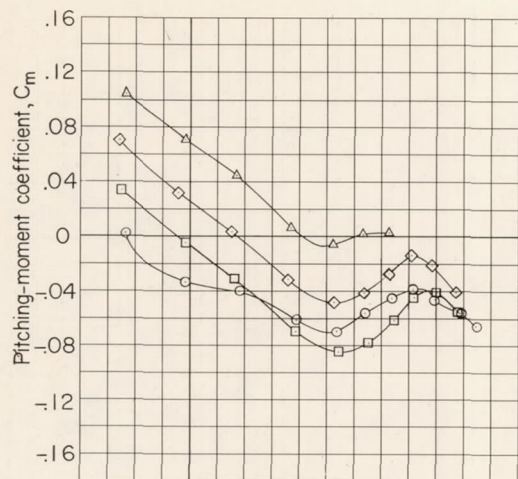
Figure 16.- Concluded.



(a)  $M = 0.70$ .

(b)  $M = 0.90$ .

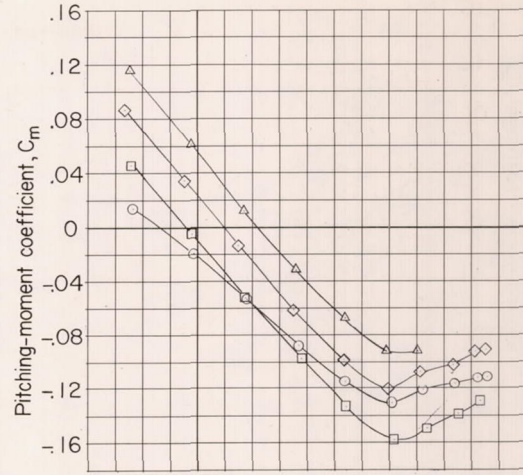
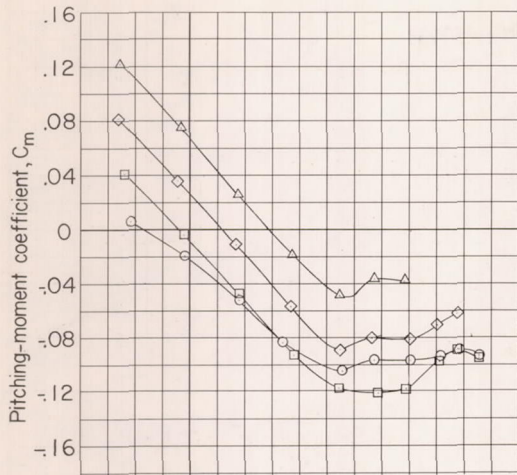
Figure 17.- Effects of stabilizer incidence on the aerodynamic characteristics of the model with buried nacelles.



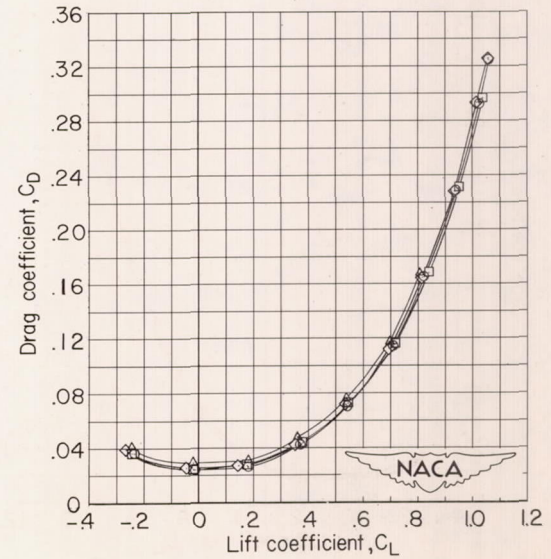
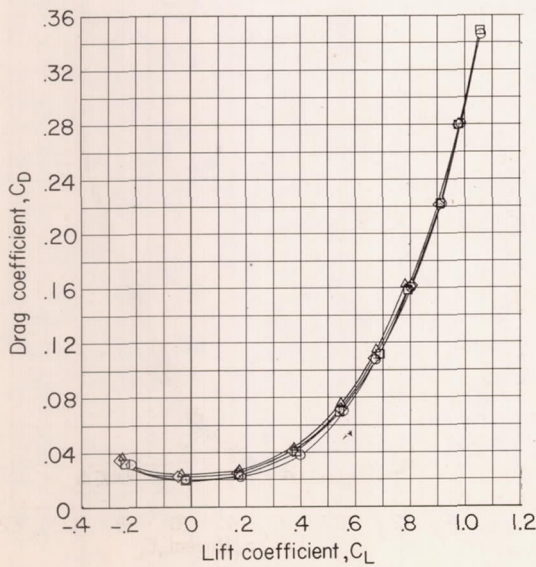
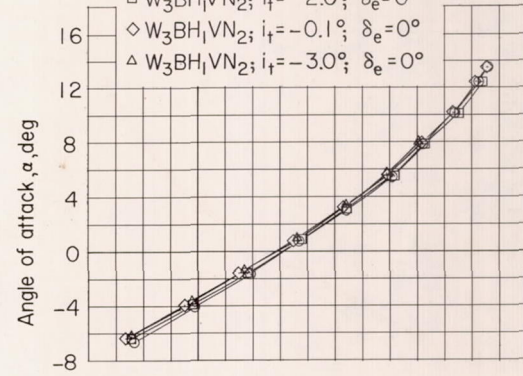
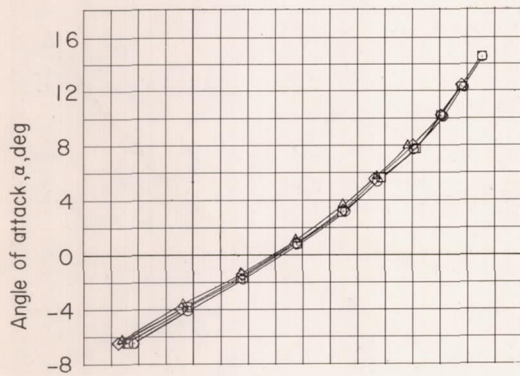
(c)  $M = 0.93$ .

(d)  $M = 0.95$ .

Figure 17.- Continued.



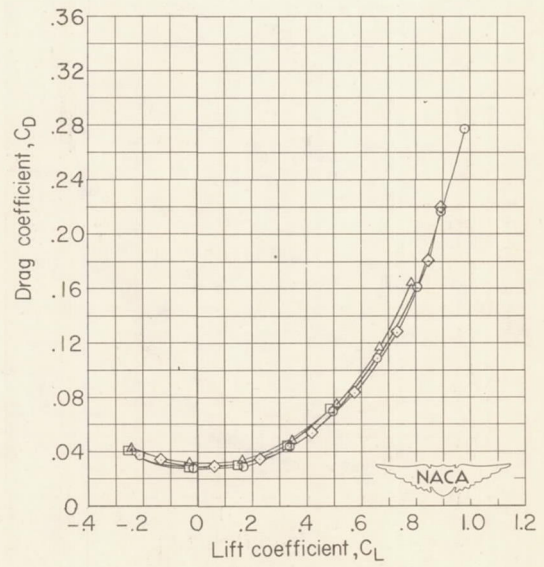
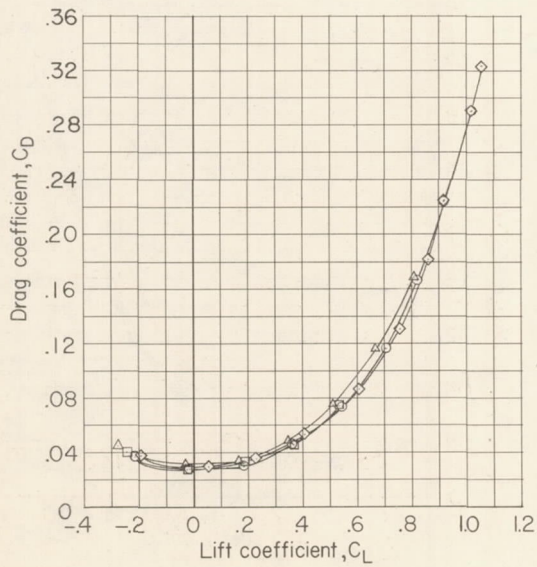
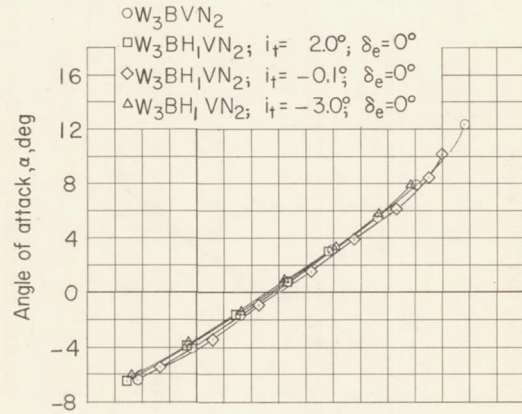
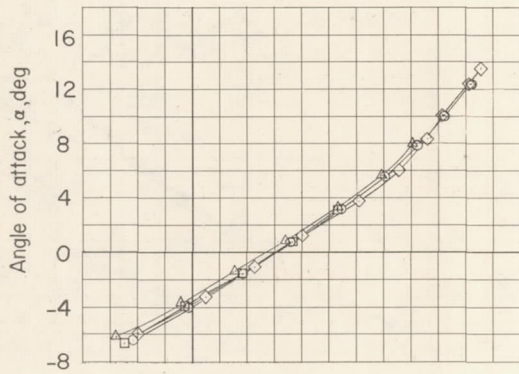
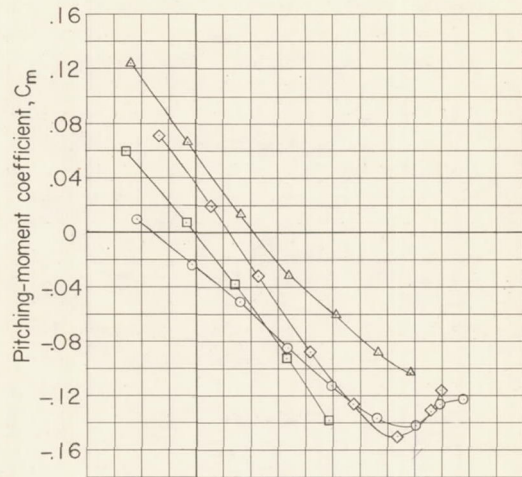
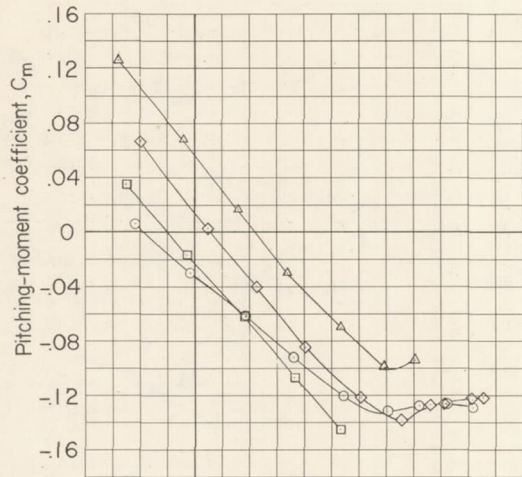
$\circ$   $W_3BVN_2$   
 $\square$   $W_3BH_1VN_2$ ;  $i_t = 2.0^\circ$ ;  $\delta_e = 0^\circ$   
 $\diamond$   $W_3BH_1VN_2$ ;  $i_t = -0.1^\circ$ ;  $\delta_e = 0^\circ$   
 $\triangle$   $W_3BH_1VN_2$ ;  $i_t = -3.0^\circ$ ;  $\delta_e = 0^\circ$



(e)  $M = 0.98$ .

(f)  $M = 1.00$ .

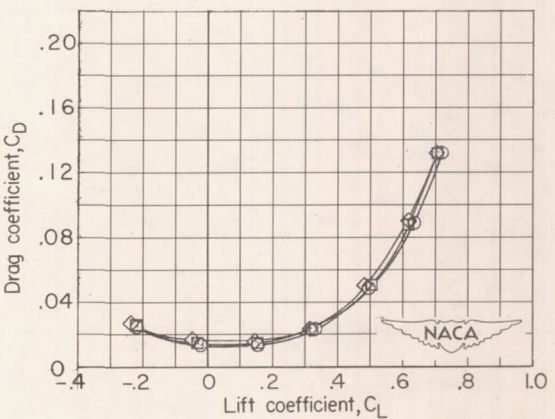
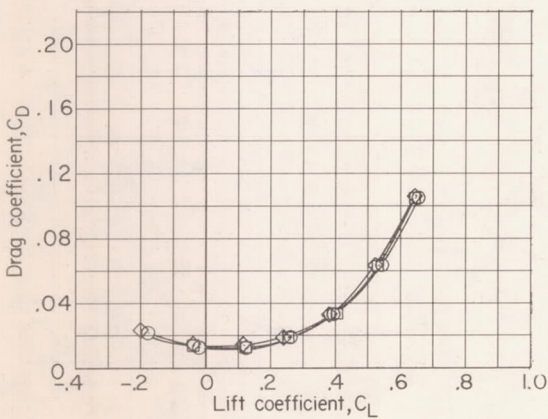
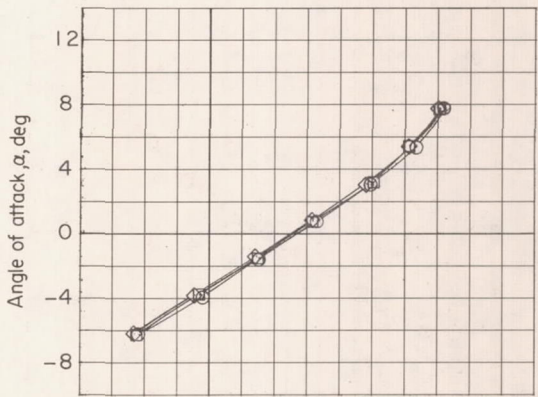
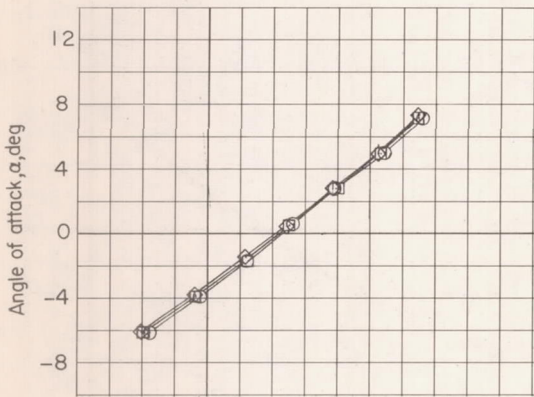
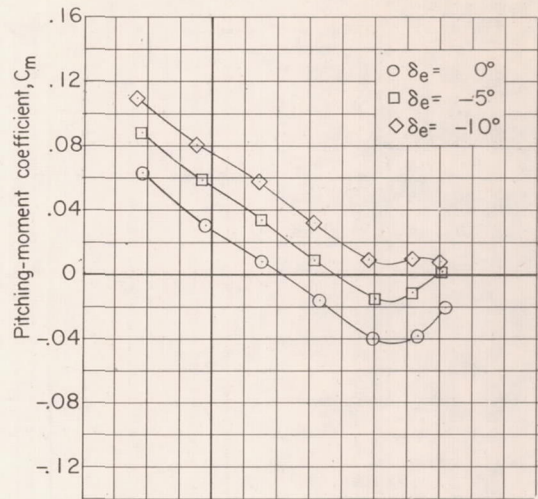
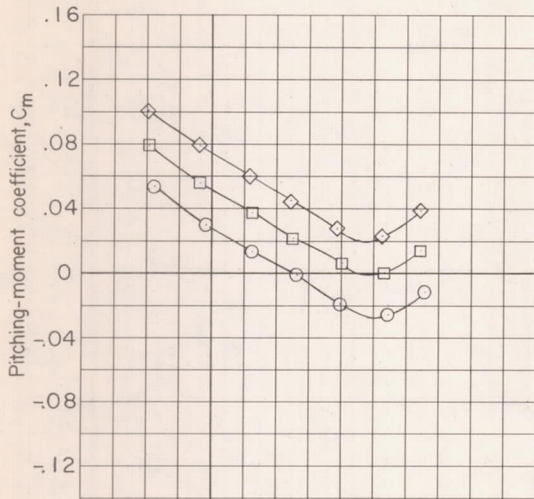
Figure 17.- Continued.



(g)  $M = 1.04$ :

(h)  $M = 1.11$ .

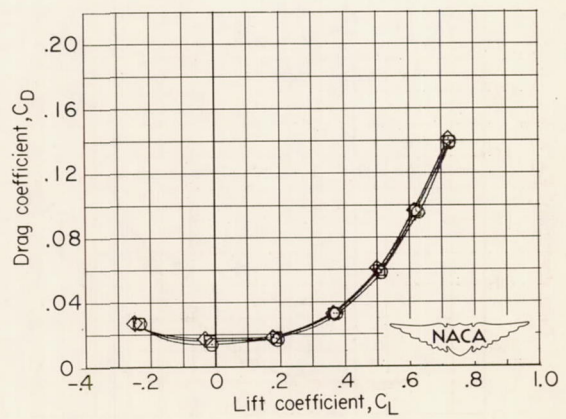
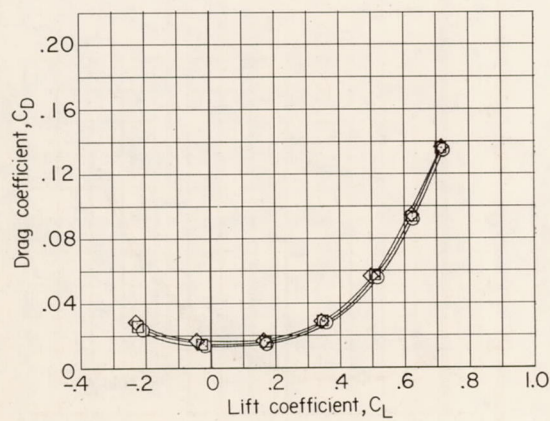
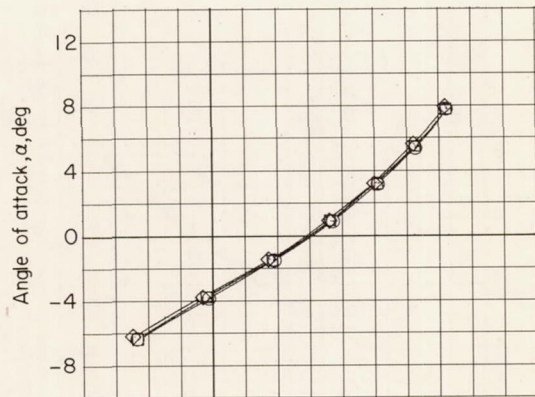
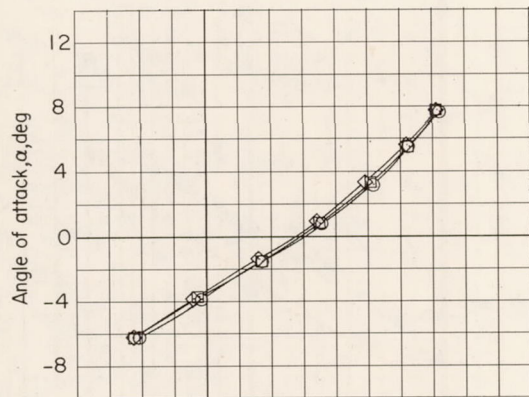
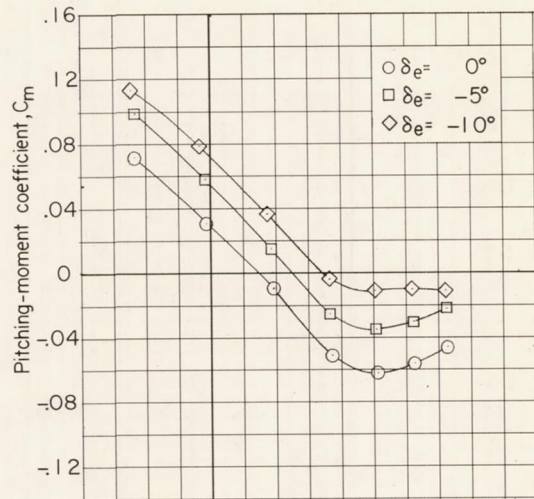
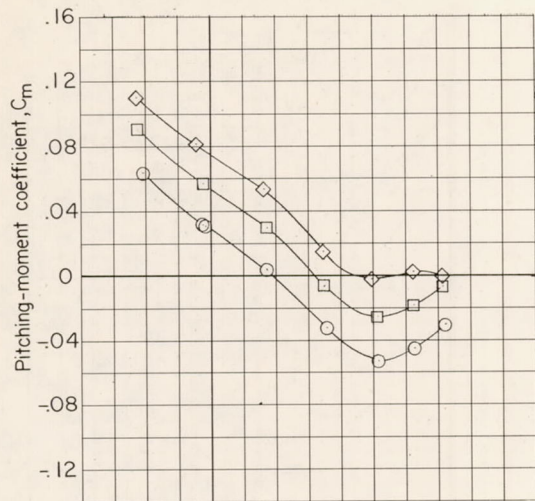
Figure 17.- Concluded.



(a)  $M = 0.70$ .

(b)  $M = 0.90$ .

Figure 18.- Effects of elevator deflection on the aerodynamic characteristics of the WBH<sub>1</sub>V configuration.

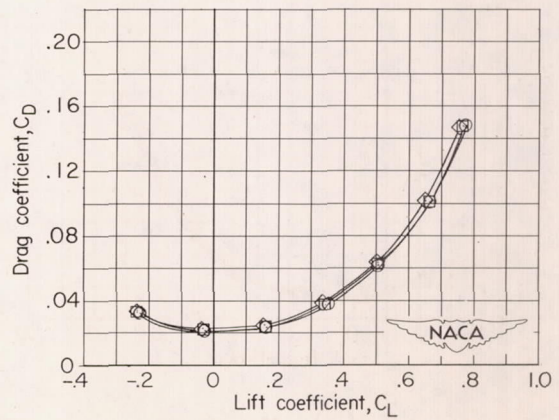
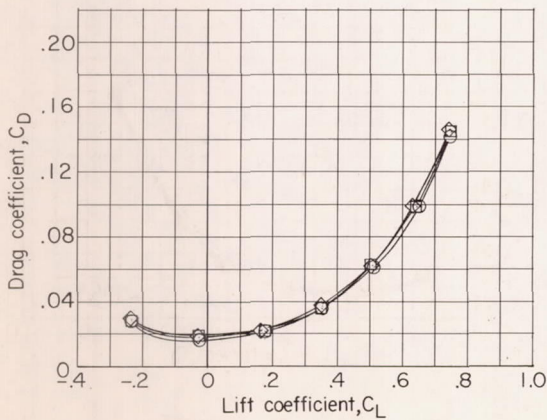
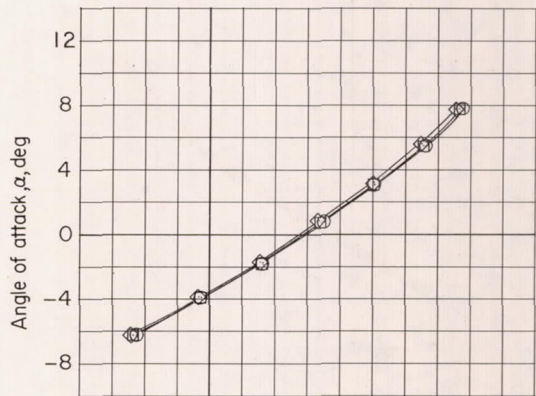
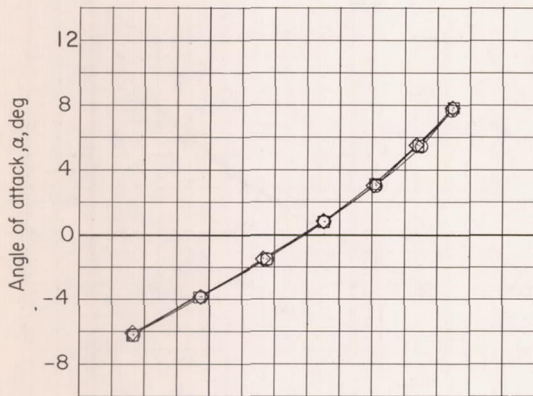
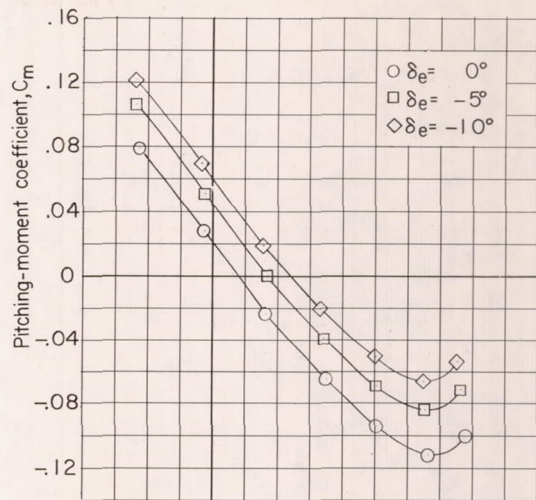
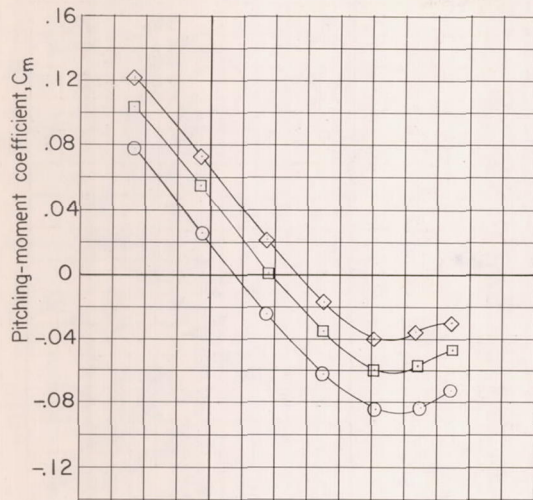


(c)  $M = 0.93$ .

(d)  $M = 0.96$ .

Figure 18.- Continued.

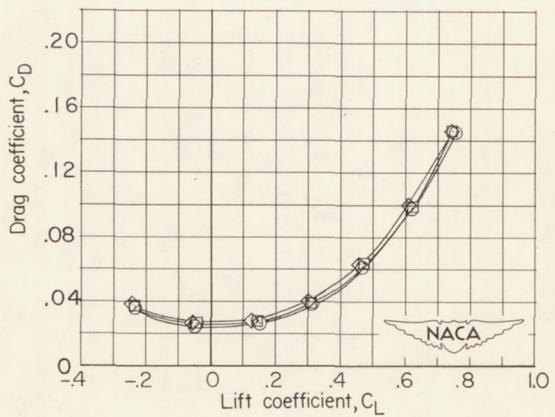
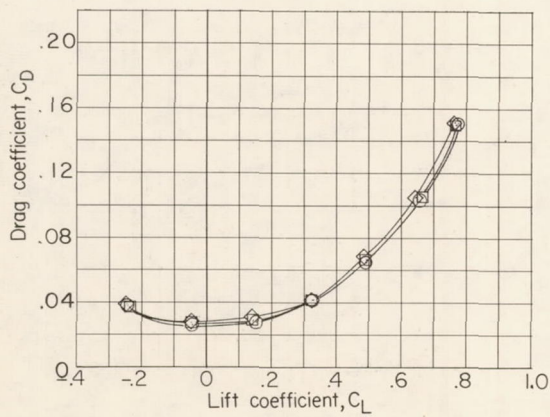
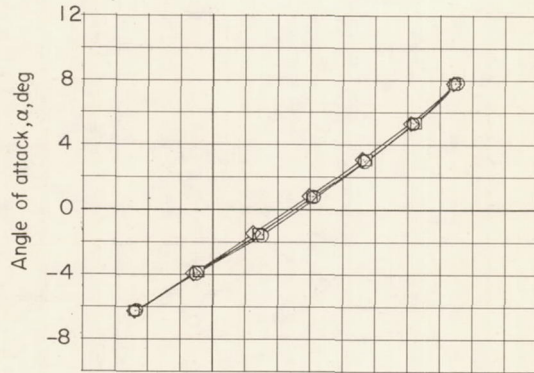
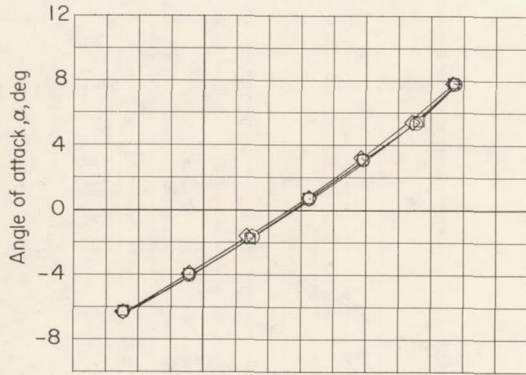
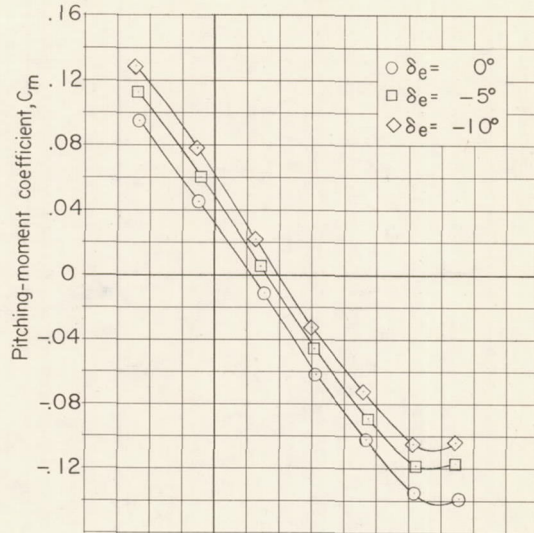
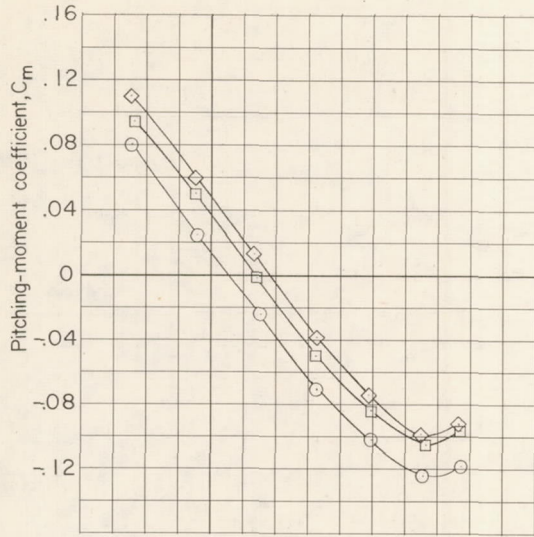




(e)  $M = 0.98$ .

(f)  $M = 1.01$ .

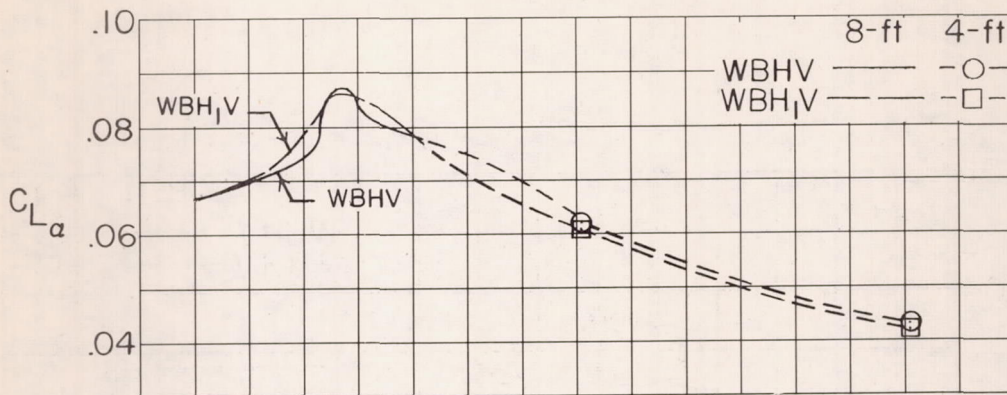
Figure 18.- Continued.



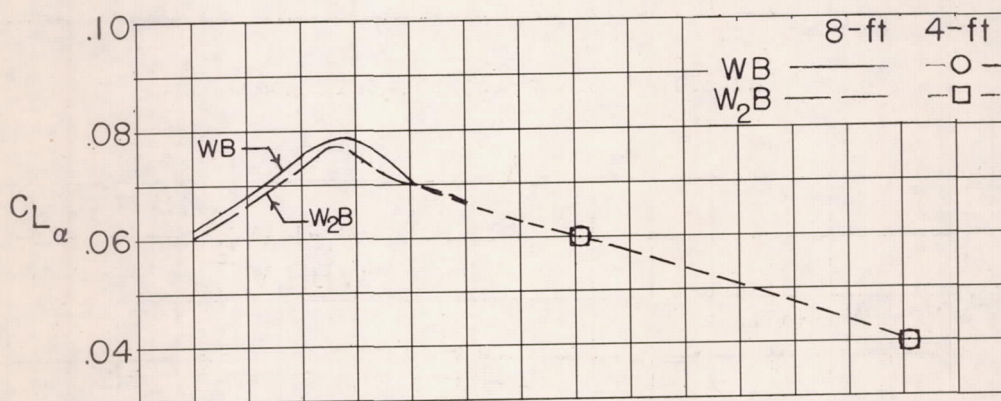
(g)  $M = 1.05$ .

(h)  $M = 1.11$ .

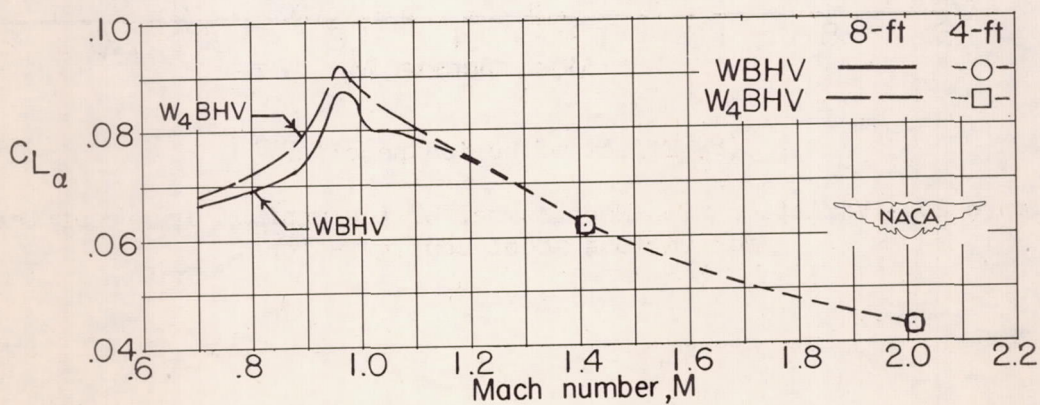
Figure 18.- Concluded.



(a) Effect of horizontal-tail location.

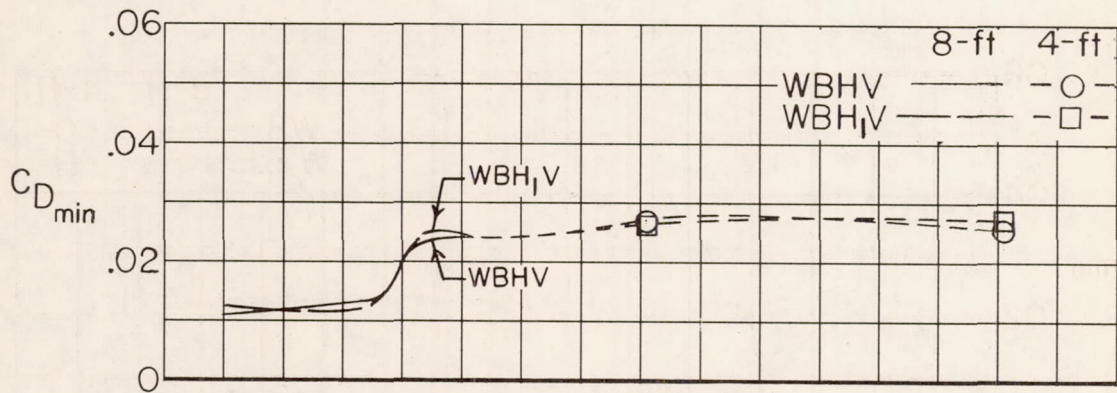


(b) Effect of wing incidence.

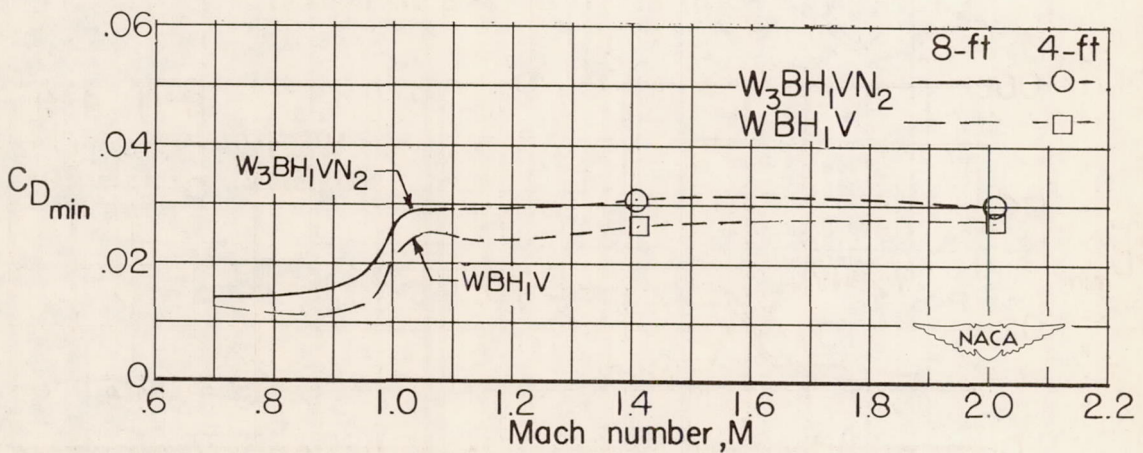


(c) Effect of wing modification.

Figure 19.- Variation with Mach number of the lift-curve slopes for various model configurations.

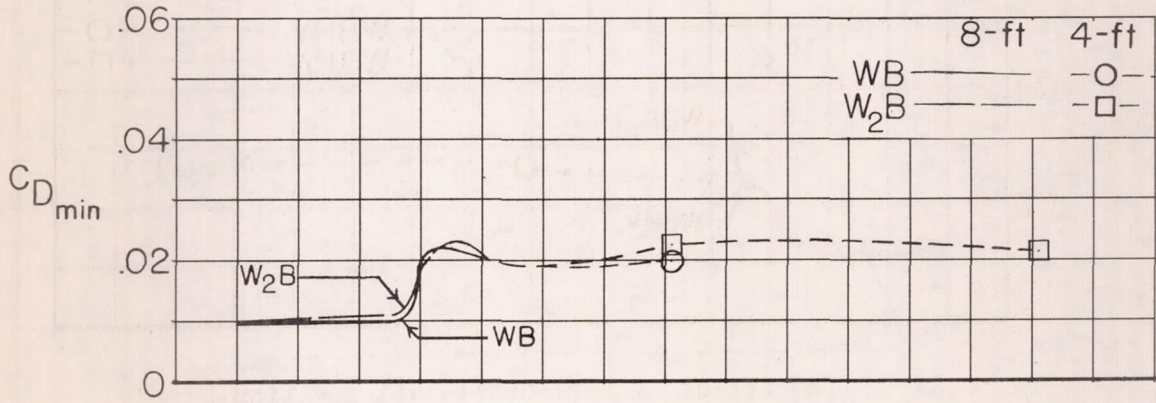


(a) Effect of horizontal-tail location.

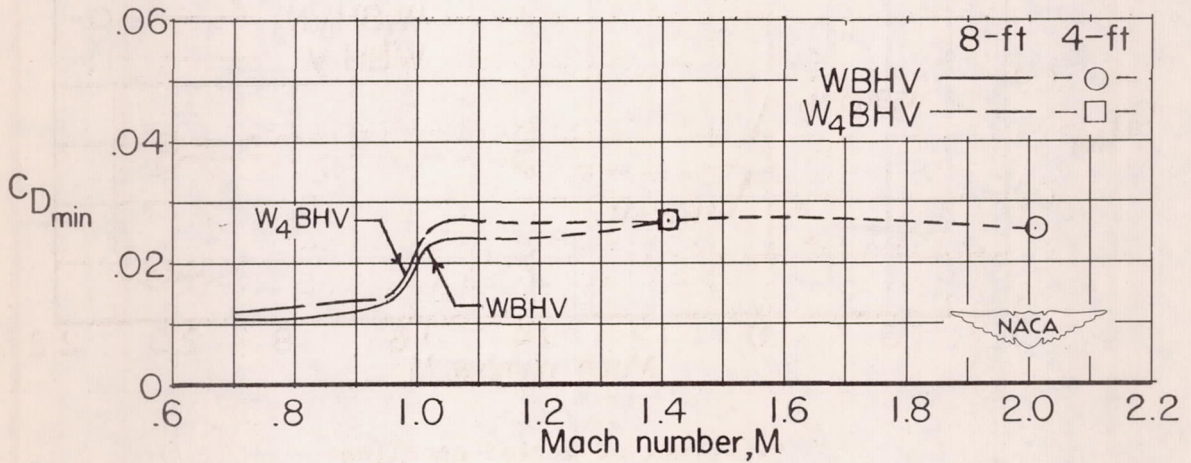


(b) Effect of buried nacelles.

Figure 20.- Variation with Mach number of the minimum drag coefficients for various model configurations.

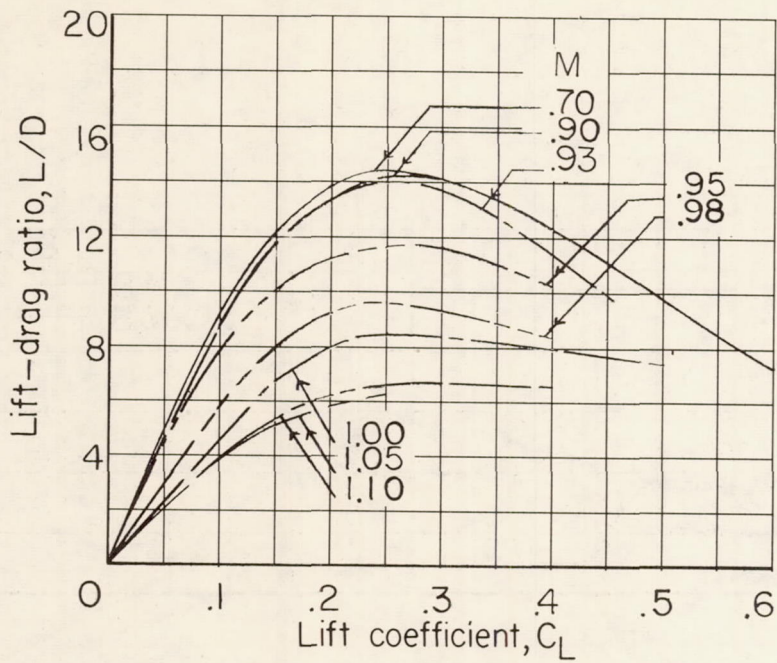


(c) Effect of wing incidence.

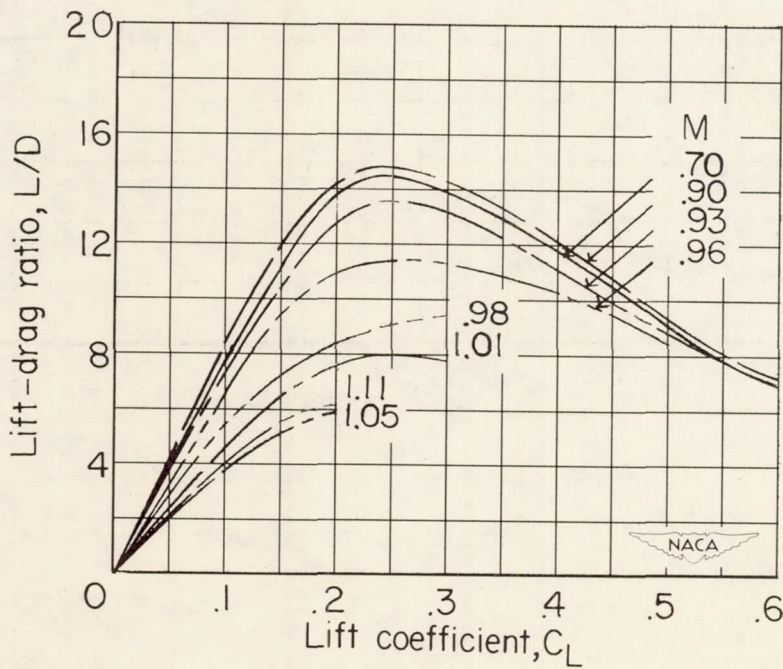


(d) Effect of wing modification.

Figure 20.- Concluded.

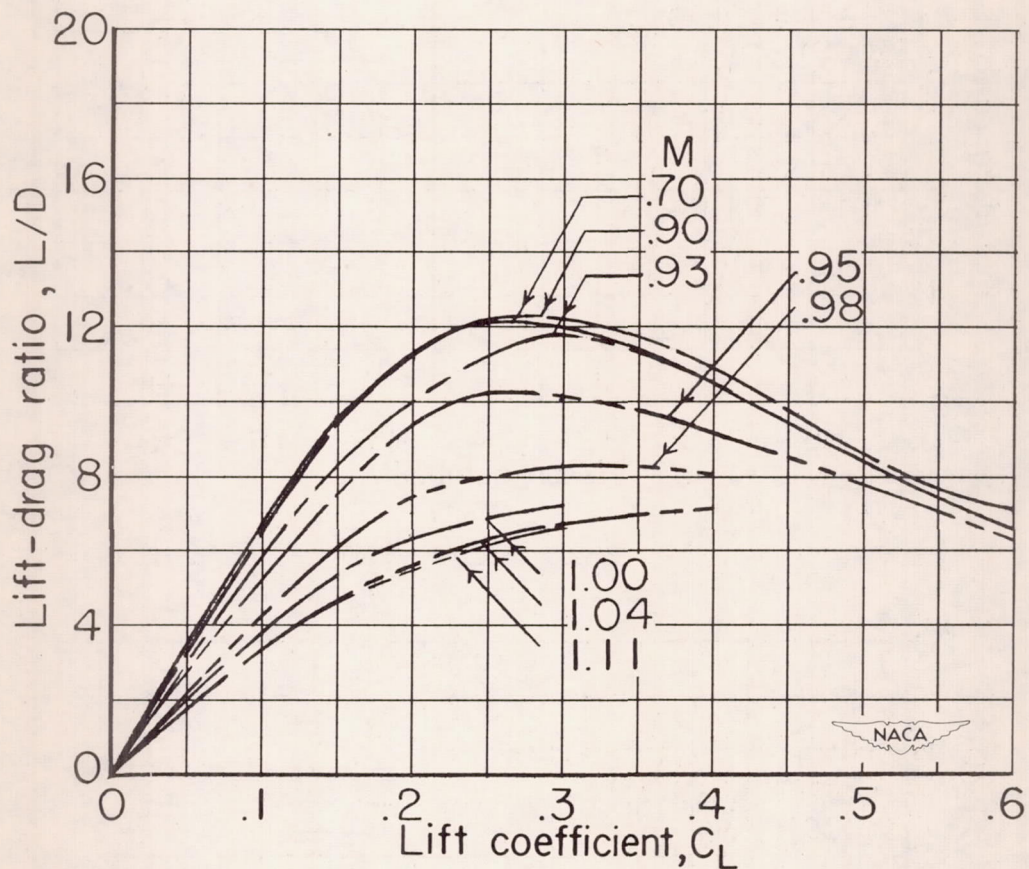


(a) Configuration WBHV.



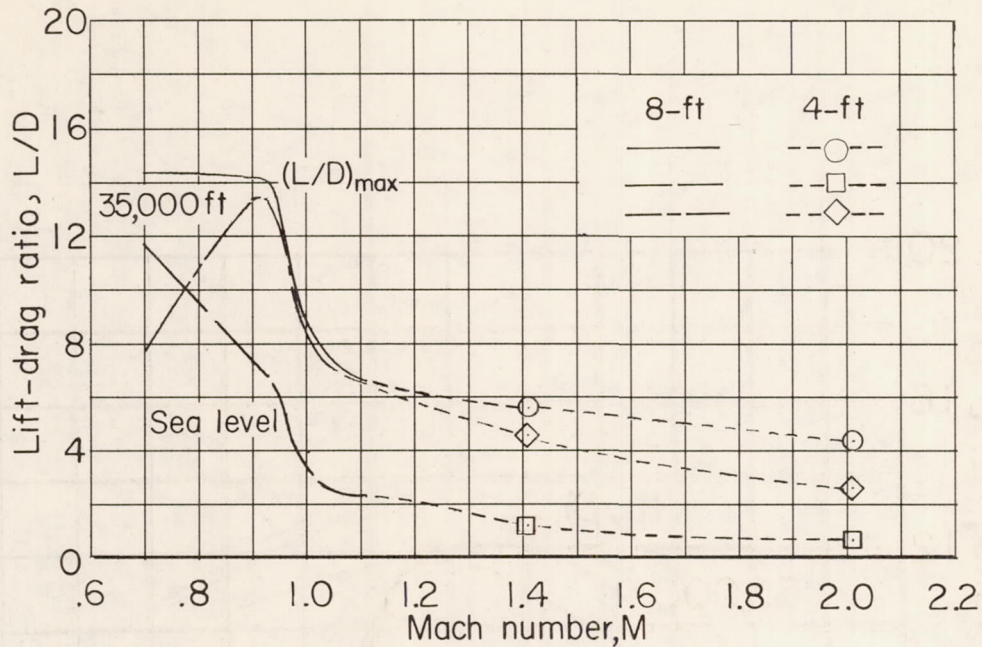
(b) Configuration WBH<sub>1</sub>V.

Figure 21.- Variation of trimmed lift-drag ratios with lift coefficient for the complete model.

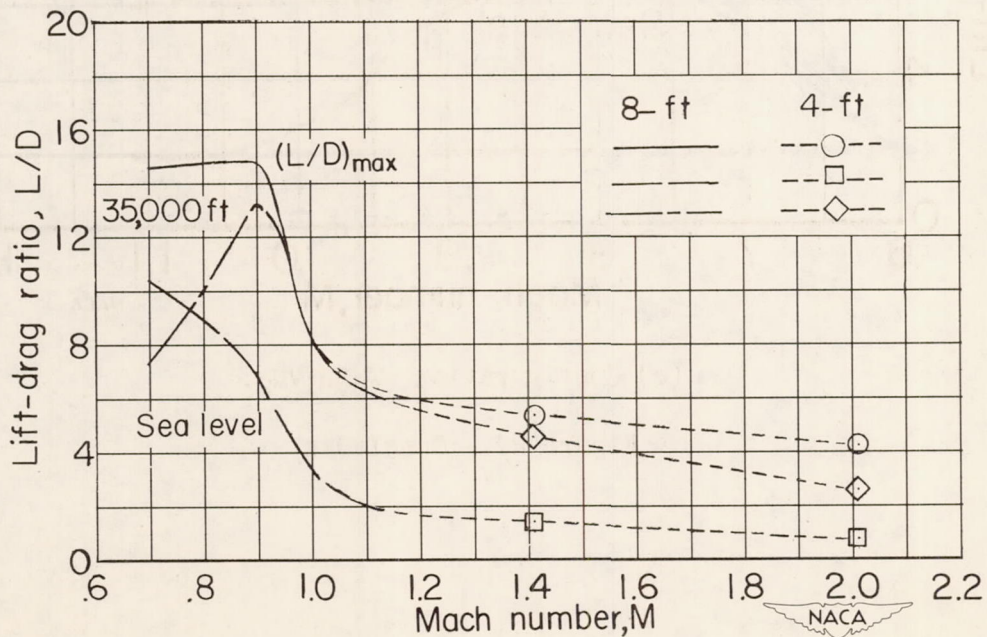


(c) Configuration  $W_3BH_1VN_2$ .

Figure 21.- Concluded.



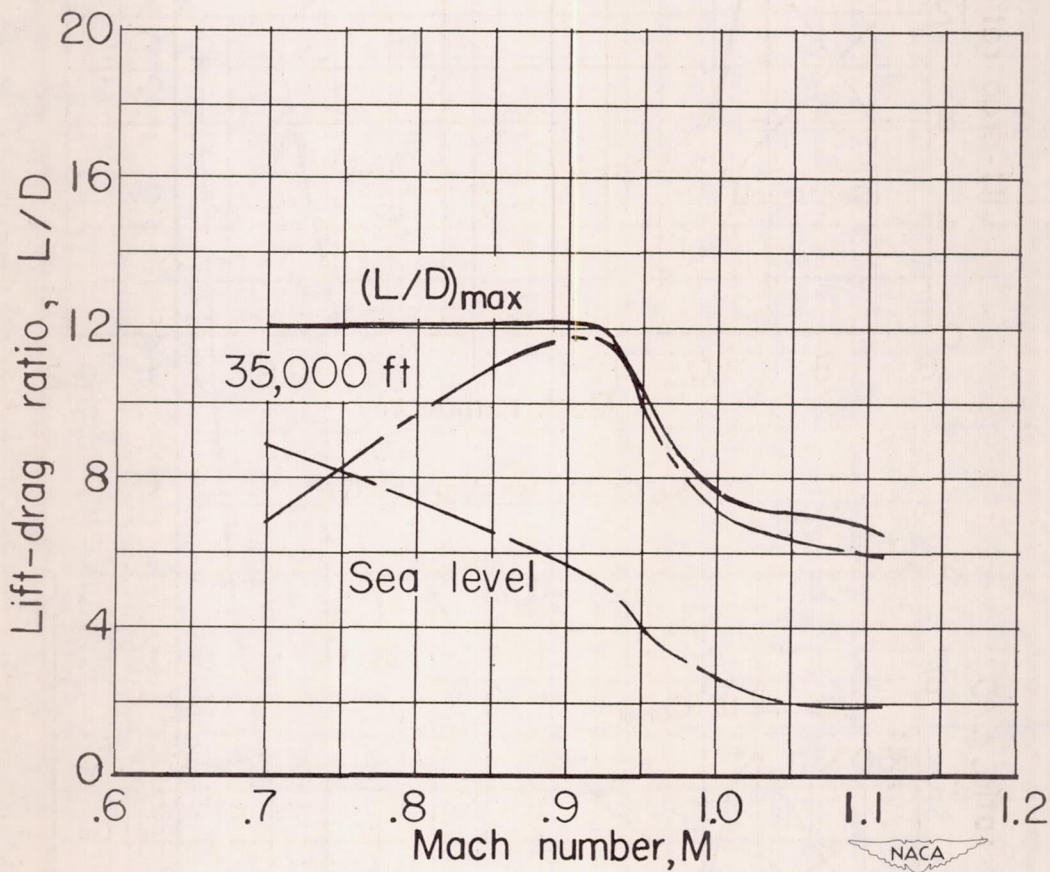
(a) Configuration WBHV.



(b) Configuration WBHV.

Figure 22.- Variation with Mach number of the maximum trimmed lift-drag ratios and the level-flight lift-drag ratios for sea level and 35,000-foot altitudes for the complete model.





(c) Configuration W<sub>3</sub>BH<sub>1</sub>VN<sub>2</sub>.

Figure 22.- Concluded.

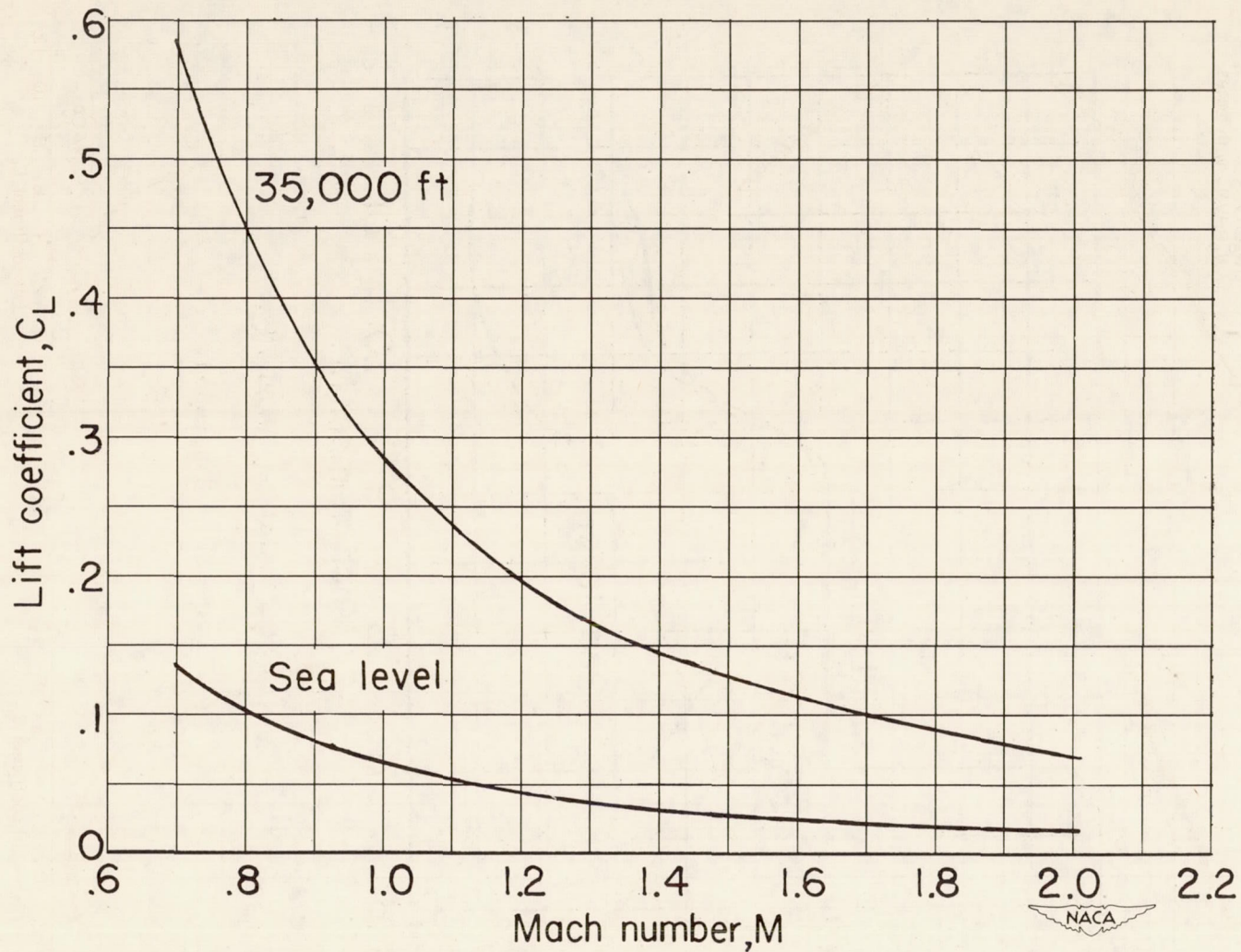
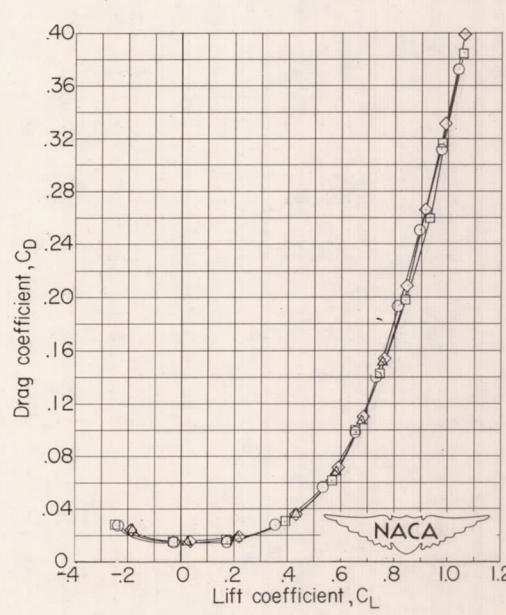
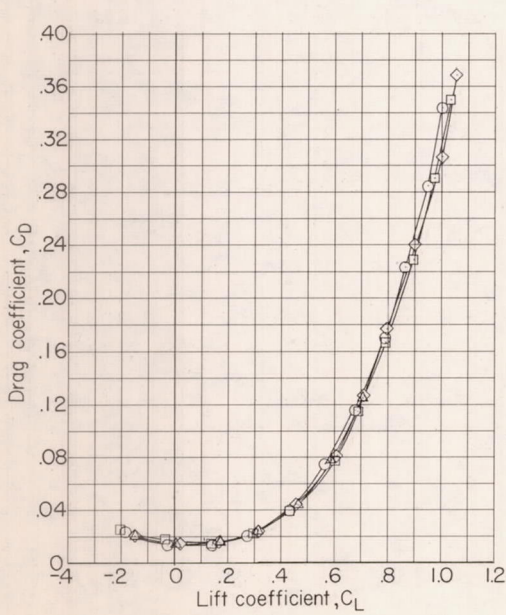
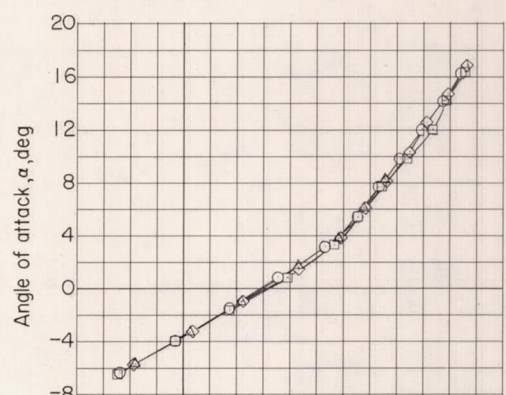
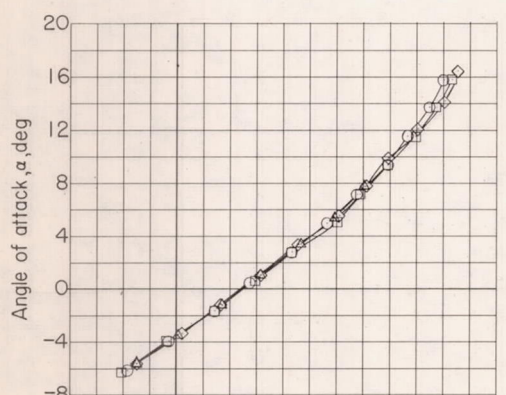
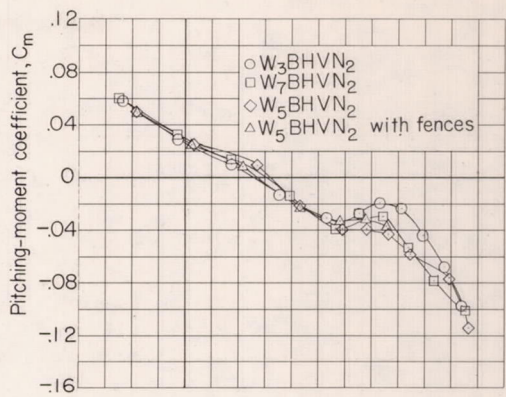
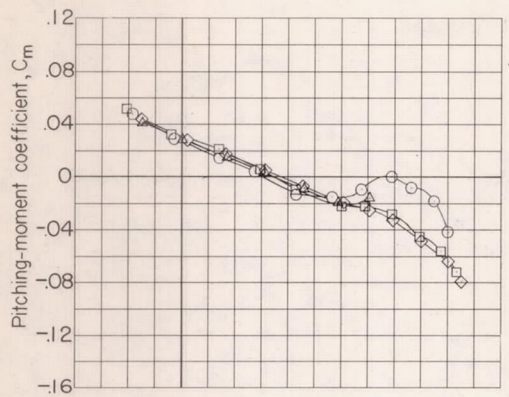


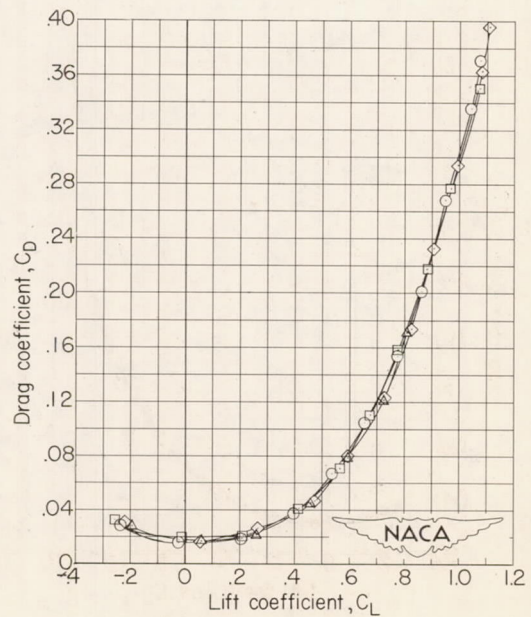
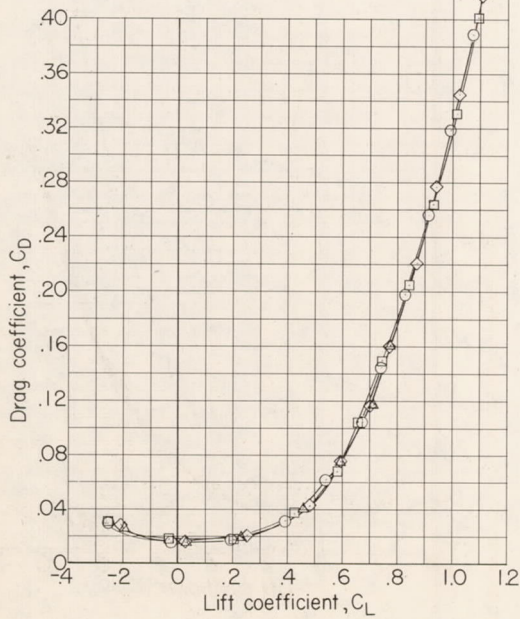
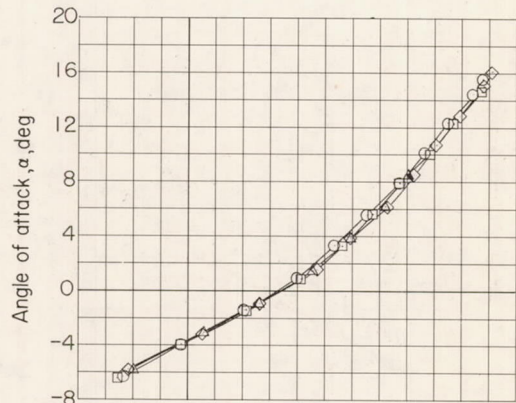
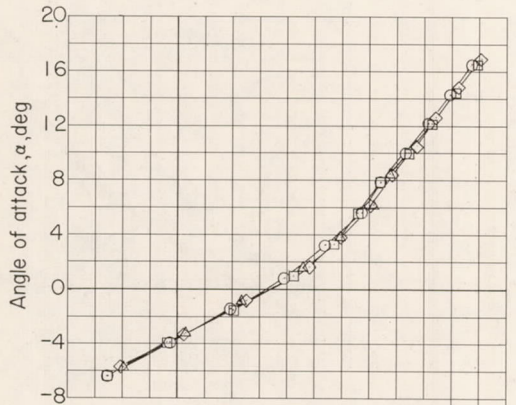
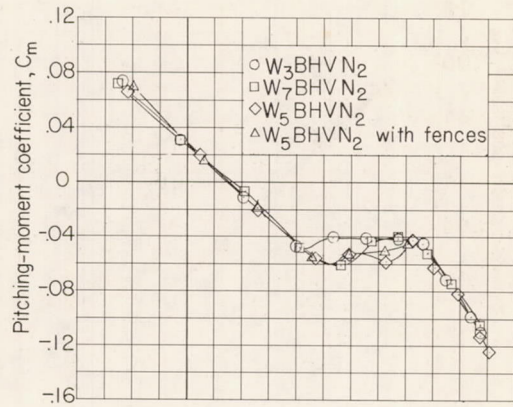
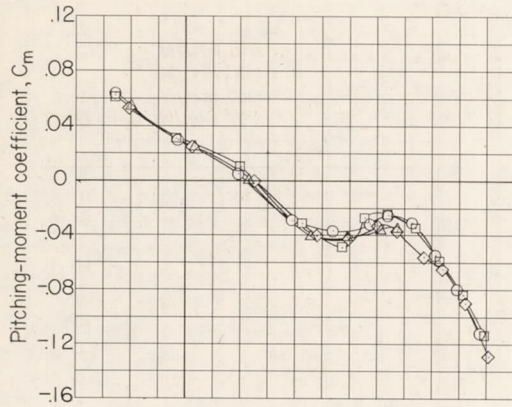
Figure 23.- Variation with Mach number of the level-flight lift coefficient for sea level and 35,000-foot altitudes. Wing loading of 100 pounds per square foot.



(a)  $M = 0.70$ .

(b)  $M = 0.90$ .

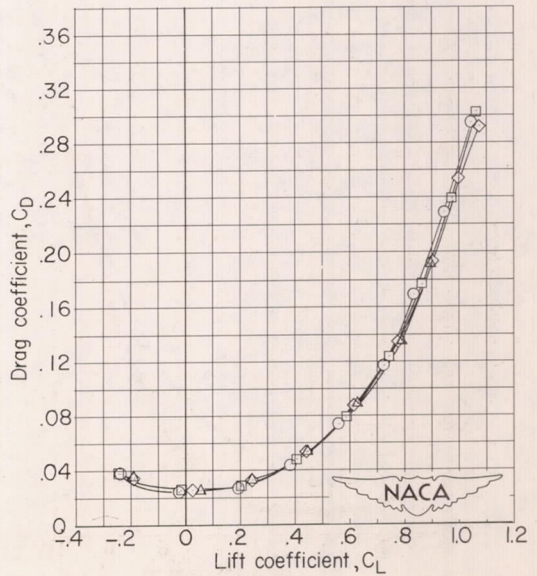
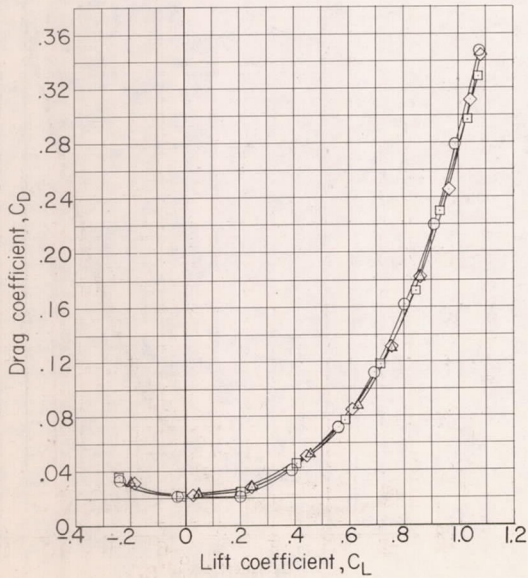
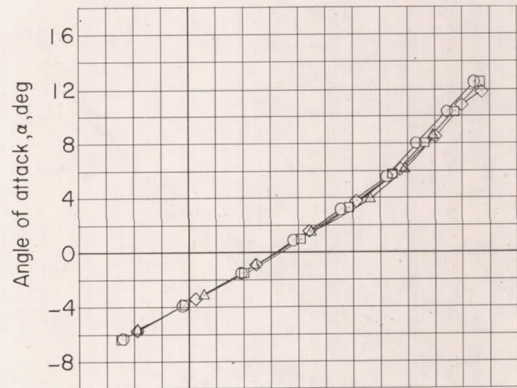
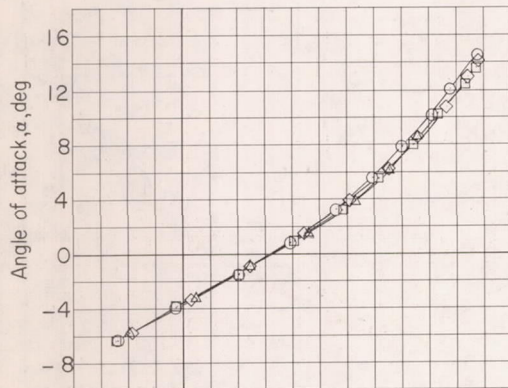
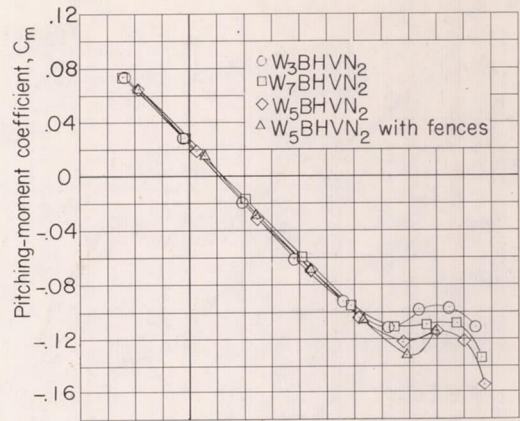
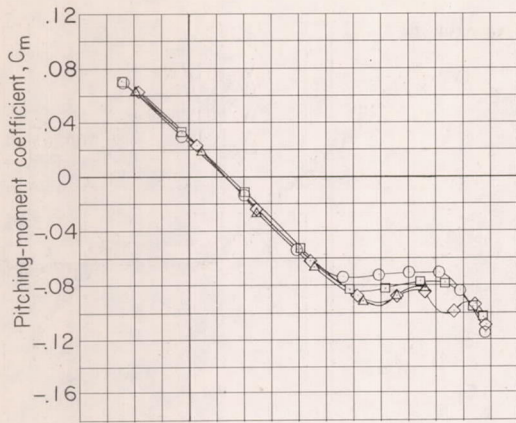
Figure 24.- Effects of leading-edge chord-extensions and fences on the aerodynamic characteristics of the model with buried nacelles.  
 $h_t = 0.06b/2$ .



(c)  $M = 0.93$ .

(d)  $M = 0.95$ .

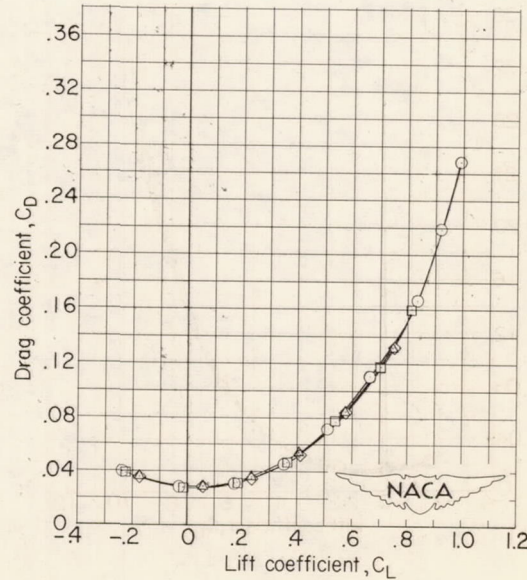
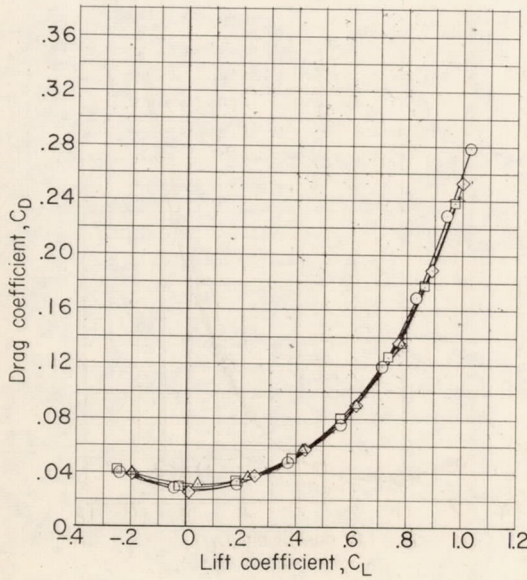
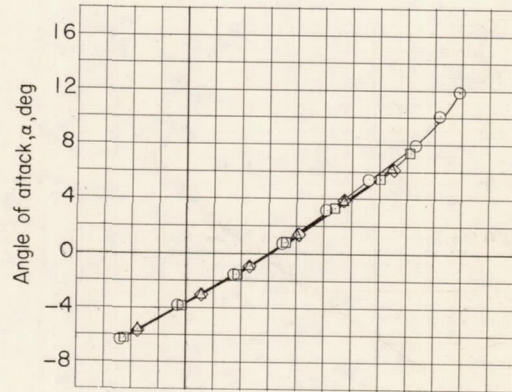
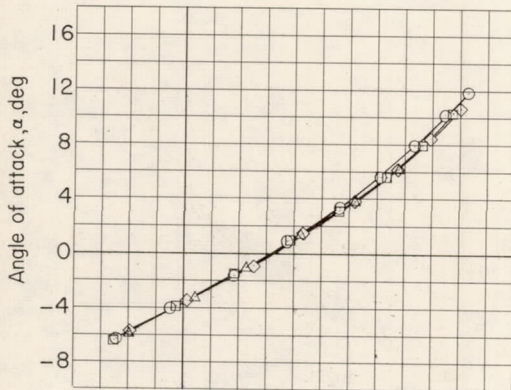
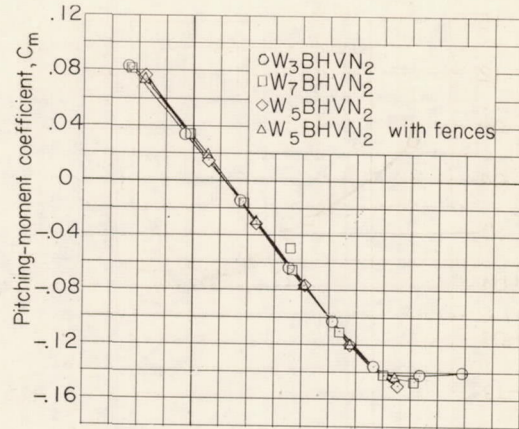
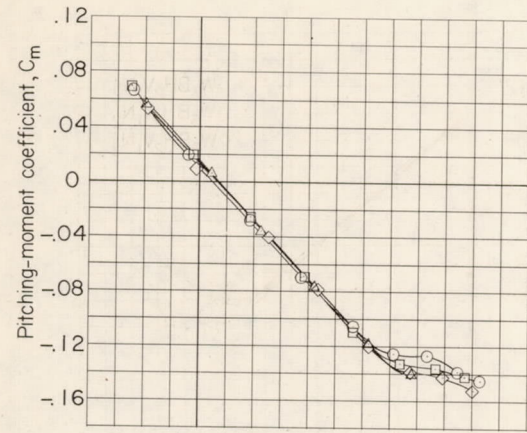
Figure 24.- Continued.



(e)  $M = 0.98$ .

(f)  $M = 1.00$ .

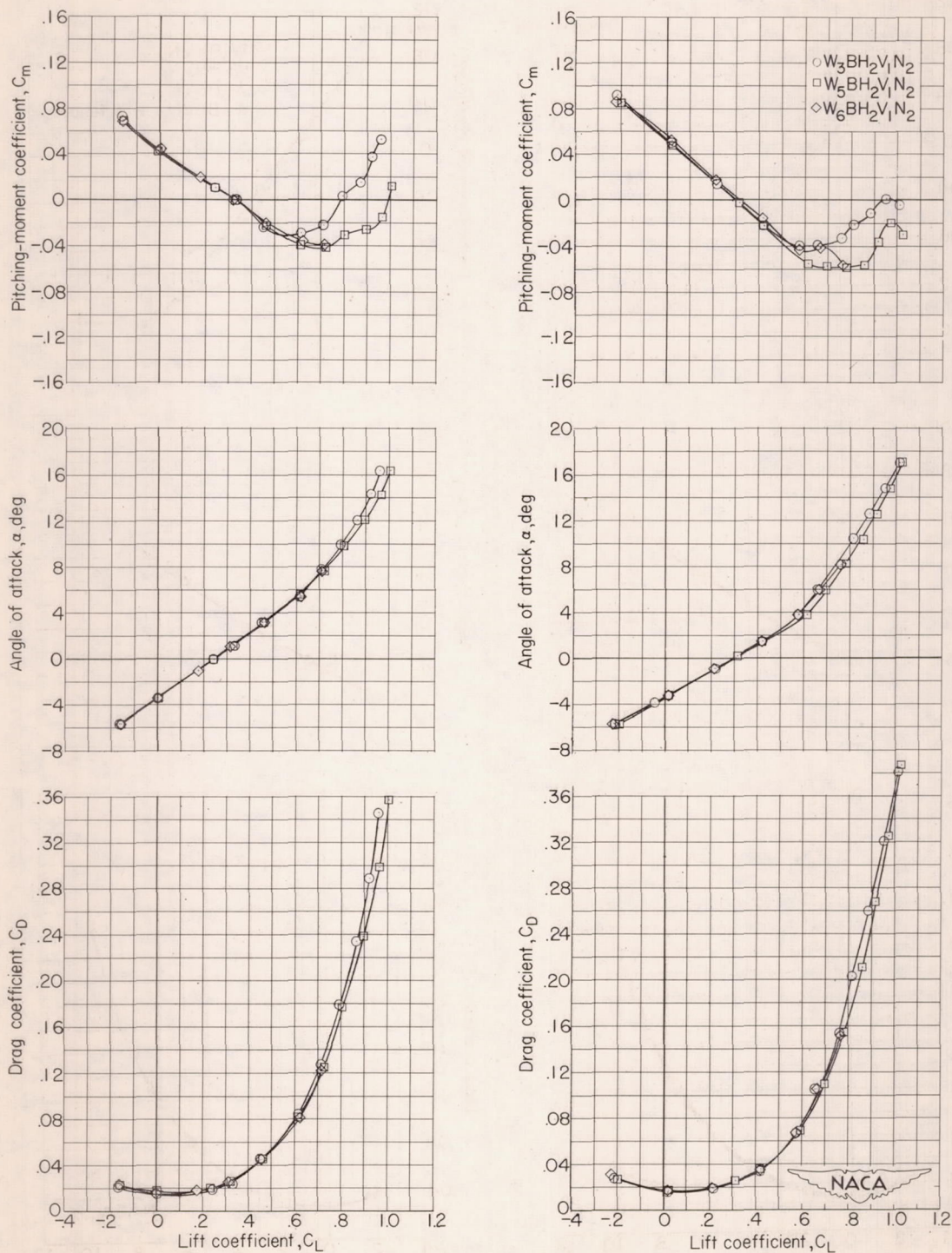
Figure 24.- Continued.



(g)  $M = 1.05$ .

(h)  $M = 1.11$ .

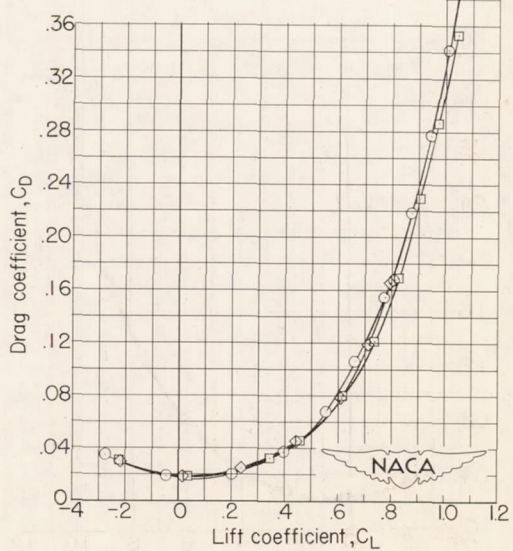
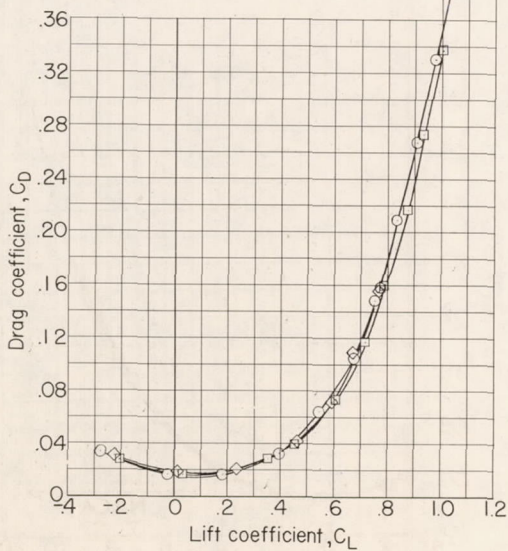
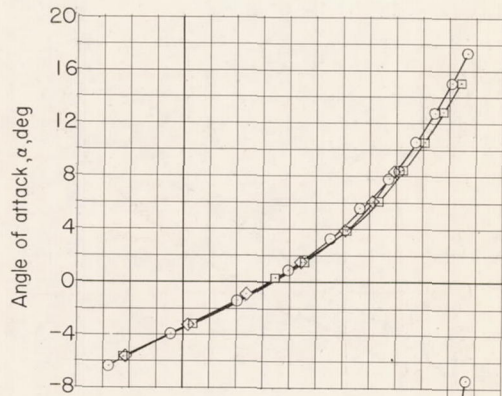
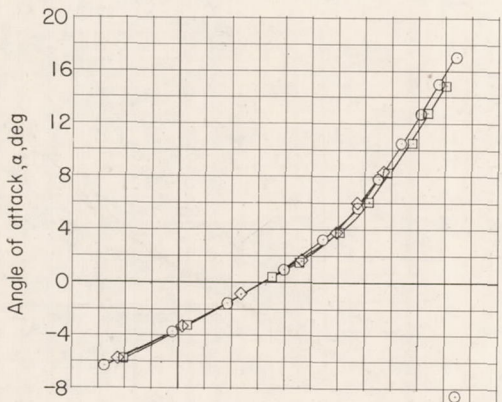
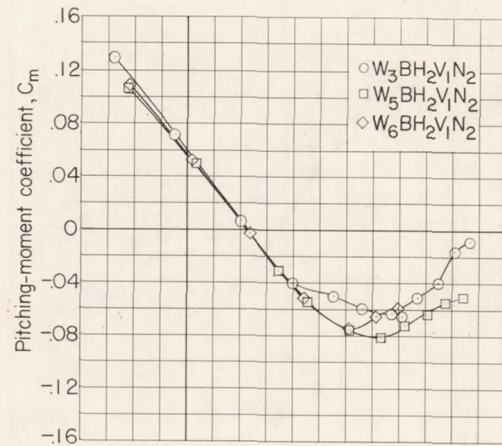
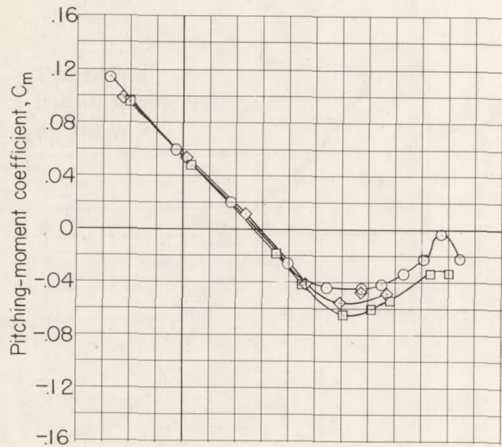
Figure 24.- Concluded.



(a)  $M = 0.70$ .

(b)  $M = 0.90$ .

Figure 25.- Effects of leading-edge chord-extensions on the aerodynamic characteristics of the model with buried nacelles.  $h_t = 0.56b/2$ .

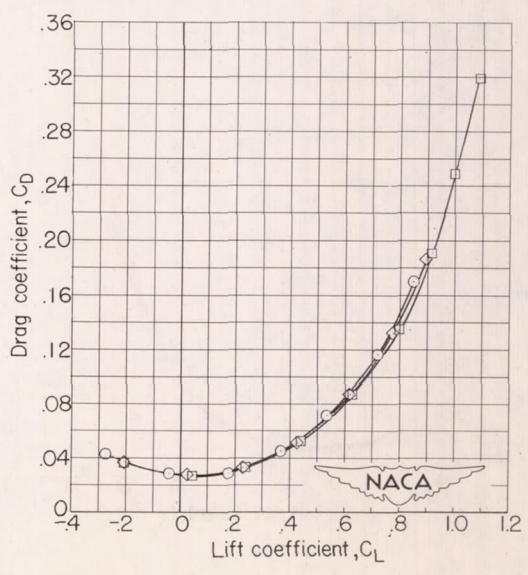
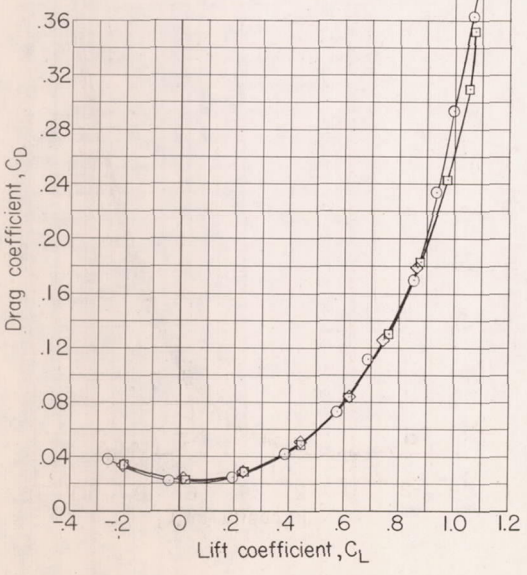
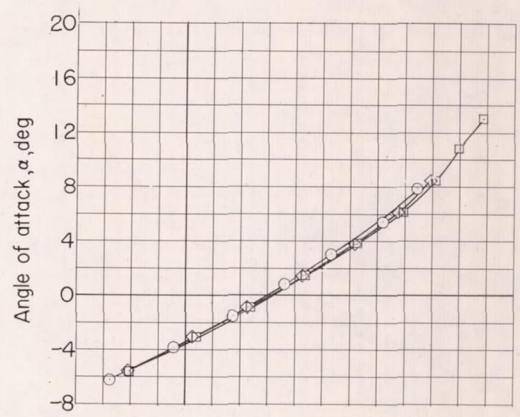
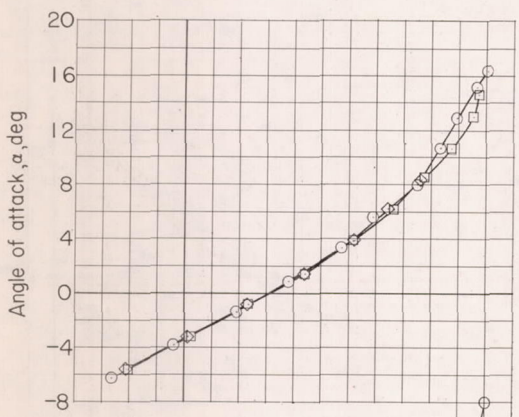
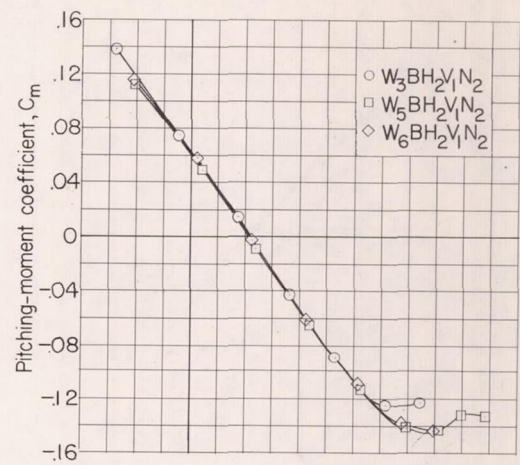
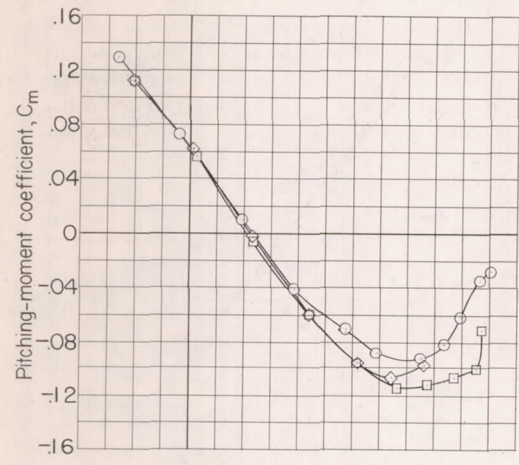


(c)  $M = 0.93$ .

(d)  $M = 0.95$ .

Figure 25.- Continued.

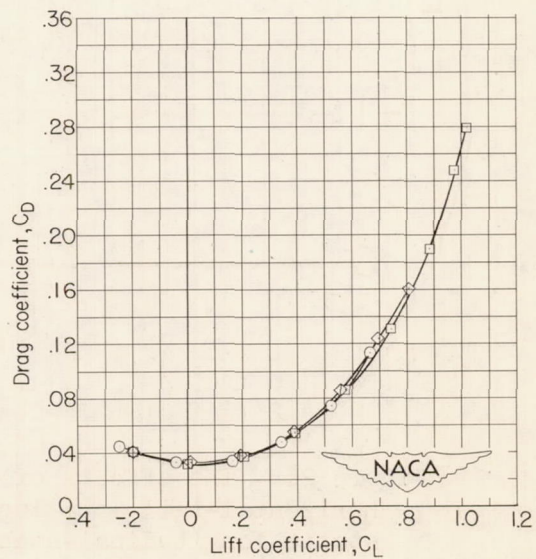
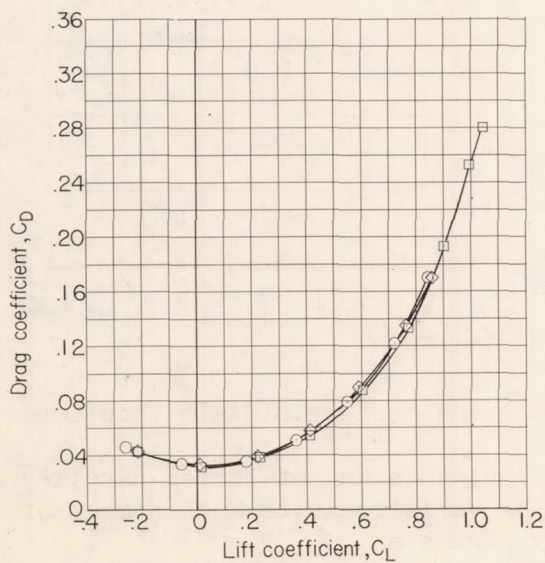
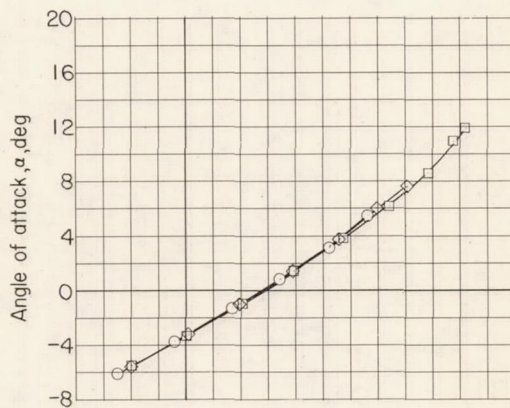
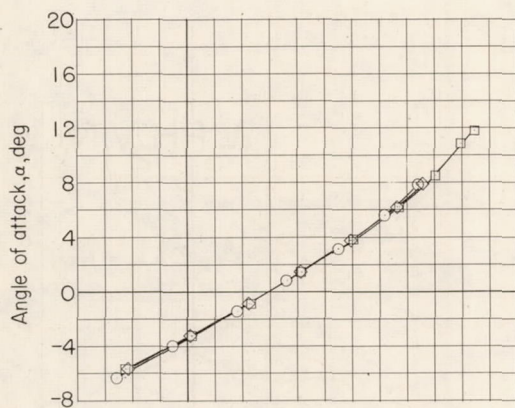
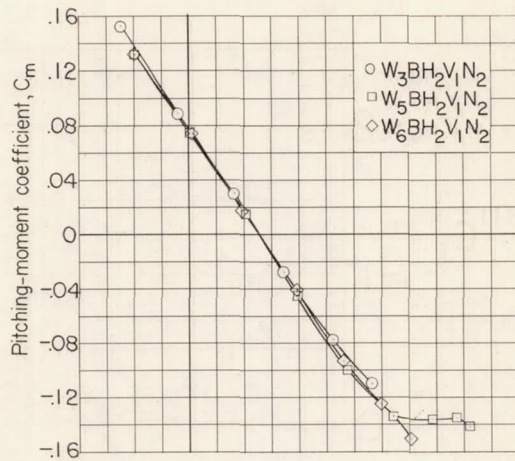
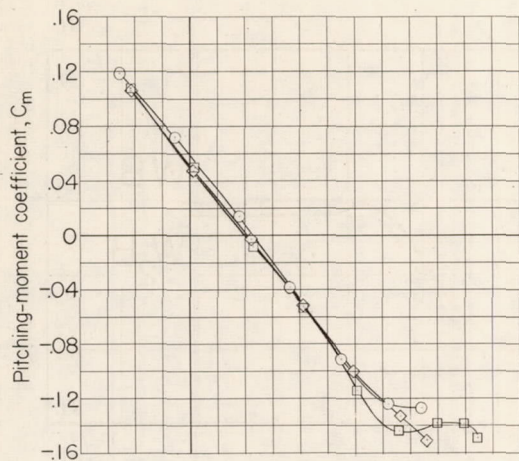




(e)  $M = 0.98$ .

(f)  $M = 1.00$ .

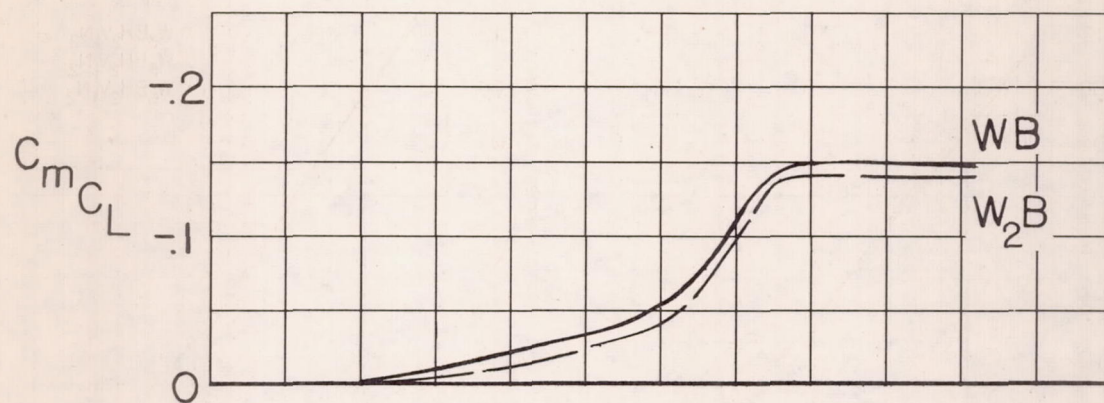
Figure 25.- Continued.



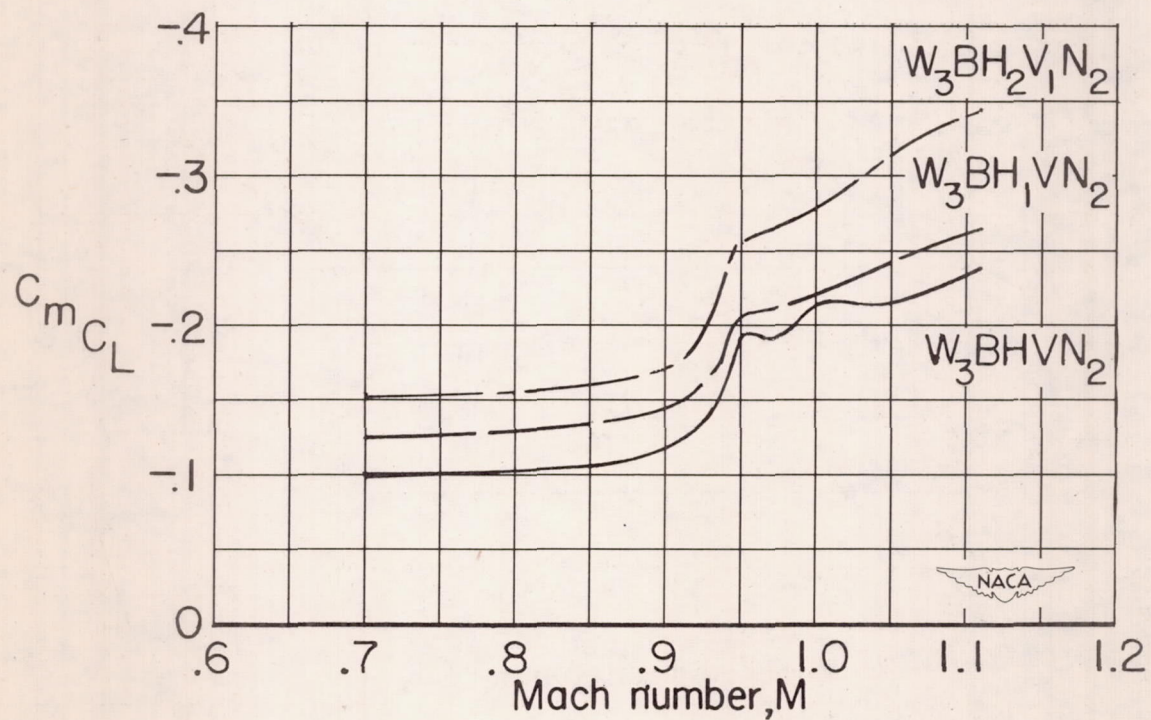
(g)  $M = 1.04$ .

(h)  $M = 1.11$ .

Figure 25.- Concluded.



(a) Effect of wing incidence.



(b) Effect of buried nacelles and horizontal-tail location.

Figure 26.- The effects of wing incidence and of buried nacelles and horizontal-tail location on the variation with Mach number of the static-longitudinal-stability parameter.

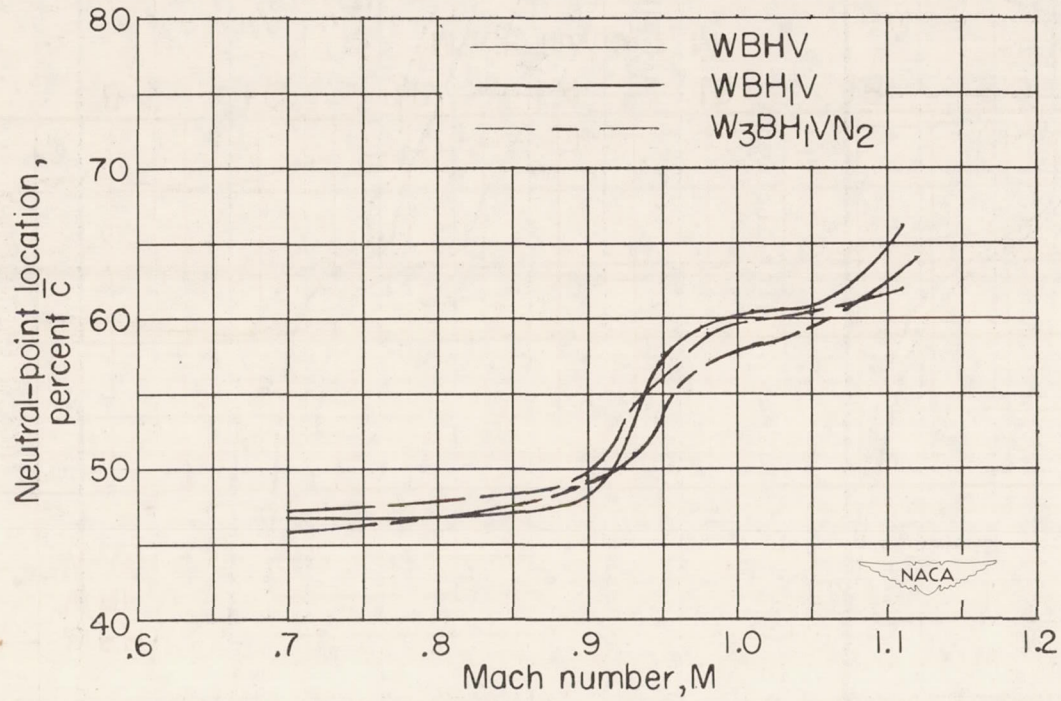


Figure 27.- Variation with Mach number of the neutral-point location for various model configurations.  $C_L = 0.3$ .

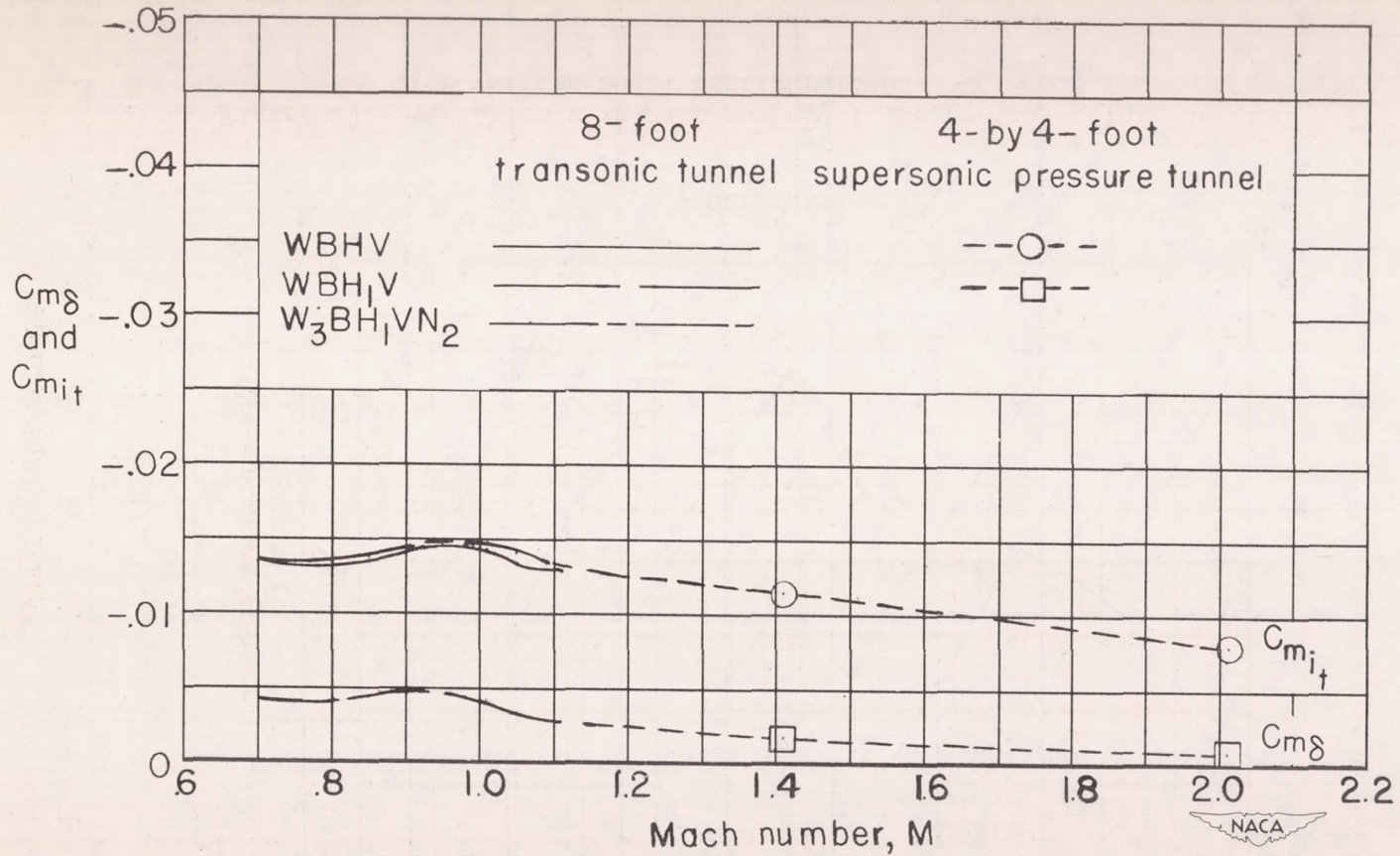
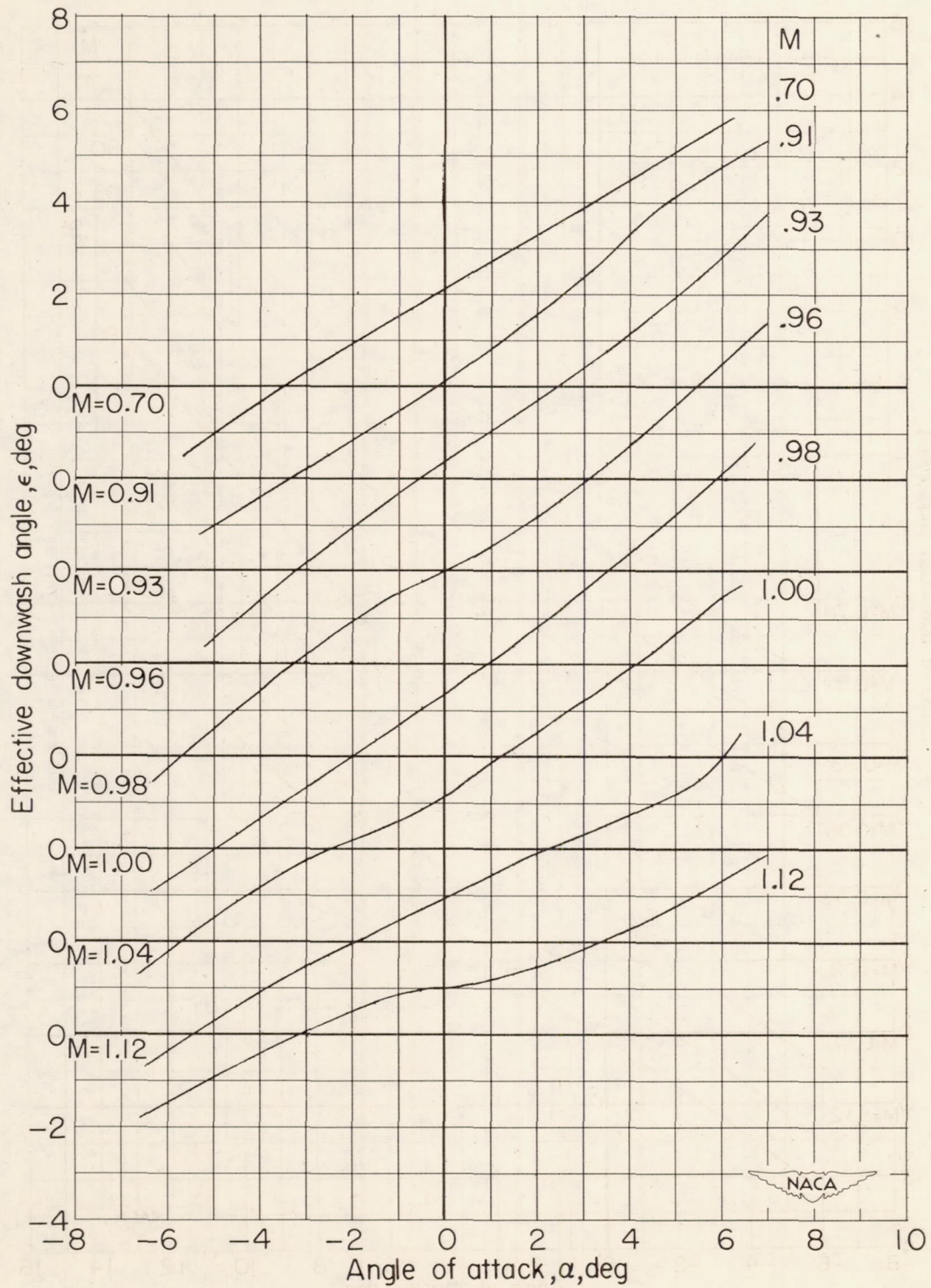
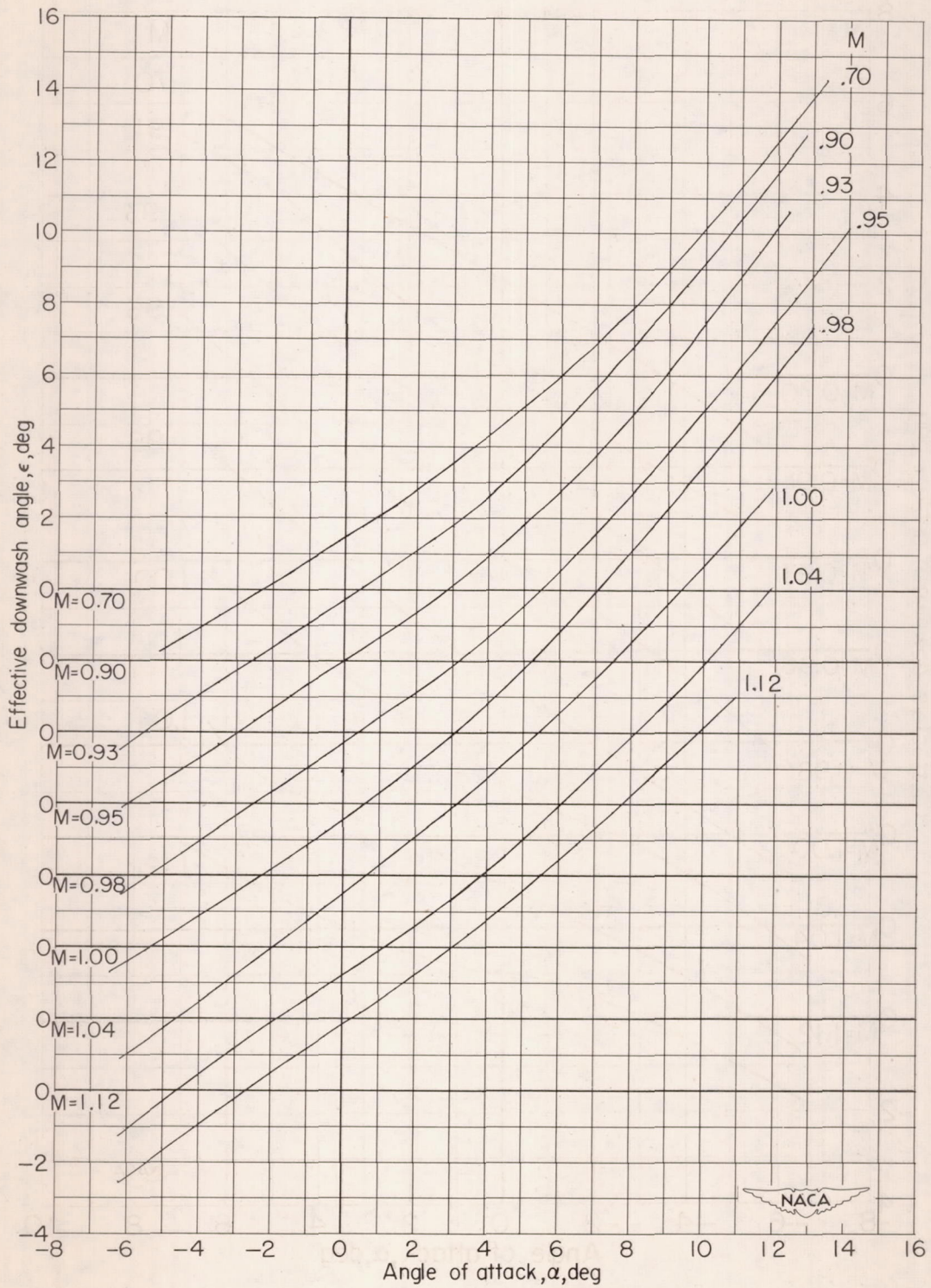


Figure 28.- Variation with Mach number of the elevator and stabilizer effectiveness parameters.



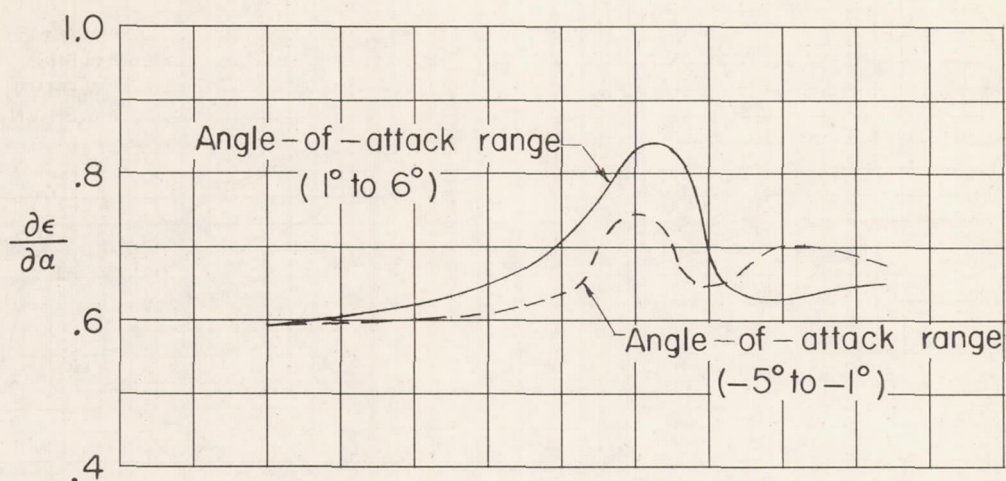
(a) Configuration WBHV.

Figure 29.- Variation of effective downwash angle with angle of attack.



(b) Configuration  $W_3BH_1VN_2$ .

Figure 29.- Concluded.



(a) Configuration WBHV.

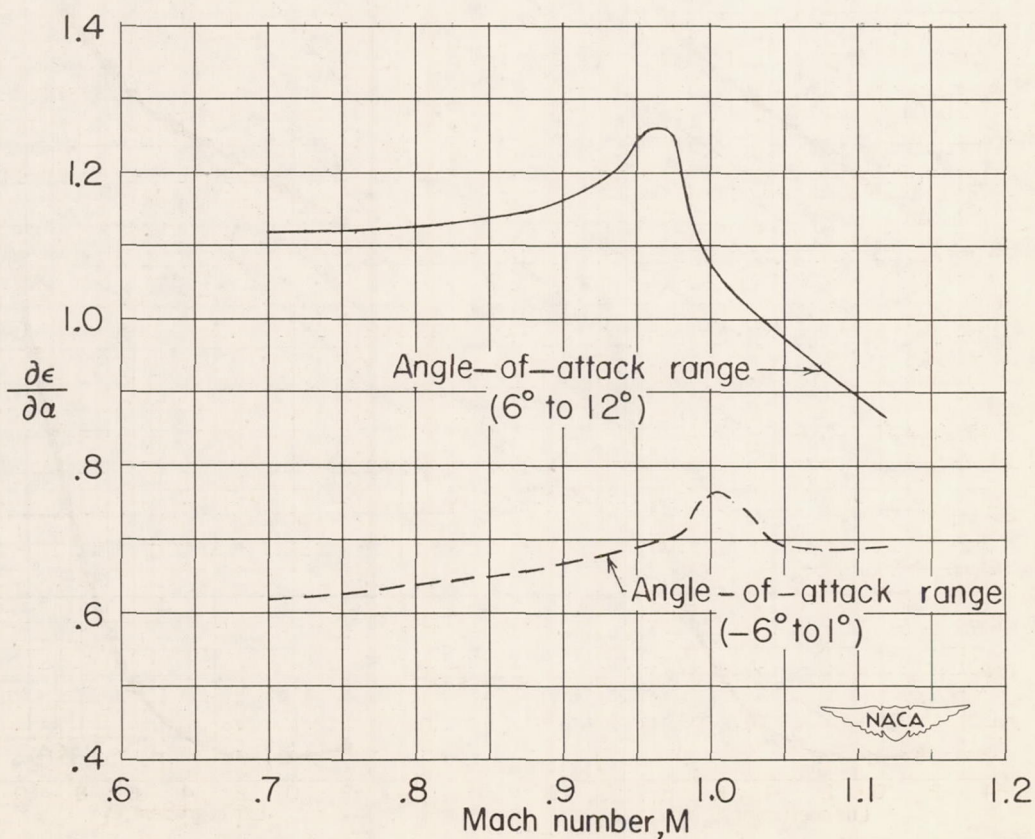
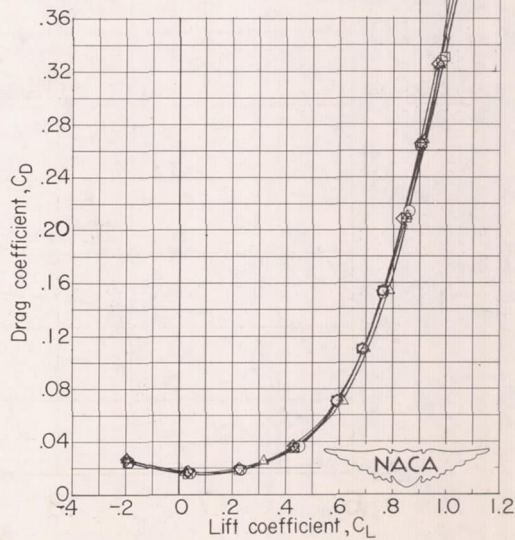
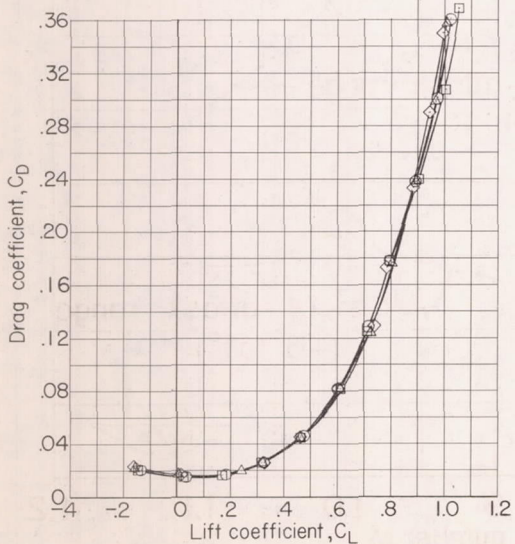
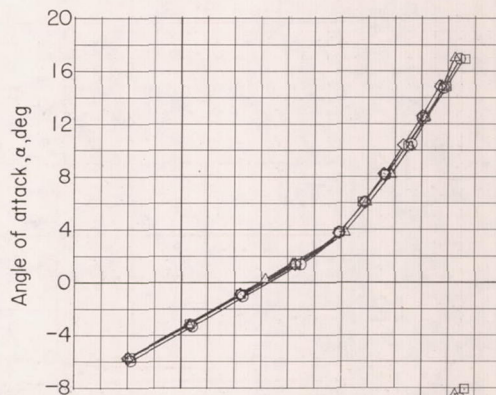
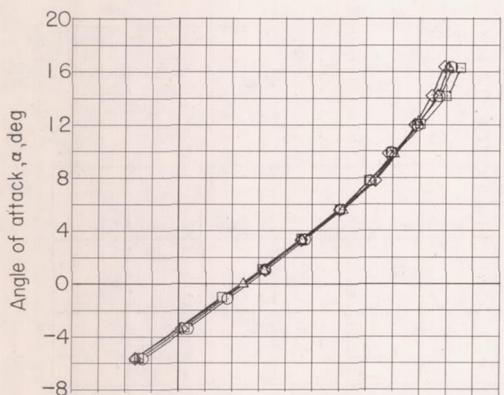
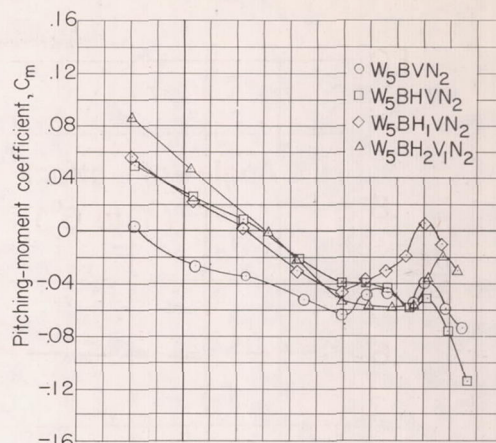
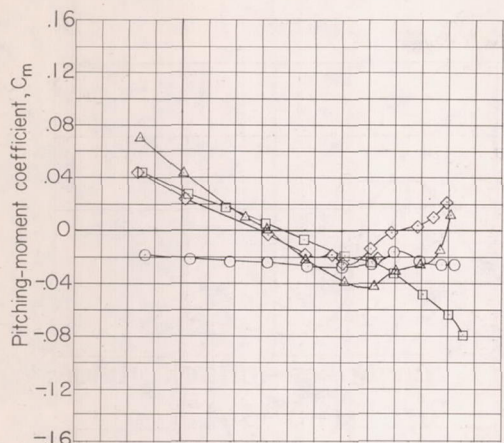
(b) Configuration W<sub>3</sub>BH<sub>1</sub>VN<sub>2</sub>.

Figure 30.- Variation with Mach number of the rate of change of effective downwash angle with angle of attack.

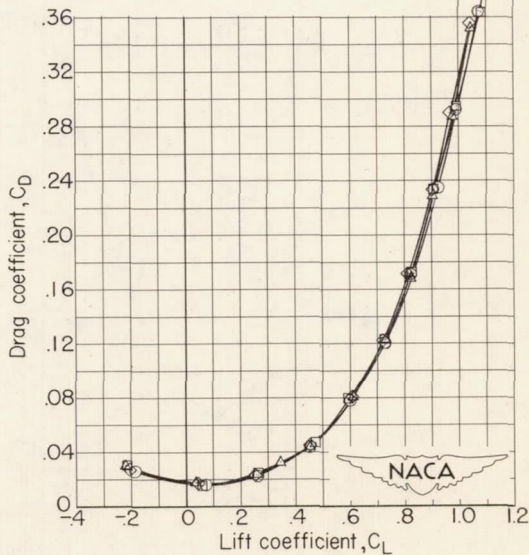
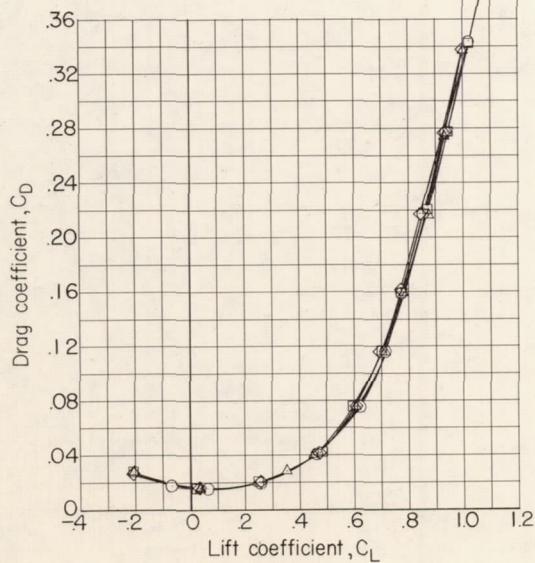
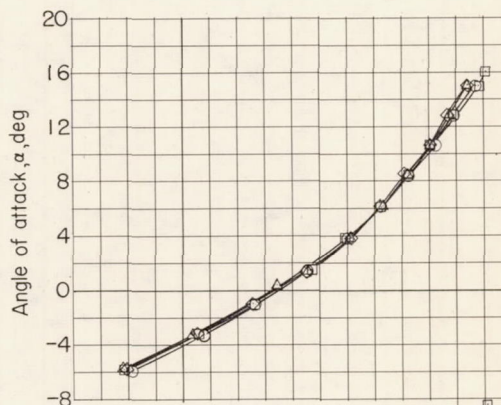
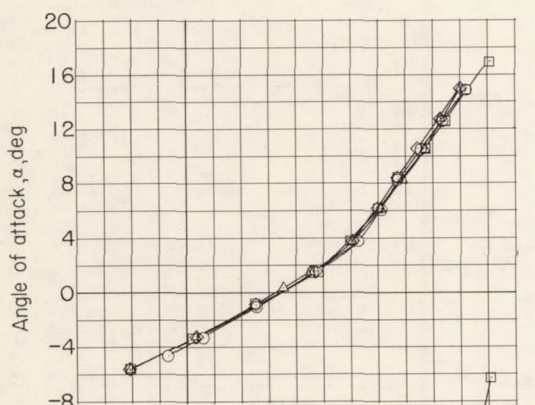
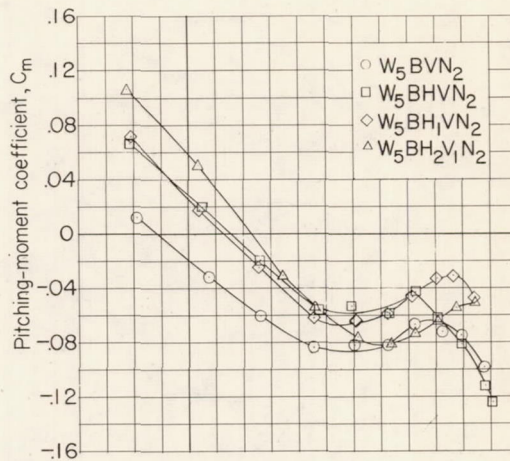
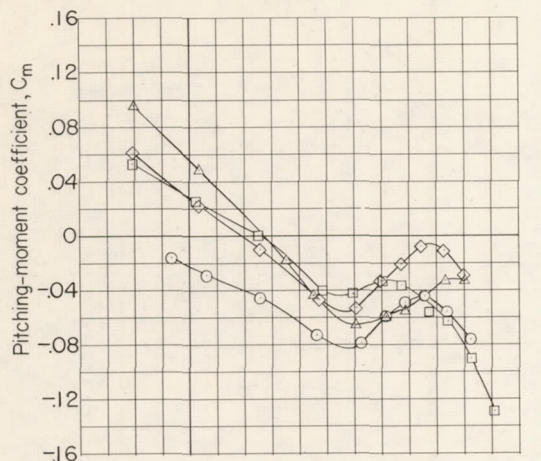




(a)  $M = 0.70$ .

(b)  $M = 0.90$ .

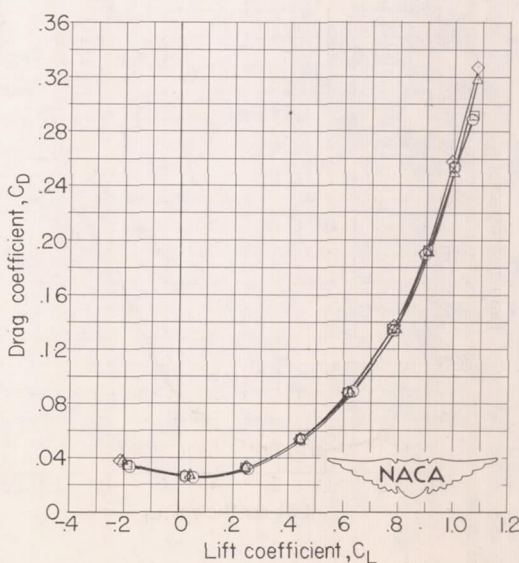
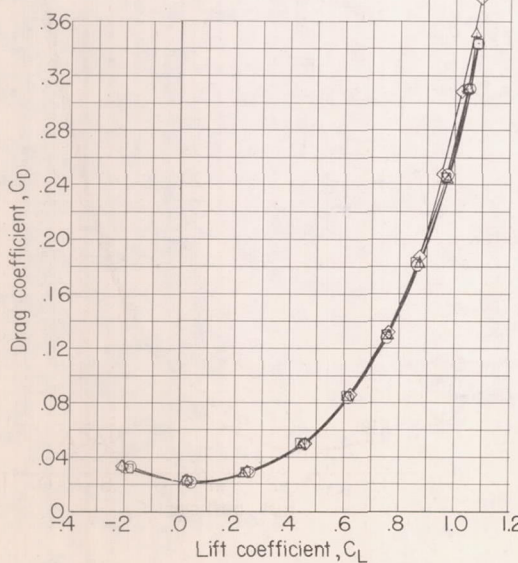
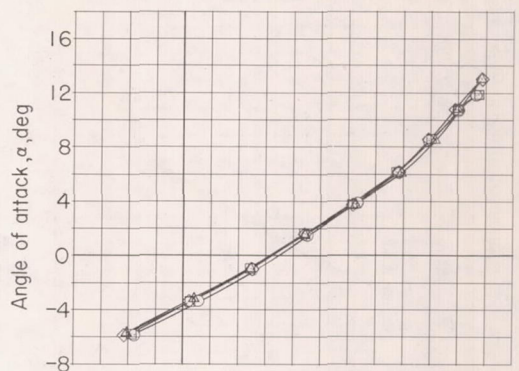
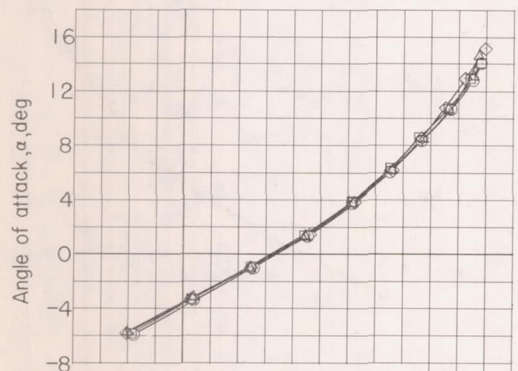
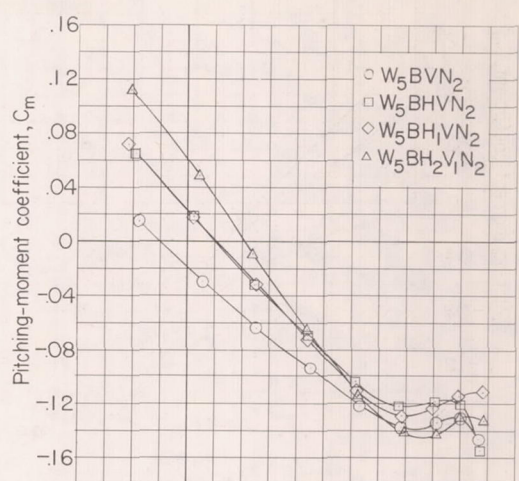
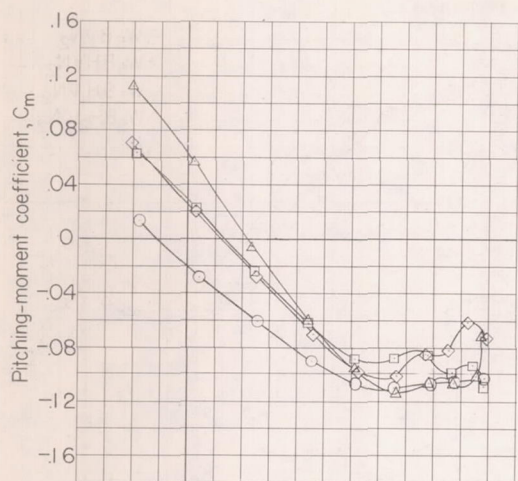
Figure 31.- Effects of vertical location of horizontal tail on the aerodynamic characteristics of the model with leading-edge chord-extensions and buried nacelles.



(c)  $M = 0.93$ .

(d)  $M = 0.95$ .

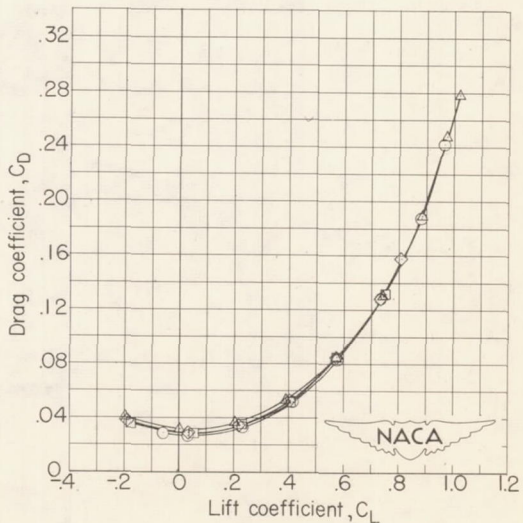
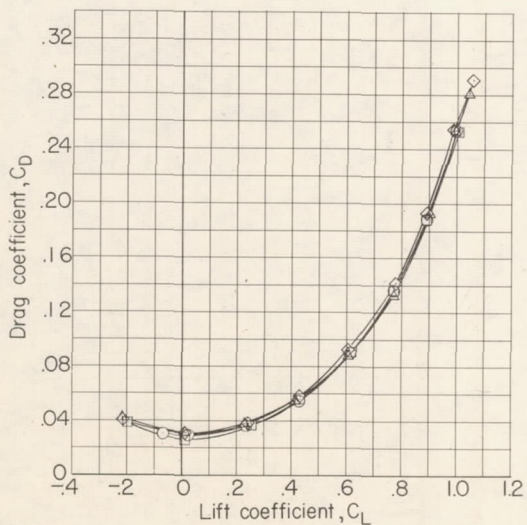
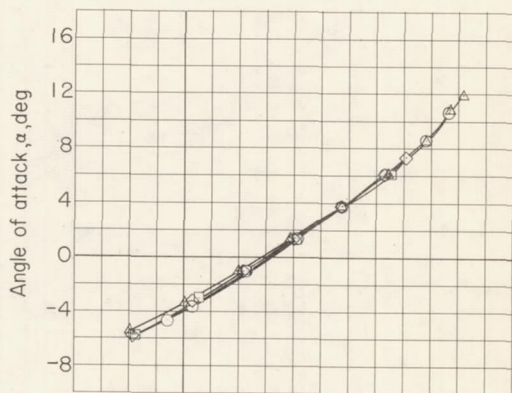
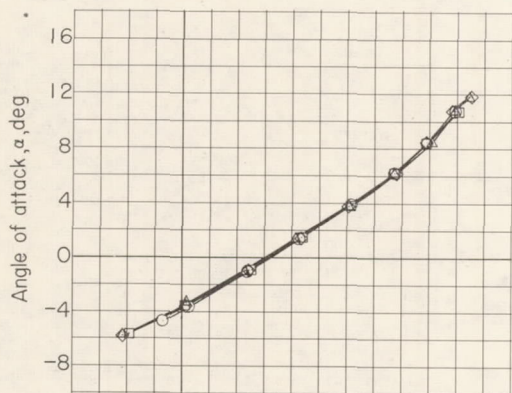
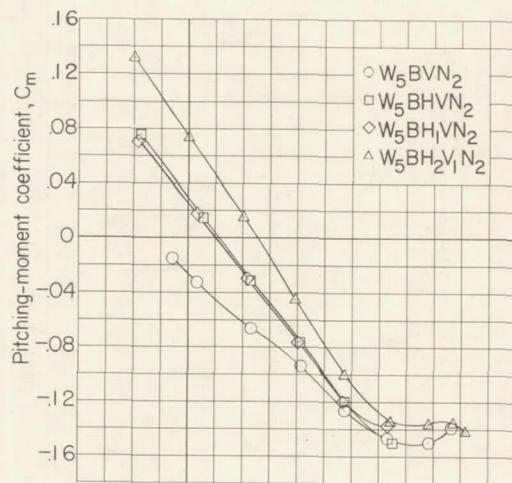
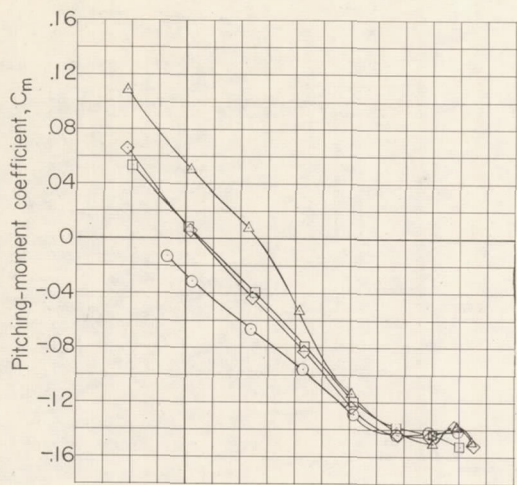
Figure 31.- Continued.



(e)  $M = 0.98$ .

(f)  $M = 1.00$ .

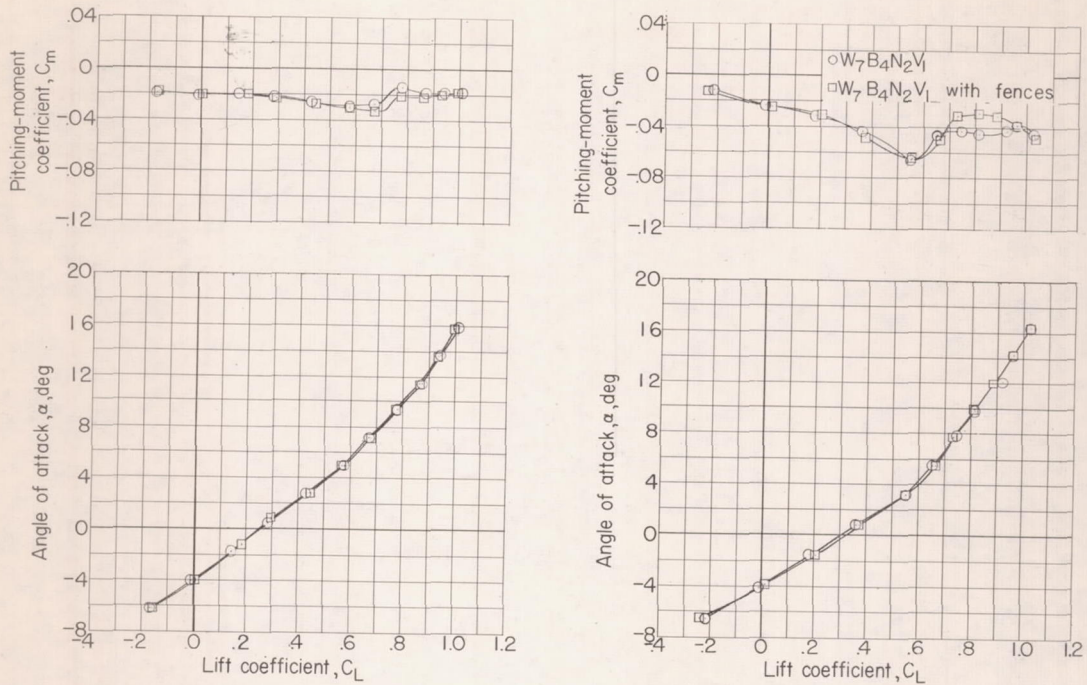
Figure 31.- Continued.



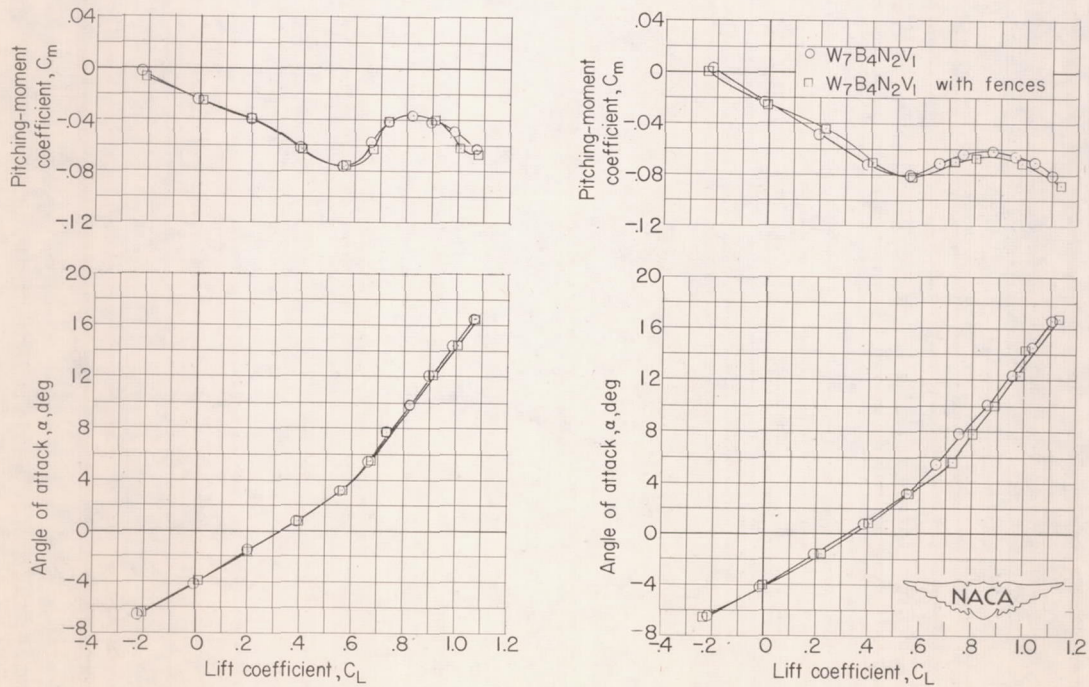
(g)  $M = 1.04$ .

(h)  $M = 1.10$ .

Figure 31.- Concluded.

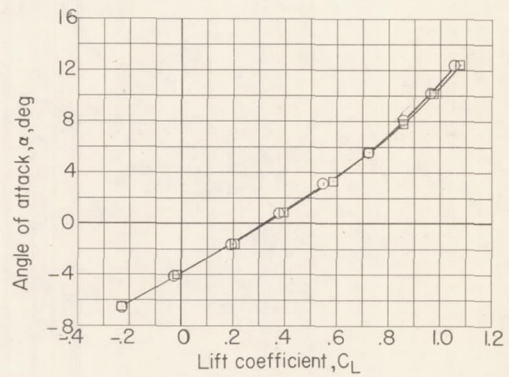
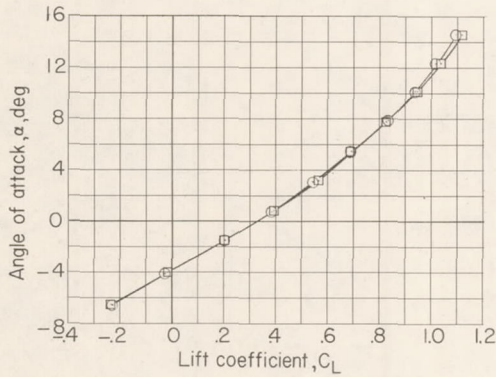
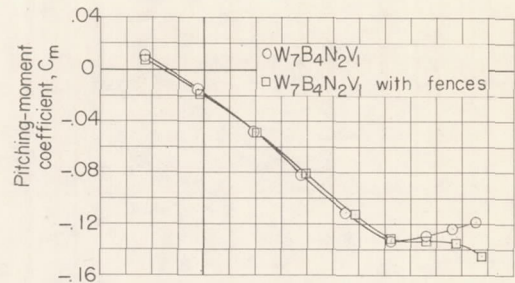
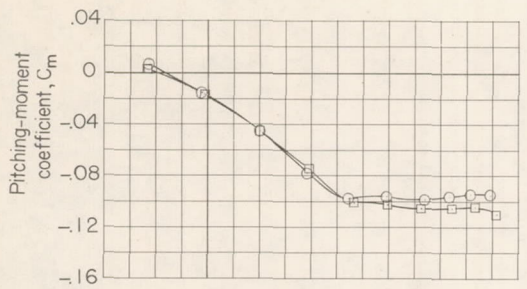


(a)  $M = 0.70$  and  $0.90$ .

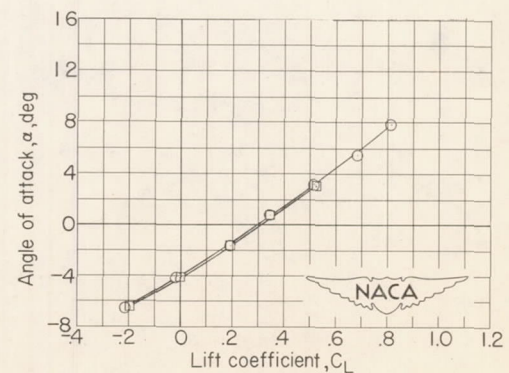
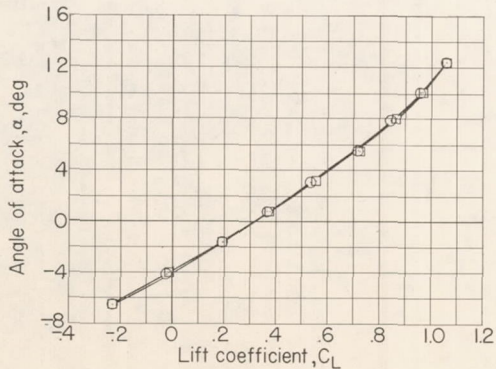
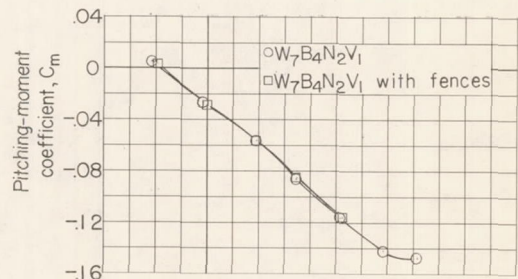
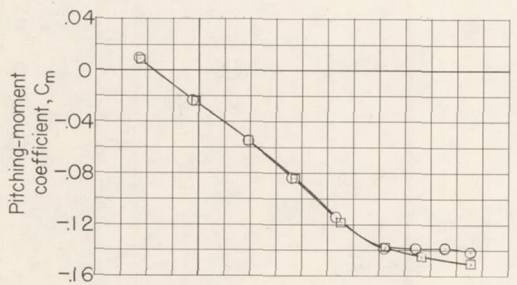


(b)  $M = 0.93$  and  $0.95$ .

Figure 32.- Effects of fences on the aerodynamic characteristics of the model with buried nacelles, shortened fuselage, and no horizontal tail.



(c)  $M = 0.98$  and  $1.01$ .



(d)  $M = 1.04$  and  $1.10$ .

Figure 32.- Concluded.

1911

CONFIDENTIAL



CONFIDENTIAL